13 Characterization, Mapping, and Monitoring of Rangelands

Methods and Approaches

Lalit Kumar, Priyakant Sinha, Jesslyn F. Brown, R. Douglas Ramsey, Matthew Rigge, Carson A. Stam, Alexander J. Hernandez, E. Raymond Hunt Jr., and Matthew Reeves

ACRONYMS AND DEFINITIONS

ASTER	Advanced Spaceborne Thermal Emission and Reflection Radiometer
DEM	Digital Elevation Model
ETM+	Enhanced Thematic Mapper Plus
EVI	Enhanced Vegetation Index
GIS	Geographic Information System
ISODATA	Iterative Self-Organizing Data Analysis Technique
LAI	Leaf Area Index
LiDAR	Light Detection and Ranging
MSS	Multispectral Scanner
MODIS	Moderate-Resolution Imaging Spectroradiometer
NDVI	Normalized Difference Vegetation Index
NDWI	Normalized Difference Water Index
NIR	Near-Infrared
NPP	Net Primary Productivity
OLI	Operational Land Imager
PAR	Photosynthetically Active Radiation
SAVI	Soil Adjusted Vegetation Index
SPOT	Satellite Pour l'Observation de la Terre, French Earth Observing Satellites
TM	Thematic Mapper
USDA	United States Department of Agriculture

13.1 INTRODUCTION

While there are many definitions of rangeland, the central theme of all these is that it is land on which the dominating vegetation is mainly grasses, grass-like plants, forbs, shrubs and isolated trees (De Cauwer et al., 2024; Arogoundade et al., 2023; Feizizadeh et al., 2023; Sharifi and Felegari, 2023; McCord and Pilliod, 2022; Matongera et al., 2021; Zhou et al., 2020; Hadian et al., 2019; Al-bukhari et al., 2018; Eddy et al., 2017; Gökalp et al., 2017). Rangelands include shrublands, natural grasslands, woodlands, savannahs, tundra and many desert regions. A distinguishing factor of rangelands from pasture lands is that they grow primarily native vegetation, rather than plants established by humans. Rangelands are also managed mainly through extensive practices such as managed livestock grazing and prescribed fire rather than more intensive agricultural practices and the use of fertilizers. Rangelands worldwide are known to provide a wide range of desirable goods

DOI: 10.1201/9781003541165-17

and services, including but not limited to livestock forage, wildlife habitat, wood products, mineral resources, water and recreation space. Large populations depend on rangelands for their livelihoods, hence effective monitoring and management is crucial for sustainable production, health and biodiversity of these systems (McCord and Pilliod, 2022; Matongera et al., 2021; Zhou et al., 2020).

Effective monitoring of rangelands has proven logistically and statistically difficult using field based monitoring methods alone due to the sheer size, range and complexity of rangelands (Hadian et al., 2019; Al-bukhari et al., 2018; Eddy et al., 2017; Gökalp et al., 2017). Mapping and monitoring of rangelands, especially those in a disturbed state or under rapid change, requires data that is extensive, accurate, timely and with regular repeat coverage. All this makes remote sensing an ideal platform for rangeland monitoring as recent developments in sensor capabilities means we have repeat coverage from multiple satellites, spectral resolutions sufficient to distinguish many rangeland vegetation species and communities, spatial resolutions allowing monitoring and management at micro-scales and costs that are a small fraction of a few decades ago. Remote Sensing data is more easily available and the systems cover almost the entire world, and certainly all the regions where rangelands occur.

There is a plethora of literature available that describe various uses of remote sensing data for rangeland monitoring, ranging from mapping species distribution, biomass, degradation, woody cover, net primary production, biodiversity, change detection, fuel loads, fire extents and frequency, invasive species encroachment, livestock foraging, etc. New methods of image classification and interpretation are regularly published, as well as novel techniques of incorporating satellite data with ancillary data to better understand rangeland dynamics (Arogoundade et al., 2023; Feizizadeh et al., 2023). Some of these applications have been discussed in the previous two chapters of this volume of the *Remote Sensing Handbook* (Second Edition, six volumes), with Reeves et al. (Chapter 11) looking at the relationship between rangeland productivity and climate, food security, fire and rangeland degradation, and Hunt et al. (Chapter 12) exploring rangeland biodiversity using different spectral, spatial and temporal satellite data.

The focus of this chapter is to present and discuss methods and approaches used in the mapping and monitoring of rangelands. We do this by presenting characterization, mapping, and monitoring of rangelands in specific applications such as: 1. Phenology and Productivity studies; 2. Fuel Analysis; 3. Biodiversity and Gap Analysis; 4. Vegetation Continuous Fields, and 5. Change Detection Analysis. We summarize some oft-used traditional means of mapping and monitoring rangelands but concentrate on newer developments in this field.

13.2 RANGELAND MONITORING METHODS USING VEGETATION INDICES

13.2.1 Rangeland Phenology

Rangeland phenology for vegetation types (shrublands, grasslands, steppes, deserts, and woodlands) is affected by environmental drivers (temperature, precipitation, sunshine) and factors such as topography (elevation, slope, aspect), edaphic conditions (variations in soil type, texture, nutrients) and latitude (Feizizadeh et al., 2023; Gökalp et al., 2017). Rangeland vegetation growth is the result of overall influence of all environmental drivers and factors and their interaction, and responds more rapidly to the environmental variations as compared to other kinds of vegetation (Reed et al., 1994a, 1994b). Since rangelands are mainly located in dry areas characterized by low and variable annual rainfall (Grice and Hodgkinson, 2002; Zhou et al., 2020), precipitation regime has a much more significant influence on rangeland vegetation among all the environmental drivers and factors (Reed et al., 1994a, 1994b). They usually respond to precipitation in a pulsed way where their phenology is dependent on discrete rainfall events in terms of productivity, density, and abundance (Rauzi and Dobrenz, 1970). Temperature has also been observed to have direct influence on phenological phases and a large number of studies have been conducted to determine the effects of temperature on the phonological timings of plants (Badeck et al., 2004; Sparks et al., 2000). Livestock grazing is another notable factor that influences rangeland phenology and has impact on rangeland vegetation (Desalew et al., 2010). The grazing-induced vegetation change is dependent on the type of livestock and the composition of vegetation types and hence an important consideration in monitoring or predicting rangeland plant phenology (Sharifi and Felegari, 2023; McCord and Pilliod, 2022).

The advent of remote sensing technology induced great changes in vegetation phenology studies by providing temporal data at regular intervals. Time-series data have been used to predict phenophase in terms of onsets and offsets of the vegetation growing season as well as budburst, flowering or leaf color changing dates. A simple way to predict the onset and/or offset of the growing season is to analyze the time series of vegetation indices (VIs). There have been many methods to determine the onset/offset dates, including thresholds, maximum rate of change, or a certain percentage of the greatest VI increase (McCord and Pilliod, 2022; Al-bukhari et al., 2018). For example, Rigge et al. (2013) evaluated the productivity and phenology of western South Dakota mixed-grass prairie in the period from 2000 to 2008 using the Normalized Difference Vegetation Index (NDVI) derived from MODIS data. They used growing-season NDVI images on a weekly basis to produce time-integrated NDVI, a proxy of total annual biomass production, and also integrated seasonally to represent annual production by cool- and warm-season species (C3 and C4, respectively). Heumann et al. (2007) studied phenological change in the Sahel and Soudan, Africa from 1982–2005. They used TIMESAT software to estimate phenological parameters from the AVHRR NDVI dataset and have found significant positive trends for the length of the growing and end of the growing season for the Soudan and Guinean regions. Kumar et al. (2002) showed that soil type has a significant impact on the early season growth variation of annual vegetation on sandy and clay soils, a fact that is utilized in the movement patterns of graziers in the Sahel.

13.2.2 Vegetation Indices in Rangeland Monitoring

13.2.2.1 What to Measure?

To be effective estimators of biomass, Leaf Area Index (LAI), or percentage cover, spectral indices must be able to differentiate vegetation features from soil features (Todd et al., 1998). For such differentiation, it is a requirement that the soils and vegetation have different reflectance patterns and the spectral index should be sensitive enough to detect the differences. Green vegetation has characteristically low reflectance in the visible portion of the spectrum (lowest in red portion of the spectrum) with a sharp increase in reflectance in the near-infrared portion (Figure 13.1). Most of the commonly used vegetation indices exploit this expected difference in near-infrared and red reflectance for vegetation discrimination and in separating them from non-vegetated areas (Sharifi and Felegari, 2023; McCord and Pilliod, 2022). For example, the Normalized Difference Vegetation Index (NDVI), computed as: NDVI = NIR−Red/NIR + Red, has been used in a wide range of practical remote sensing applications (e.g., Tucker et al., 1985). The NDVI values range between −1 to +1, with dense vegetation having a high NDVI while soil values are low but positive, and water is negative due to its strong absorption of NIR. Tucker (1979) tested various combinations of the red, NIR, and green bands to predict biomass, water and chlorophyll content of grass plots. A strong correlation was observed between NDVI values and chlorophyll content and crop characteristics such as green biomass and leaf water content. Sellers (1985) used a canopy radiative transfer model to show that NDVI is near-linearly related to area-averaged net carbon assimilation and plant transpiration, even at different values of fractional vegetation cover (fc) and LAI over an area of interest.

The TM Tasseled Cap green vegetation index (GVI) is a linear combination of the six reflecting wavebands of Landsat TM (Crist, 1983). The GVI coefficients with the highest values are for the red (negatively loaded) and the near-infrared (positively loaded) wavebands.

13.2.2.2 Soil Reflectance Variation

As compared to vegetation, soil reflectance patterns are usually quite different and generally increase linearly with increasing wavelength: from visible to near-infrared to mid-infrared (Figure 13.1).

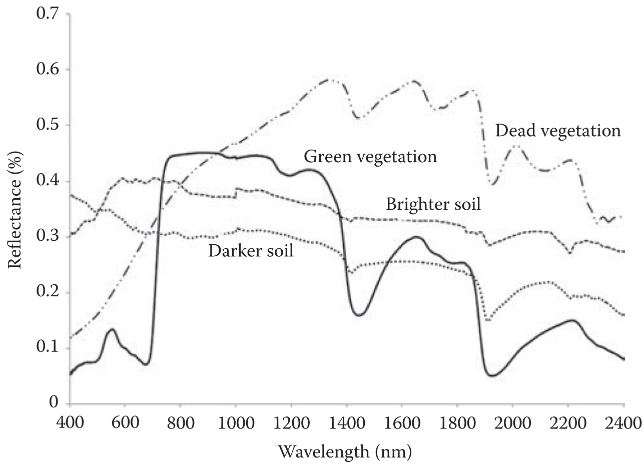

FIGURE 13.1 Idealized representation of spectral reflectance curves for green and dead vegetation, and light and dark soils.

Unlike vegetation, soil usually has high reflectance in the visible wavelengths and low reflectance in the near-infrared wavelengths. Figure 13.1 illustrates the contrast in reflectance patterns between dark (low reflecting) and light (high reflecting) soils. The difference between reflectance of soil and vegetation, in case of high reflecting soils, can be small in the near-infrared wavelengths (Eddy et al., 2017; Gökalp et al., 2017).

Soil reflectance properties vary considerably with soil type, texture, moisture content, organic matter content, color, and the presence of iron oxide (McCord and Pilliod, 2022). Low reflecting soils are usually dark, high in organic matter or moisture, containing iron oxides, and/or coarse textured. Dry soils show high reflectance values in visible, near-infrared, and mid-infrared regions of the spectrum. In contrast wet soils show low reflectance values for these regions (Bowers and Hanks, 1965).

13.2.2.3 Soil Background Impacts on Spectral Indices

In rangelands and semi-arid regions, background soil effects lead to soil-vegetation spectral mixing, a major concern in vegetation identification from spectral indices using remote sensing data. Soil, plant and shadow reflectance components mix interactively to produce composite reflectance (Richardson and Wiegand, 1990). The knowledge on soil reflectance variations for different soil types and conditions and their interaction with vegetation reflectance is essential to differentiate the soil and vegetation reflectance patterns. This helps in assessing the potential effectiveness of remote sensing techniques to map spatial distribution of plant species or communities and estimate biomass (De Cauwer et al., 2024; Sharifi and Felegari, 2023; McCord and Pilliod, 2022; Al-bukhari et al., 2018).

Generally, the values of ratio based indices, such as the normalized vegetation index, tend to increase with dark or low reflecting soil backgrounds (De Cauwer et al., 2024; Hadian et al., 2019; Al-bukhari et al., 2018; Elvidge and Lyon, 1985; Huete et al., 1985; Todd and Hoffer, 1998, 1997). However, a few studies have shown that the Tasseled Cap green vegetation index (GVI) decreases with low reflecting soil backgrounds (Huete et al., 1985; Huete and Jackson, 1987). The influence of soil type and moisture content on vegetation index was found less for Landsat TM derived GVI as compared to NDVI when estimating percentage green vegetation cover, based on a two component soil and vegetation model (Todd and Hoffer, 1997). Where soil effects on NDVI are a problem, alternative VIs such as the Soil Adjusted Vegetation Index (e.g., Huete, 1988) or the scaled difference vegetation index (Jiang et al., 2006) can be used.

13.2.2.4 Vegetation Reflectance Variation

The relationship between biomass and spectral indices can also be affected by vegetation condition, distribution and structure (Sharifi and Felegari, 2023; McCord and Pilliod, 2022; Todd et al., 1998). The loss in chlorophyll content due to drying of vegetation alters spectral reflectance characteristics in the visible and infrared regions. This phenomena is a very common occurrence in semi-arid rangelands such as the shortgrass steppe (Hadian et al., 2019). In case of drying vegetation, the reflectances in both the visible and in the mid-infrared regions of the spectrum increase significantly. The reflectance patterns of dead or dry plant material are more similar to soil than to healthy green vegetation (Matongera et al., 2021). Both dry vegetation and most soils have high reflectance in the visible and mid-infrared regions (Hoffer and Johannsen, 1969) and hence the spectral similarities introduce difficulties in remote sensing applications in rangelands.

For a given region, if dry or senescent biomass forms a significant portion of total vegetation present, the spectral distinction between vegetation and soil background is altered (Todd et al., 1998). For bright soil, spectral bands such as Red or indices such as Tasseled Cap brightness index, which are responsive to scene brightness, should help in vegetation discrimination in the presence of dry and/or senescent vegetation which appear less bright than the soil background.

Todd et al. (1998) found that the RED index, which responds to surface brightness, estimated vegetation cover on high reflecting soils more accurately than vegetation indices because dry vegetation was less bright than the soil background.

The grazing pattern and intensity also change the relative proportions of the standing dead and green biomass (Matongera et al., 2021; Sims and Singh, 1978a, 1978b) and cover characteristics (Milchunas et al., 1989) of plant communities within the rangelands. With increasing grazing intensity, the amount of standing dead plant material as well as litter decreases; however, in the absence of grazing, there will be considerable amount of both green and dry vegetation present. The presence of dead and/or drying plant material causes spectral confusion between this dead/drying plant material and the soil background and hence creates difficulties in estimating biomass using remote sensing techniques. Therefore, comparisons between grazed and ungrazed sites can provide insights into the impacts of senescence on biomass detection. In addition, grazing intensity varies considerably with topography (Milchunas et al., 1989), therefore information on the effectiveness of various remote sensing indices in detecting biomass under different grazing intensities could be useful in developing models across landscapes with heterogeneous grazing patterns. The field methods used to sample vegetation may also affect possible relationships between remote sensing indices and biomass.

13.2.2.5 Overview of Vegetation Indices

Vegetation indices combine reflectance measurements from different portions of the electromagnetic spectrum to provide information about vegetation cover on the ground (De Cauwer et al., 2024; Matongera et al., 2021; Zhou et al., 2020). Healthy green vegetation has distinctive reflectance in the visible and near-infrared regions of the spectrum. In the visible region, and in particular red wavelengths, plant pigments strongly absorb the energy for photosynthesis, whereas in the near-infrared region the energy is strongly reflected by the internal leaf structures. This strong contrast between red and near-infrared reflectance has formed the basis of many different vegetation indices. When applied to multispectral remote sensing images, these indices involve numeric combinations of the sensor bands that record land surface reflectance at various wavelengths.

One of the most promising applications of satellite data is the estimation of net primary productivity over time and space. The use of satellite derived vegetation indices has been useful for estimating net productivity (Al-bukhari et al., 2018). Vegetation indices are not a direct measure of biomass or primary productivity, but establish empirical relationships with a range of vegetation/climatological parameters (Weiser et al., 1986) such as: (a) Fraction of Absorbed Photosynthetically Active Radiation (FAPAR); (b) Leaf Area Index (LAI); and (c) Net Primary

Productivity (NPP). They are simple to understand and their implementation is fast as most of them use spectral band values in a mathematical formulation (e.g., ratio, difference, etc.). While maintaining sensitivity to vegetation temporal characteristics and seasonality, most of these indices reduce sensitivity to topographic effects, soil background, view/Sun angle and atmosphere to some extent. While many vegetation indices have been developed over the years, Table 13.1 lists a few of these and provides references for further investigation (McCord and Pilliod, 2022; Matongera et al., 2021).

TABLE 13.1
Vegetation Indices Commonly Used in Rangeland Studies

	Vegetation Index	Formula
1	SR—Simple Ratio	$\left[SR = \frac{\rho_{NIR}}{\rho_R}\right]$
2	EVI—Environmental Vegetation Index (Birth and McVey, 1968)	$\left[EVI = \frac{\rho_{IR}}{\rho_R}\right]$
3	NDVI—Normalized Difference Vegetation Index (Rouse et al., 1974)	$\left[NDVI = \frac{\rho_{IR} - \rho_R}{\rho_{IR} + \rho_R}\right]$
4	PVI—Perpendicular Vegetation Index (Richardson and Wiegand, 1977)	$\left[PVI = \sqrt{\left(\rho R_{soil} - \rho R_{veg}\right)^2 + \left(\rho IR_{soil} - \rho IR_{veg}\right)^2}\right]$
5	SAVI—Soil-Adjusted Vegetation Index (Huete, 1988)	$\left[SAVI = (1+L)\frac{(\rho_{IR} - \rho_R)}{(\rho_{IR} + \rho_R + L)}\right]$ L is a correction factor whose values range from 0 (high vegetation cover) to 1 (low vegetation).
6	TSAVI—Transformed SAVI (Baret et al., 1989)	$\left[TSAVI = \frac{a^*(\rho_R - a^*\rho_{IR} - b)}{(\rho_R + a^*\rho_{IR} - a^*b))}\right]$
7	Kauth-Thomas transformation [Tasseled cap, K-T] (Kauth and Thomas, 1976)	GVI= − 0′2728(TM1) − 0′2174(TM2) − 0′5508(TM3) + 0′722(TM4) + 0′0733(TM5) − 0′1648(TM7)
8	GNDVI—Green NDVI (Gitelson et al., 1996)	$\left[NDVI_g = \frac{(\rho_{NIR} - \rho_{green})}{(\rho_{NIR} + \rho_{green})}\right]$
9	GEMI—Normalized Difference Vegetation Index (Pinty and Verstraete, 1992)	$\left[GEMI = \eta(1 - 0.25\eta)\frac{(\rho_R - 0.125)}{(1 - \rho_R)}\right]$
10	EVI—Enhanced Vegetation Index (MODIS) Huete et al., 2002)	$\left[EVI = G\frac{\rho_{NIR} - \rho_{red}}{\rho_{NIR} + C_1 * \rho_{red} - C_2 * \rho_{blue} + L}\right]$ L = canopy background adjustment that addresses nonlinear, differential NIR and red radiant transfer through a canopy, and C1, C2 are the coefficients of the aerosol resistance term, which uses the blue band to correct for aerosol influences in the red band.
11	II—Infrared Index Hardisky et al., 1983)	$\left[II = \frac{(TM4 - TM5)}{(TM4 + TM5)}\right]$
12	MSI—Moisture Stress Index (Rock et al., 1985)	$\left[MSI = \frac{TM5}{TM4}\right]$

13.2.2.6 Vegetation Indices (VIs) as Proxies for Other Canopy Attributes

13.2.2.6.1 VIs and LAI

The leaf area index (LAI) is an estimate of the total leaf area per unit area (Glenn et al., 2008). LAI links vegetation indices to photosynthesis through the absorbed photosynthetically active radiation (Tucker and Sellers, 1986). When light travels through a series of leaves the transmission and therefore reflectance in near infrared of the electromagnetic radiation decreases (McCord and Pilliod, 2022). On the other hand, the uppermost leaf layers of a green vegetation canopy strongly absorb the red portion of the spectrum and therefore reduce their transmittance to successive leaf layers. The relation between LAI and vegetation indices varies among vegetation types (Peterson et al., 1987). In the case of saturated LAI, the ability to estimate biomass using vegetation indices is constrained, however, in rangelands, such as the shortgrass steppe, LAI saturation is improbable (Sharifi and Felegari, 2023; McCord and Pilliod, 2022).

LAI is derived mathematically and has no direct relationship to fPAR or processes that depend on fPAR (Glenn et al., 2008). LAI is related to light interception by a canopy (Ri) by:

$$\mathrm{Ri} = \mathrm{Rs}(1 - \exp - \mathrm{kLAI})$$

where k is a factor that accounts for leaf angles and other factors that affect absorption of Rs within a canopy (Monteith and Unsworth, 1990). Vertical leaved (erectophiles) plants typically absorb less light per unit leaf area than plants with relatively horizontal leaves (planophiles). Within a stand, the coefficient k also varies with respect to plant arrangements. Single stand plants receive light from all sides of their canopy as compared to dense stands of plants which receive light from the top of the canopy. The fraction of light absorbed by the canopy (fPAR) depends not only on Ri but also on the spectral properties of the leaves. The reflective surfaces present in some leaves reduce the heat gain while other surfaces absorb nearly all of the incident radiation between the visible bands (400 and 700 nm). Therefore, a correlation can easily be established between LAI and NDVI for single plant species grown under uniform conditions (Asrar et al., 1985). However, the same is not the case with mixed canopies, often the case in remote sensing data, in which a single pixel contains several landscape units.

13.2.2.6.2 VIs and Fractional Cover (fc)

Models use fractional vegetation cover to divide the landscape into areas of vegetation and bare soil (Zhou et al., 2020; Hadian et al., 2019; Glenn et al., 2007; Kustas and Norman, 1996; Anderson, 1997; Timmerman et al., 2007). Different methods are used in these models to estimate carbon and moisture fluxes from vegetation and bare soil and the fraction of the landscape that is vegetated (Glenn et al., 2008). Typically, a landscape unit is partitioned into bare soil and vegetation through the use of vegetation indices (VIs). For example, NDVI values derived from satellite images and ranging from −1 to +1 are rescaled between 0 and 1 to represent bare soil at values near 0 and 100% vegetation cover at values near to 1 to get fc for a given pixel or area of interest in the scene. Depending on the models used, the scaling is done linearly or in a nonlinear way to represent the vegetation type of interest. Some models require both LAI and fc often estimated by VIs (Anderson, 1997). In a few cases, ground-based information relating to vegetation species and canopy characteristics are also included to improve the estimates. Sometimes average leaf angles for a particular type of landscape are used to predict both fc and LAI from VIs (Anderson, 1997).

For partially vegetated scenes with LAI in the range of 1–3, Hadian et al. (2019) found VIs to be much more closely related to fc than to LAI in case of clumped vegetation, and the relationships between NDVI and fc to be nonlinear. They showed that, for partially vegetated scenes of uniform vegetation type, VIs were a good measure of fc. Other studies on a variety of landscape types have also reported strong linear (McCord and Pilliod, 2022) or nonlinear (Al-bukhari et al., 2018) relationships between VIs and fc. However, at 100% cover, different plant species may have different VIs due to differences in chlorophyll content and canopy structure, and thus create a potential practical problem in using VIs to estimate fc over mixed scenes. Amiri and Shariff (2010), in their study of vegetation cover assessment in semi-arid rangelands of Iran, used 26 different VIs to determine suitable indices for vegetation cover and production assessment, and found a significant relationship between NDVI derived from ASTER data with the vegetation cover. In another study, Ajorlo and Abdullah (2007) examined four vegetation indices (NDVI, SAVI, PVI and RVI) to assess rangeland degradation in semi-arid parts of the Qazvin province, Iran. The results showed that NDVI was a more powerful index for assessing the rangeland degradation as compared to other indices. McCord and Pilliod (2022) used NDVI and ratio vegetation index (RVI) in grassland study and found good correlation between fresh herbage yields and RVI and NDVI ($P < 0.01$) in four grassland types with correlation coefficient (r) >0.679. Fresh herbage yields correlated better with RVI than with NDVI for lowland meadow, hill desert steppe, and mountain meadow, but not for plains desert steppe. Matongera et al. (2021) monitored grassland health with remote sensing approaches and assessed the effectiveness of remote sensing in grassland monitoring. They found that it was challenging to use remotely sensed data in mixed grasslands because the large proportion of dead material complicated analysis for indices that were not developed for heterogeneous landscapes, especially in conservation areas. They investigated the relationship between remote sensing data and grassland biophysical measurement, including aboveground biomass and plant moisture content, in the native mixed prairie ecosystem with its high litter component. Their results indicated that the NDVI was not suitable for biomass estimation although a moderate relationship was found between NDVI and plant moisture content. Compared to NDVI, leaf area index (LAI) provided promising results on both biomass and plant moisture content estimation. John et al. (2008) evaluated the utility of MODIS-based productivity (GPP and EVI) and surface water content (NDSVI and LSWI) in predicting species richness in the semi-arid region of Inner Mongolia, China. They found that these metrics correlated well with plant species richness and could be used in biome- and life form-specific models (De Cauwer et al., 2024; Matongera et al., 2021; Zhou et al., 2020).

Although, different vegetation indices are used in assessing the rangeland degradation, there are still challenges facing the classification of vegetation species in degraded areas where the reflectance is strongly affected by the soil background as a result of relatively sparse vegetation and atmospheric conditions.

13.2.3 Case Study: Rangeland Phenology and Productivity in the Northern Mixed-Grass Prairie, North America

13.2.3.1 Introduction

Rangelands across the northern plains of North America are predominantly mixed-grass prairie communities and can be dominated by either C_3 (cool-season) or C_4 (warm-season) grass species. These mixed-grass communities exhibit different growth dynamics or phenological patterns that can be detected from satellite remote sensing (Sharifi and Felegari, 2023; McCord and Pilliod, 2022; Matongera et al., 2021; Zhou et al., 2020; Gökalp et al., 2017; Rigge et al., 2013; Tieszen et al., 1997). Although remote sensing cannot detect traditional phenological events such as budding and flowering in individual plants (Tieszen et al., 1997; White et al., 2009), it can detect important landscape-level phenological measures such as the onset of the growing season, the end of the growing season, rate of green-up, and peak vegetation vigor based on satellite image time series over a growing season (De Cauwer et al., 2024; Matongera et al., 2021; Gökalp et al., 2017; Kovalskyy and Henebry, 2012; Reed et al., 1994b; Tao et al., 2008; van Leeuwen et al., 2010). In this case study, conducted in the Bad River watershed in western South Dakota, USA, the spatial and temporal dynamics of rangelands as measured by remote sensing indicators or "phenological metrics" varied related to climate, management, and plant photosynthetic pathway (Rigge et al., 2013).

Land management, livestock grazing, invasive species, and prolonged droughts have the potential to change rangeland plant community structure and therefore contribute to altered phenological patterns (De Cauwer et al., 2024; Matongera et al., 2021; Gökalp et al., 2017; Foody and Dash, 2007; Tieszen et al., 1997)). These factors also have the potential to modify ecosystem goods and services (Matongera et al., 2021). One benefit in monitoring rangelands is to detect and mitigate any damaging trends caused by land management (Paruelo and Lauenroth, 1998).

Biomass production in rangelands by C_3 and C_4 plants displays significantly different phenological timing that is detectable utilizing satellite remote sensing. Information on rangeland phenological dynamics has been applied to assessing rangeland health monitoring, due to inferences that can be made about community composition and presence of invasive species (Arogoundade et al., 2023; McCord and Pilliod, 2022; Eddy et al., 2017; Boyte et al., 2014; Rigge et al., 2013; Tateishi and Ebata, 2004). For example, rangeland plant communities dominated by either C_3 or C_4 species can be identified through their unique and asynchronous phenological time series signals (Foody and Dash, 2007). Grasses with C_3 pathways are most active during the cooler spring and fall seasons, while many C_4 grasses are adapted to the hot and dry summer months (Arogoundade et al., 2023; Zhou et al., 2020; Gökalp et al., 2017; Foody and Dash, 2007; Tieszen et al., 1997; Wang et al., 2010). State-and transition models indicate that cool-season (C_3) grasses tend to dominate historic plant climax communities in many ecological sites of the northern mixed prairie, while shortgrass (C_4) species generally increase under disturbance such as heavy, continuous, season-long grazing (U.S. Department of Agriculture, 2008). Furthermore, phenological differences are useful for identifying vegetation types. For example, in western South Dakota, riparian vegetation tends to be dominated by C_4 species while upland vegetation communities consist primarily of C_3 plants. In late summer, this difference allows for the detection of a clear riparian vegetation signal (Kamp et al., 2013).

In the northern mixed-grass prairie, the majority of C_3 production occurs in spring and fall, and most C_4 production occurs in summer, although there is both spatial and temporal overlap in production (Ode et al., 1980). For example, both C_3 and C_4 plants actively produce biomass in mid- to late June with no clear separation between the timing of their production (Ode et al. 1980). In midsummer (1 July to 31 August) production is typically dominated by C_4 grasses in the study area and was therefore used to define the warm-season period (Ode et al., 1980; Wang et al., 2010).

13.2.3.2 Methods

13.2.3.2.1 Study Site

The Bad River watershed of western South Dakota (~lat 45°N, long 101°W) is dominated by the Clayey ecological site description in the Major Land Resource Area classification (U.S. Department of Agriculture, 2008). The topography of this region is generally typified by long, smooth slopes, with steeper slopes along well-defined waterways. Bedrock throughout the watershed is Pierre Shale, resulting in soils with a high clay content and low permeability. The climate is semiarid, receiving an average of 398 mm precipitation annually over the 2000–2008 period of which 80% occurred during the growing season of April to September. Annual precipitation is highly variable, with drought and insufficient moisture common (Matongera et al., 2021). The daily mean temperature ranges from 32°C in July to 14°C in January, with a yearly mean of 8°C (Smart et al., 2007). Analysis was constrained to pixels classified in the National Land Cover Database 2006 as herbaceous cover (Fry et al., 2011).

The study area vegetation is mixed-grass rangeland dominated by C_3 grasses including western wheatgrass (*Pascopyrum smithii Rybd.*) and green needlegrass (*Stipa viridula Trin. & Rupr.*; Smart et al. 2007). Shortgrasses (C_4) include buffalograss (*Bouteloua dactyloides Nutt.*) and blue grama (*Bouteloua gracilis H.B.K.*). Midgrasses are typically C_4 species such as little bluestem (*Schizachyrium scoparium [Michx.] Nash*) and sideoats grama (*Bouteloua curtipendula [Michx.] Torr.*). Little forb and succulent cover exists (Sims and Singh et al., 1978a, 1978b).

13.2.3.2.2 Input Data

Moderate Resolution Imaging Spectroradiometer (MODIS) satellite time series data provided an ideal balance between spatial resolution and temporal repeat, and are therefore well-suited for

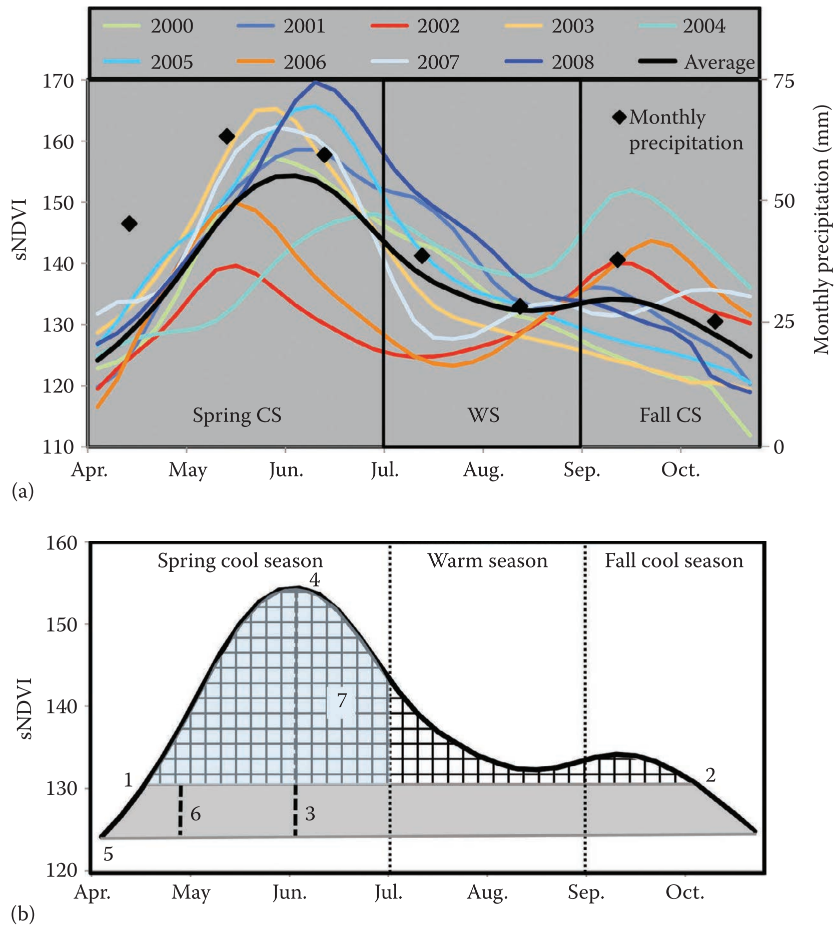

FIGURE 13.2 (a) Phenological profiles for Bad River watershed, South Dakota, USA, from 2000–2008 where years are colored according to growing-season precipitation (shown on the secondary vertical axis). Colors range from red (for dryer growing seasons to blue (for relatively wetter growing seasons). The left third of the graph shows the spring cool season (CS), the middle shows the warm season (WS), and the right thirds shows the fall CS. (b) Illustration of idealized phenological profile and main phenological indicators used in the study. The entire gridded area corresponds to the growing season time integrated NDVI (TIN) and the blue gridded area corresponds to the spring CS integrated NDVI. (Based on Figure 13.1 and 13.3 in Rigge et al. 2013.)

phenology studies across relatively large regions. This study is based on 9 years (2000–2008) of eMODIS weekly composite Terra MODIS imagery at 250-m resolution (van Leeuwen et al., 2010). NDVI values were calculated and rescaled to a range of 0 to 200 to simplify calculations by eliminating negative values. Hereafter, rescaled NDVI will be referred to as sNDVI (scaled NDVI).

Annual variability in rangeland phenology and productivity as shown in MODIS sNtDVI time series plots (Figure 13.2a) is fairly common (Tieszen et al., 1997), where complex herbaceous communities respond to highly variable inter- and intra-annual precipitation (Lauenroth and Sala, 1992; Smart et al., 2007).

13.2.3.2.3 Phenological Analysis

Several measures calculated on a pixel by pixel basis were utilized in this study to describe the phenology of rangeland communities (Table 13.2). The start of the season was calculated for each pixel as the first point in time each year when sNDVI reached 20% of the total growing-season sNDVI

TABLE 13.2
Phenological Measures Calculated from Input MODIS Time Series Profiles

	Remote Sensing Phenological Metric	Description/Notes
1	SOS: Start of season	Time of first occurrence of sNDVI >= 20% of growing season amplitude (within a calendar year)
2	EOS: End of season	Time of last occurrence of sNDVI >= 20% growing season amplitude (within a calendar year)
3	AMP: Amplitude	Difference between the growing season minimum sNDVI and the growing season peak NDVI
4	$sNDVI_{peak}$	Value of peak growing season NDVI
5	$sNDVI_{min}$	Value of minimum growing season NDVI
6	Baseline	Values of <=20% of growing season amplitude (within a calendar year) that are eliminated
7	TIN_{GS}	Summation of sNDVI from Apr 1– Oct 1 where sNDVI is >= 20% of growing season amplitude

amplitude of that year (van Leeuwen et al., 2010). The total growing season amplitude was calculated as the difference between the peak sNDVI value (during the April 1 to October 31 growing season) and the minimum sNDVI value during this period. Similarly, the end of the season was the time at which the sNDVI value dropped below 20% of the total growing-season sNDVI amplitude. This approach better approximated the total seasonal biomass production than simply averaging NDVI across the entire growing season. TIN served as a proxy for growing-season total biomass production. Because TIN is influenced by the magnitude and duration of mNDVI values, the saturation effects that occur at larger leaf area index values (Huete et al., 2002) are minimized. The TIN of the spring cool season (start of season to 30 June) was also used in this study (Figure 13.2b).

Since phenological profiles can reveal community species composition and vegetation communities (McCord and Pilliod, 2022; Matongera et al., 2021; Zhou et al., 2020; Gökalp et al., 2017; Reed et al., 1996; Tateishi and Ebata, 2004) and phenology can strongly influence biomass production (Smart et al., 2007), the combined geospatial data on cool-season grasses and TIN was combined to create a watershed-level vegetation map (Figure 13.3). The per-pixel 2000–2008 average TIN was grouped into three classes: (1) within one standard deviation of the study area mean, (2) below one standard deviation of the mean, and (3) above one standard deviation of the mean. A similar approach was used to group the 2000–2008 average cool-season percentages into three classes. The TIN and cool season percentage classes were integrated to form nine vegetation classes, representing the average of the 2000–2008 conditions.

Table 13.3 provides vegetation class numbers, generally indicative of the plant community state, with higher numbers closely approaching the western wheatgrass/green needlegrass community (historic climax plant community of the Clayey ecological site) and lower numbers generally indicative of the blue grama/buffalograss plant community (Smart et al., 2007; U.S. Department of Agriculture, 2008). Classes marked with "+" indicated TIN or CS% over one standard deviation higher than the study area average, "N" indicated TIN or CS% within one standard deviation of the average, and "–" indicated TIN or CS% below one standard deviation of the average.

Spatial patterns of vegetation classes are useful for describing topographic, edaphic, and land management influences on plant communities (Figure 13.3). For example, areas with both low cool-season percentage and low TIN (class 1) were likely dominated by buffalograss and blue grama, both low-producing C_4 species. This community was reported to result from strong grazing pressure (Smart et al., 2007; U.S. Department of Agriculture, 2008) in the Clayey ecological site, but might stem from lower than normal warm-season moisture in Pierre Shale/badland outcrops.

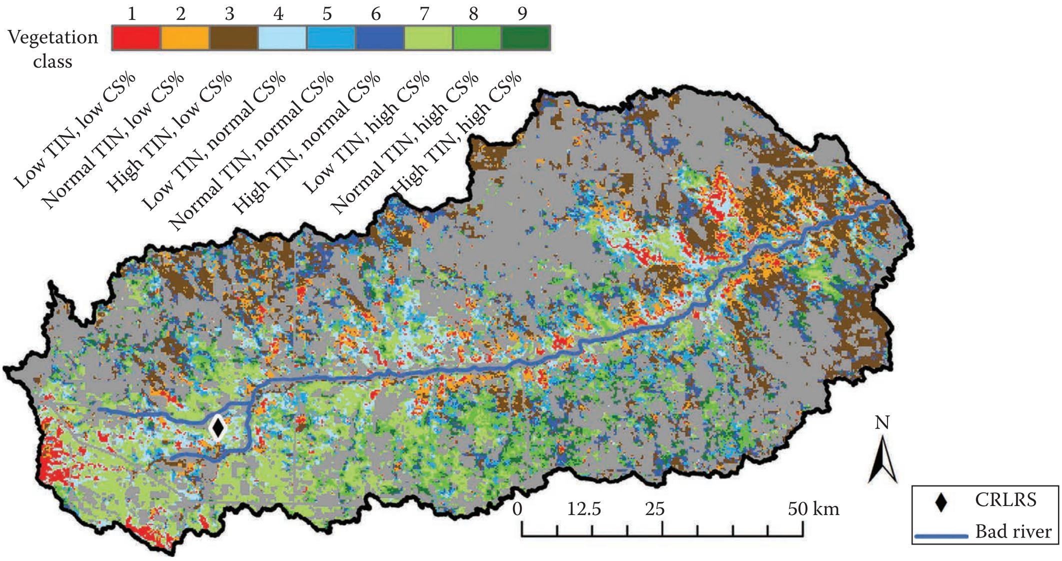

FIGURE 13.3 Nine vegetation classes derived from growing season time-integrated NDVI (TIN) and average cool season percentage (CS%) in the Bad River watershed, South Dakota, USA, shaded gray in the inset map. Light gray areas denote non-rangeland vegetation types that were excluded from this analysis. The Cottonwood Range and Livestock Research Station (CRLRS) is located in the southwest. (Based on Figure 13.6 in Rigge et al. 2013.)

TABLE 13.3
Bad River Watershed Rangeland Vegetation Classes

Vegetation Class	TIN	CS%	Area (%)	Mean TIN	Mean CS%
1	–	–	4.7	268.2	74.5
2	N	–	8.8	329.0	74.7
3	+	–	19.1	389.4	73.7
4	–	N	10.2	279.2	80.3
5	N	N	12.8	327.3	80.0
6	+	N	10.3	376.7	79.8
7	–	+	18.1	270.1	85.7
8	N	+	11.5	325.0	85.0
9	+	+	4.5	370.7	84.7

13.2.3.2.4 Validation Methods

Validation is a critical, yet challenging, component of phenological studies based on remote sensing. Methods were performed based on field plot data and carbon flux tower data. The field plot data were collected for two distinct plant communities (mixed-grass and midgrass-dominated) in fields that were retained under long-term grazing management practices (Dunn et al., 2010). Field-measured vegetation data estimated species composition by weight in late June (peak cool-season biomass) and early August (peak warm-season biomass). A nonrandom sampling scheme consisted of 14 plots per field represented local variation in soil type, slope, and aspect. The remotely sensed yearly average TIN and cool-season percentage for each field were regressed against the corresponding field-measured average biomass production and cool-season percentage data. The comparison of remotely sensed growing season TIN and phenology to field vegetation data collected at the Cottonwood Range and Livestock Research Station (CRLRS) in the Bad River watershed suggested that the remote observations were successful in describing actual conditions (Rigge et al., 2013). Field-measured cool-season biomass production and cool-season TIN were greater on the midgrass-dominated pastures than the mixed-grass pastures, following the expected pattern (Sims and Singh, 1978a, 1978b; Smart et al., 2007). Overall, the relationship between field-measured annual biomass production and TIN by pasture was strong ($R^2 = 0.69$, $P < 0.01$, $n = 24$).

A carbon flux tower located on a mixed-grass plant community pasture at the CRLRS was used for validation at that site. Thirty-minute flux tower quality-controlled ecosystem data for 2007 and 2008 were modeled using nonlinear light response curves driven by photosynthetically active radiation (PAR), soil temperature, and vapor pressure deficit to partition carbon fluxes associated with PAR (i.e., gross primary productivity) from those associated with total ecosystem respiration (Gilmanov et al., 2010). Gross photosynthesis (PG) data were calculated as the sum of day CO_2 flux and respiration minus the rate of change in atmospheric CO_2 storage below the tower. Phenological metrics from the flux tower data were generated using the same methods employed for MODIS data, making the results generated from both datasets more directly comparable. Flux tower PG data were strongly related to sNDVI values ($R^2 = 0.67$, $P < 0.01$) at the overlapping pixel. Similarly, the accumulation of TIN and PG throughout both growing seasons were related ($R^2 > 0.90$ in both years).

13.2.3.2.5 Conclusions

Information on the timing and magnitude of biomass production can be a useful tool for assessment of rangeland health (De Cauwer et al., 2024; McCord and Pilliod, 2022; Eddy et al., 2017; Gökalp et al., 2017). Species diversity and variable weather across the northern mixed-grass prairie make modeling native rangelands problematic. However, the MODIS-based phenological indicators were successful in capturing important characteristics of plant community phenology and productivity. The results of this study clarify the spatial and temporal dynamics (inter and intra-annual) of phenology and biomass production in response to precipitation in this region.

This approach could be useful to land managers in adjusting the stocking rate and season of grazing to 1) maximize rangeland productivity and profitability (Dunn et al., 2010) and 2) achieve conservation objectives, through improving understanding of management impacts to rangeland phenology and production. Maps such as these might also be useful to identify areas where land degradation may be occurring or is likely to occur if current management practices are continued. Further, if the phenological metrics of a patch (e.g., pasture) of land is dramatically different than the surrounding landscape or contrasts with the general landscape gradient, it can be presumed that land management practices on that parcel, not climate, soils, or topography, are primarily responsible. These specific parcels can then be the focus of best management practices, field examination, and data collection.

13.2.4 Rangeland Fuel Load Assessment

Knowledge of the spatial distribution of fuels is critical when characterizing susceptibility of landscapes to wildfire and for estimating expected fire behavior (Arroyo et al., 2008). In the simplest terms the susceptibility of a rangeland landscape to wildfire is a function of expected fire weather, topography, probability of ignition, juxtaposition of the landscape, and fuel bed characteristics. Many rangelands are dominated by small diameter fuel components, which respond very quickly to environmental conditions such as heating, relative humidity and precipitation (Cheney and Sullivan, 1997). In addition, the high surface area to volume ratio, high packing ratios and small sizes make rangeland fuels characteristically prone to ignition and very high rates of spread. For example, under extreme fire weather conditions, grassland fires can exceed 28 km hr^{-1} making rangeland fires unpredictable. The temporal and spatial variability of fuels add to this uncertainty.

Productivity of rangeland varies much more on an inter-annual, proportional basis than that of forests (Zhou et al., 2020; Hadian et al., 2019; Briggs and Knapp, 1995; Le Houerou and Hoste, 1977; Teague et al., 2008; Zhang et al., 2010). As a result, the fuel bed properties associated fire behavior characteristics and potential risk can change commensurately. In addition, rangelands are the most extensive kind of land cover, occupying nearly 33% of ice-free land globally (Ellis and Ramankutty, 2008). In the coterminous U.S.A. alone there is an estimated 268 million ha that often occur across large, open, remote expanses prone to high and gusty winds. The high variability and large areas inherent in rangeland systems suggest that regular monitoring is needed for properly addressing the fire danger situation.

Regular monitoring of fuels is needed for both strategic (Kaloudis et al., 2005) and tactical purposes (Reeves et al., 2009). Strategic assessment involves planning and resource allocation modeling. In contrast, tactical uses of wildland fuel data involve specific fire behavior projections and assessment for determining things such as arrival time, risks to resources, and suppression tactics.

A complete evaluation of wildland fuels requires accounting for all fuel bed characteristics including such components as fuel bed depth, vegetation structure and species composition, litter, fuel moisture, fuel quantity of various size classes (Sharifi and Felegari, 2023; Gökalp et al., 2017; Anderson, 1982; Scott and Burgan, 2005; Ottmar et al., 2007; Sandberg et al., 2001). The diameters of the fuel particles can be classified based on their time lag. Larger diameter fuels have longer time-lags because they respond more slowly to changes in environmental conditions. The time lag categories most often used for fire behavior and danger assessment include 1hr, 10hr, 100hr, and 1000hr corresponding to diameter ranges of 0–0.635 cm, 0.635–2.54 cm, 2.54–7.62 cm, and 7.62–20.32 cm, respectively. These fuel bed components are most strongly influenced by the kinds and amounts of vegetation. The pressing need for timely information, dynamic nature of rangeland vegetation and fuels, and paucity of plot data suggest that remote sensing can play a significant role in the evaluation of rangeland fuels.

Remote sensing has long been used to evaluate vegetation conditions at spatial scales and spatial resolutions varying from plot level evaluation (Blumenthal et al., 2007) to global assessment at 8 km^2. Mere vegetation classification, however, is generally not sufficient for quantifying fuel conditions. As a result, many approaches have been derived for using remote sensing to evaluate wildland fuels (Riaño et al., 2002; Riaño et al., 2003; Rollins, 2009; Reeves et al., 2009; Arroyo et al., 2008). Most methods for quantifying fuels across the landscape involve a combination of remote sensing techniques (e.g., spectral analysis for species composition, structure and production; LiDAR for vegetation structure) and modeling or expert systems (Keane and Reeves, 2011). Use of satellite remote sensing for capturing temporal dynamics of fuel bed properties is usually most successful for characterizing the herbaceous biomass response. These biomass estimates can subsequently be converted to fuel loadings (1-hour time lag category). With woody vegetation the situation is more complicated and quantifying fuels can be accomplished by first determining vegetation structure (height and cover) (e.g., McCord and Pilliod, 2022; Eddy et al., 2017; Gökalp et al., 2017; Chopping et al., 2006; Vierling et al., 2012). Yet another method is to first determine stand structure (stand cover and height) and species composition and then using allometric relationships to estimate individual fuel components (Means et al., 1996). Once the appropriate fuel bed attributes have been estimated it is often necessary to invoke expert systems to crosswalk stand level fuel attributes into a fuel model depending on the intended use of the data. This is a critical step because describing all fuel characteristics in an area is exceedingly difficult given the extreme spatial and temporal variation of fuel bed components (Arroyo et al., 2008; Keane, 2013). As a result, description of fuel properties relevant to fire behavior or effects is normally based on classification schemes, which summarize large groups of fuel characteristics. These classes are expressed as "an identifiable association of fuel elements of distinctive species, form, size arrangement, and continuity that will exhibit characteristic fire behavior under defined burning conditions" (Merrill and Alexander, 1987).

Commonly used fuel classification systems include Surface Fire Behavior Fuel Models (Sharifi and Felegari, 2023; Zhou et al., 2020; Eddy et al., 2017; Gökalp et al., 2017; Anderson, 1982; Scott and Burgan, 2005) and Fuel Loading Models (Lutes et al., 2009). The reason for this is that most fire behavior or fire affects processors such as Farsite (Lutes et al., 2009), FlamMap (Lutes et al., 2009), Behave (Andrews and Bevins, 2003) and Promethius (Lutes et al., 2009) require stylized fuel models or standardized classifications of fuel components. In the United States, many decision support systems and tactical evaluations utilize FarSite and Flammap which generally require stylized fuel models from either Anderson (1982) or Scott and Burgan (2005). Prometheus, on the other hand, is widely used in Canada and components of it have been used in the U.S.A., Spain, Portugal, Sweden, Argentina, Mexico, Fiji, Indonesia and Malaysia (www.nrcan.gc.ca/forests/fires/14470) to estimate fire spread and uses fuel models from the Canadian Forest Fire Danger Rating System (CFFDRS) (Wotton, 2009).

13.2.5 Case Study: Using Remote Sensing to Aid Rangeland Fuel Analysis

This case study focuses on the rangelands of the coterminous U.S.A. where, in places, annual aboveground rangeland production can vary by more than 150% in extreme years. Prominent fire decision support systems in the U.S.A. presently require the Surface Fire Behavior Fuel Models (FBFM) (Anderson, 1982; Scott and Burgan, 2005). As a result, here we present a case study using remote sensing to inter-annually quantify 1-hour time lag fuels for informing mapping processes designed to predict surface FBFMs for all coterminous U.S.A (Figure 13.4).

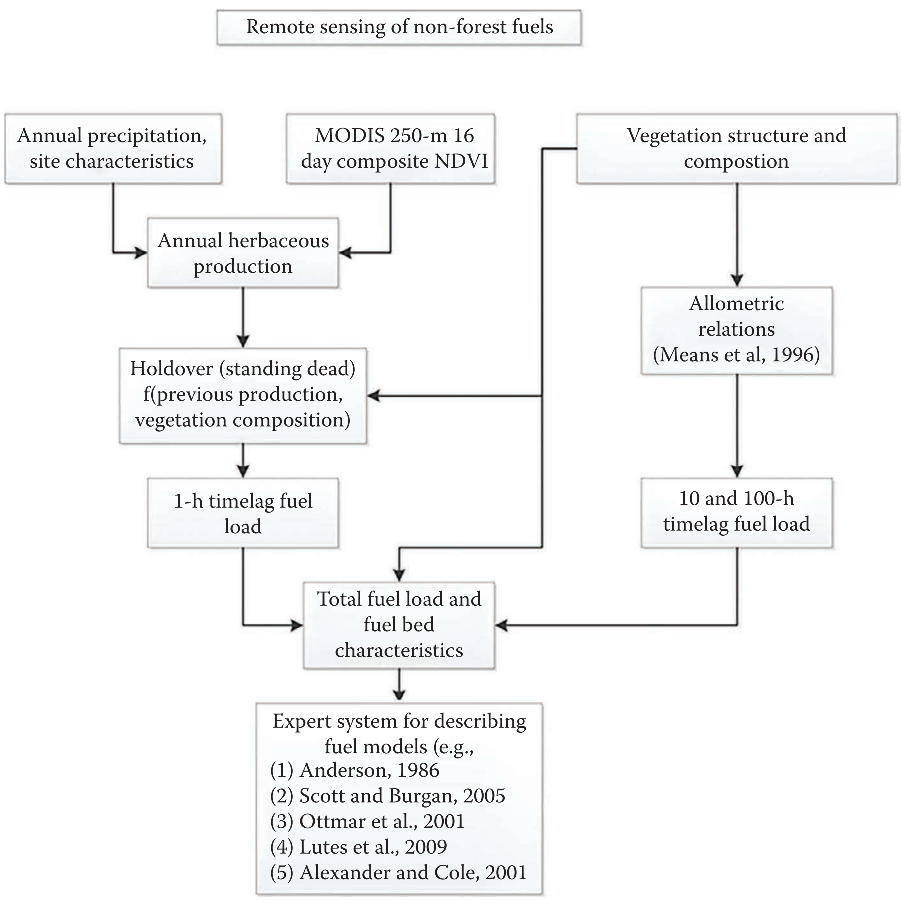

FIGURE 13.4 Fuel flowchart.

The fine fuels of rangelands are driven primarily by grasses and forbs. Capturing these inter-annual fuel dynamics requires a relatively high repeat cycle and reasonably good spatial resolution, both of which are inherent in the 250 m^2 16-day composite MODIS Normalized Difference Vegetation Index (NDVI) from the Moderate Resolution Imaging Spectroradiometer (MODIS). From the 23 periods in each year from 2000 to 2012 the annual maximum NDVI was chosen to correlate with ground observations of aboveground productivity. Since spatially explicit, consistent, comprehensive ground data do not exist, production estimates from the Soil Survey Geographic database (SSURGO; www.nrcs.usda.gov/wps/portal/nrcs/detail/soils/survey/?cid=nrcs142p2_053627) were used as a surrogate for plot based ground data. For each soil type in the SSURGO database, the expected annual production based on normal (mean), drought (low) and above average (high) growing conditions is available. Thus, for each soil site, represented as a soil map unit, there are three data points representing expected annual production. Annual maximum NDVI, gridded annual precipitation from the PRSIM project, and the Biophysical Settings (BPS) data layer were used to develop a model for predicting annual production and, ultimately, 1-hr time lag fuels through time. For precipitation, the maximum, minimum, and mean annual total precipitation from 2000 to 2012 was selected to correspond with the high, mean and low productivity for each BPS type. Likewise, the maximum, minimum, and mean annual maximum from 2000 to 2012 was also selected to correspond with the rangeland productivity from the SSURGO soil types. For each BPS type, the range of annual production, range of annual precipitation, and annual maximum NDVI was spatially averaged. For example, average mean annual maximum NDVI, annual summation of precipitation and rangeland productivity were averaged for all shortgrass prairie BPS. The annual productivity model resulted in a simple combination of these predictors and their interactions as

$$\begin{gathered}\text{AnnualProduction} = (\text{Y int}) + (\text{Precip}_{\text{annsum}} * 0.141) + \\ (\text{NDVI}_{\text{annmax}} * 3.0056) + \text{BPS} + (\text{Precip}_{\text{annsum}} * \text{BPS} * -0.1138) + \\ (\text{NDVI}_{\text{annmax}} * \text{BPS} * -1.2961)\end{gathered}$$

where AnnualProduction is the estimated annual production of rangeland biomass, $\text{Precip}_{\text{annsum}}$ is the annual sum of precipitation for a BPS unit and the $\text{NDVI}_{\text{annmax}}$ is the average annual maximum NDVI. This model resulted in an R^2 value of 0.94, a bias estimate of 1.43, and a mean absolute error (MAE) of 164 kg $ha^{-1.}$

This relationship between NDVI, precipitation and site specific (BPS) coefficients enabled estimates of rangeland annual production from 2000 to 2012.

After quantifying annual production, estimates of standing dead residue ("holdover"), which add considerably to the total fuel load on a rangeland site, were estimated. This was accomplished using a simple decay function represented in Figure 13.4. As a result, for a given year, the total 1-hr fuel load can be described as function of the following form f(annual production + holdover $_{t-1}$ + holdover $_{t-2}$, holdover $_{t-3}$). These fine fuel loads were combined with estimates of 10- and 100-hour time lag fuels of the woody components (e.g., shrubs) of each stand. This was accomplished by combining the cover, height, and species composition from the LANDFIRE project, and quantifying woody biomass and 10- and 100-hour time lag fuels using allometric equations from Means et al. (1996) (Figure 13.4). Once the full suite of fuel characteristics were known, surface FBFMs from the Scott and Burgan (2005) suite were estimated for average fuel conditions and then modulated through time based on the inter-annual change in 1-hour time lag fuel loads (Figure 13.5). Figure 13.5 demonstrates how remote sensing is used with climate and site characteristics to estimate 1-hr time lag fuels every year. In addition in Figure 13.5, the amount of deviation (as a percent of the 12-year average) in 2000, 2005 and 2011 are shown for the southwestern Ecological Province (Bailey and Hogg, 1986). Finally, the resulting change in the distribution of surface FBFMs can be seen in panel C for all three years presented. Note the large increase in 1-hr time lag fuels in 2005 in the Southwestern Ecoregion. This corresponds to a large increase in rainfall and a strong NDVI signal resulting in very high biomass and subsequent changes to surface FBFMs suggesting much

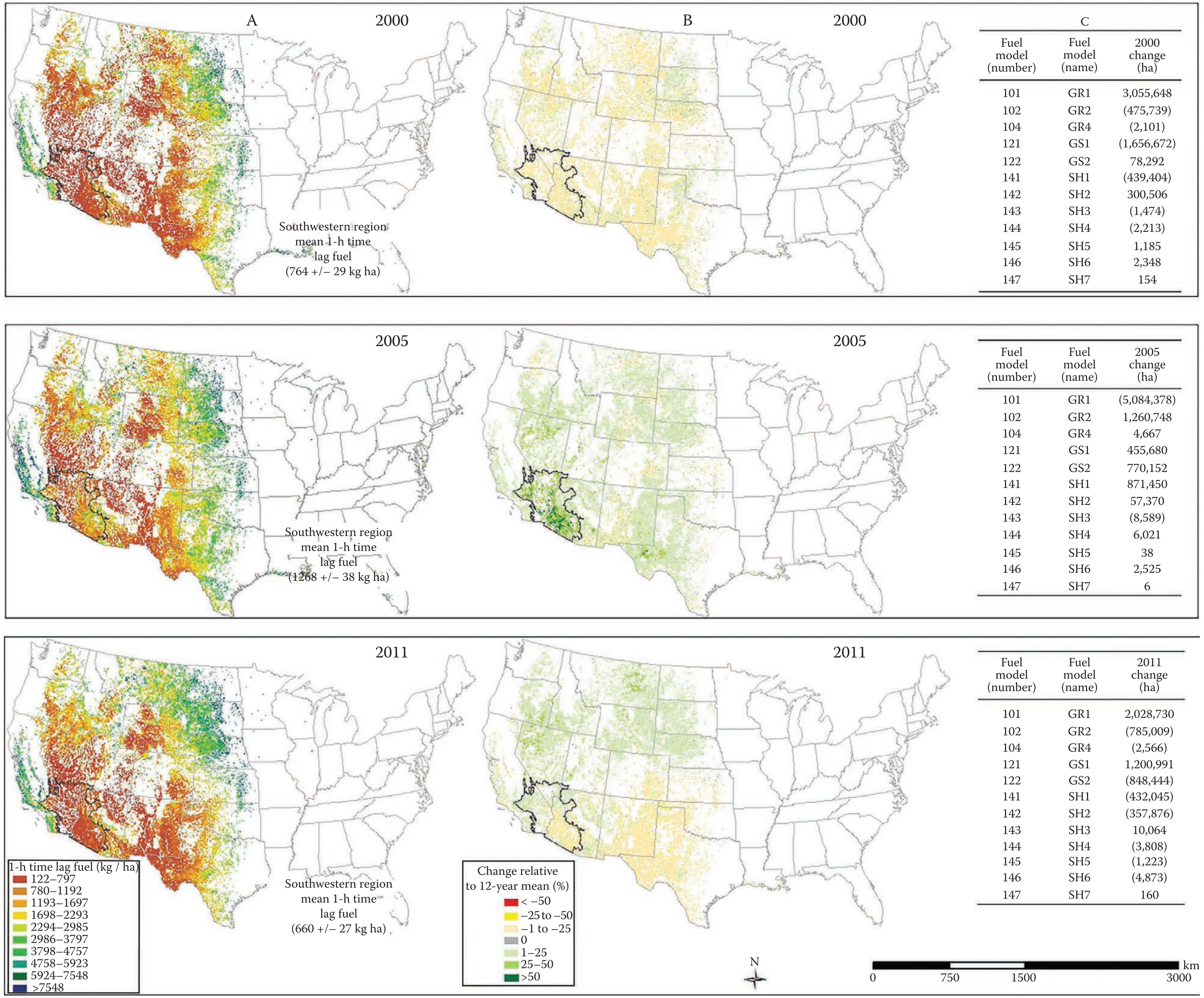

Fuel model (number)	Fuel model (name)	2000 change (ha)
101	GR1	3,055,648
102	GR2	(475,739)
104	GR4	(2,101)
121	GS1	(1,656,672)
122	GS2	78,292
141	SH1	(439,404)
142	SH2	300,506
143	SH3	(1,474)
144	SH4	(2,213)
145	SH5	1,185
146	SH6	2,348
147	SH7	154

Fuel model (number)	Fuel model (name)	2005 change (ha)
101	GR1	(5,084,378)
102	GR2	1,260,748
104	GR4	4,667
121	GS1	455,680
122	GS2	770,152
141	SH1	871,450
142	SH2	57,370
143	SH3	(8,589)
144	SH4	6,021
145	SH5	38
146	SH6	2,525
147	SH7	6

Fuel model (number)	Fuel model (name)	2011 change (ha)
101	GR1	2,028,730
102	GR2	(785,009)
104	GR4	(2,566)
121	GS1	1,200,991
122	GS2	(848,444)
141	SH1	(432,045)
142	SH2	(357,876)
143	SH3	10,064
144	SH4	(3,808)
145	SH5	(1,223)
146	SH6	(4,873)
147	SH7	160

FIGURE 13.5 Fuel modulation.

greater flame lengths and spread rates (the GR1 is reduced and GR2 is substantially increased). As an example, under the identical environmental parameters with an open wind speed of 24 km hr^{-1}, a GR2 surface FBFM results in a spread rate of 9 times greater than a GR1.

This brief case study demonstrates a method for using high temporal resolution satellite remote sensing for quantifying fuels in rangeland landscapes. The important characteristics of a sensor for characterizing fine fuels across large landscapes in a timely manner suggest satellites with relatively high repeat frequencies and appropriate spectral channels for modeling changes in aboveground biomass. Application of the methods outlined here are limited to regions where sufficient numbers of spatially explicit measures (or estimates as in the present work) of biomass or fuels are available.

13.3 RANGELAND VEGETATION CHARACTERIZATION

13.3.1 Rangeland Biodiversity and Gap Analysis

Rangeland biological diversity (biodiversity) refers to the variety and variability among living organisms and the environments in which they occur and is recognized at species, ecosystem and landscape level (Al-bukhari et al., 2018; Eddy et al., 2017, Gökalp et al., 2017). The goal of biodiversity conservation is to reverse the processes of biotic impoverishment at each of these levels of organization. Gap analysis provides a quick overview of the distribution and conservation status of several components of biodiversity (Scott et al., 1993). Gap Analysis is the process by which the distribution of species and vegetation types are compared with the distribution of different land management and land ownership classifications. It seeks to identify gaps (vegetation types and species that are not represented in the network of biodiversity management) that may be filled through establishment of changes in land management practices (Scott et al., 1993). The goal here is to ensure that all ecosystems and areas rich in species diversity are represented adequately in biodiversity management areas. Gap Analysis uses vegetation types and vertebrates as indicators of biodiversity. Maps of existing vegetation are prepared from satellite imagery and other sources and entered into a geographic information system (GIS). Because the mapping is carried on a regional scale, the smallest area identified on vegetation maps is generally 100 ha. Vegetation maps are verified through field checks and aerial photographs. Predicted species distributions are based on existing range maps and other distributional data, combined with information on the habitat of each species. Distribution maps for individual species are overlaid in the GIS to produce maps of species richness. An additional GIS layer of land ownership and management status allows identification of gaps in the representation of vegetation types and centers of species richness in biodiversity management areas through a comparison of the vegetation and species richness maps with ownership and management status maps. Gap Analysis is a powerful and efficient first step towards setting land management priorities. It provides focus, direction, and accountability for conservation efforts. Areas identified as important through Gap Analysis can then be examined more closely for their biological qualities and management needs (Scott et al., 1993).

13.3.2 Case Study: Vegetation Continuous Fields with Regression Trees

13.3.2.1 Introduction

The sagebrush ecosystem is an important and distinguishing natural system of the U.S. Intermountain West. However, an estimated 40% of its pre-European settlement distribution has been reduced due to conversion to agriculture, urban/suburban growth, energy development, invasion by exotic plants, and encroachment by woodlands among others (Wisdom et al., 2005). The sagebrush ecosystem is an example of many other globally distributed natural systems that have been impacted by similar disturbances. Monitoring land cover change, across vast landscapes, in an efficient manner is touted by many to be a significant strength of digital remote sensing. The holistic view of remotely sensed data allows us to evaluate landscapes in their entirety. Traditional, field-based, monitoring systems are limited to specific locations whose characteristics are then extrapolated across the entire landscape. The number of field-based samples required to characterize landscapes with statistical certainty is often cost prohibitive and in some cases impossible to acquire due to access restrictions. The temporally systematic, landscape level monitoring that remote sensing offers coupled with modern statistical modeling approaches can provide land managers with much of the information necessary for effective planning and management.

Traditional image interpretation techniques that convert digital remote sensing data into discrete land cover maps have been used to monitor landscapes (Jin et al., 2013; Vogelmann et al., 2012). These techniques rely on the ability to accurately classify and map vegetation types at multiple time intervals to determine how change has occurred at the vegetation community level. A limitation of this technique is the assumption that adjacent vegetation community types have discrete boundaries (sharp ecotones) and that variation within the community is typically ignored. The reality is that sharp ecotones between community types, while they exist, are typically not the norm. Further, the spatial variation of vegetation cover within a mapped community type is often an important diagnostic of community condition. In traditional classification of imagery, this information is lost.

This case study describes the use of digital remote sensing data coupled with field-based measurements and advanced statistical modeling techniques to map vegetation continuous fields (VCF) in the sagebrush ecosystem. Vegetation Continuous Fields (VCF) is a relatively new concept that attempts to model percent canopy cover of specific vegetation types using remotely sensed imagery as its primary input. This technique has been used to estimate canopy cover of woody and herbaceous vegetation, as well as bare ground, on a global basis (De Cauwer et al., 2024; McCord and Pilliod, 2022; Defries et al., 2000; Sexton et al., 2013). A series of VCFs consist of several continuous response surfaces (one for each cover type) in which every pixel value corresponds to a percent canopy cover estimate predicted through a regression model. The VCF offers an advantage over traditional discrete classifications because areas of heterogeneity within vegetation community types are better represented (Hansen et al., 2002).

The objectives of the case study were to: (a) Test the effectiveness of a regression tree algorithm (Random Forest) to model estimates of percent cover, and (b) Develop a series of Vegetation Continuous Fields models for shrubs, woodland, herbaceous vegetation and bare ground for a semiarid shrub-steppe landscape.

13.3.2.2 Methods

13.3.2.2.1 Study Area

Our research was conducted in the northwest corner of Box Elder County, Utah (114°2′31. 2″ – 112°43′40. 8″ West longitude and 41°6′ 27. 36″–41°59′ 59. 64″ North latitude) depicted in Figures 13.6 and 13.7. The area covers 1,742,860 ha, with approximately 60% of the county occupied by the Great Salt Lake and barren playa bottoms. Of the remaining area, salt desert scrub occupies about one fifth of the area while big sagebrush shrubland and steppe covers nearly the same amount (19%). Pinyon-juniper ecosystems are an important part of the landscape making up 12% of the area. The remainder consists of greasewood flats, montane sagebrush steppe, xeric mixed sagebrush shrubland and invasive annual grasslands (Program, 2004). The elevation ranges from 1,278 m in the lowlands close to the Great Salt Lake to 3,027 m at the peak of the Raft River range. The mean elevation is 1,520 m.

13.3.2.2.2 Field Data

Field-based estimates of percent canopy cover for shrubs, trees, herbaceous (grasses and forbs) vegetation, and bare-ground were used to develop the VCF models. These data were prepared as

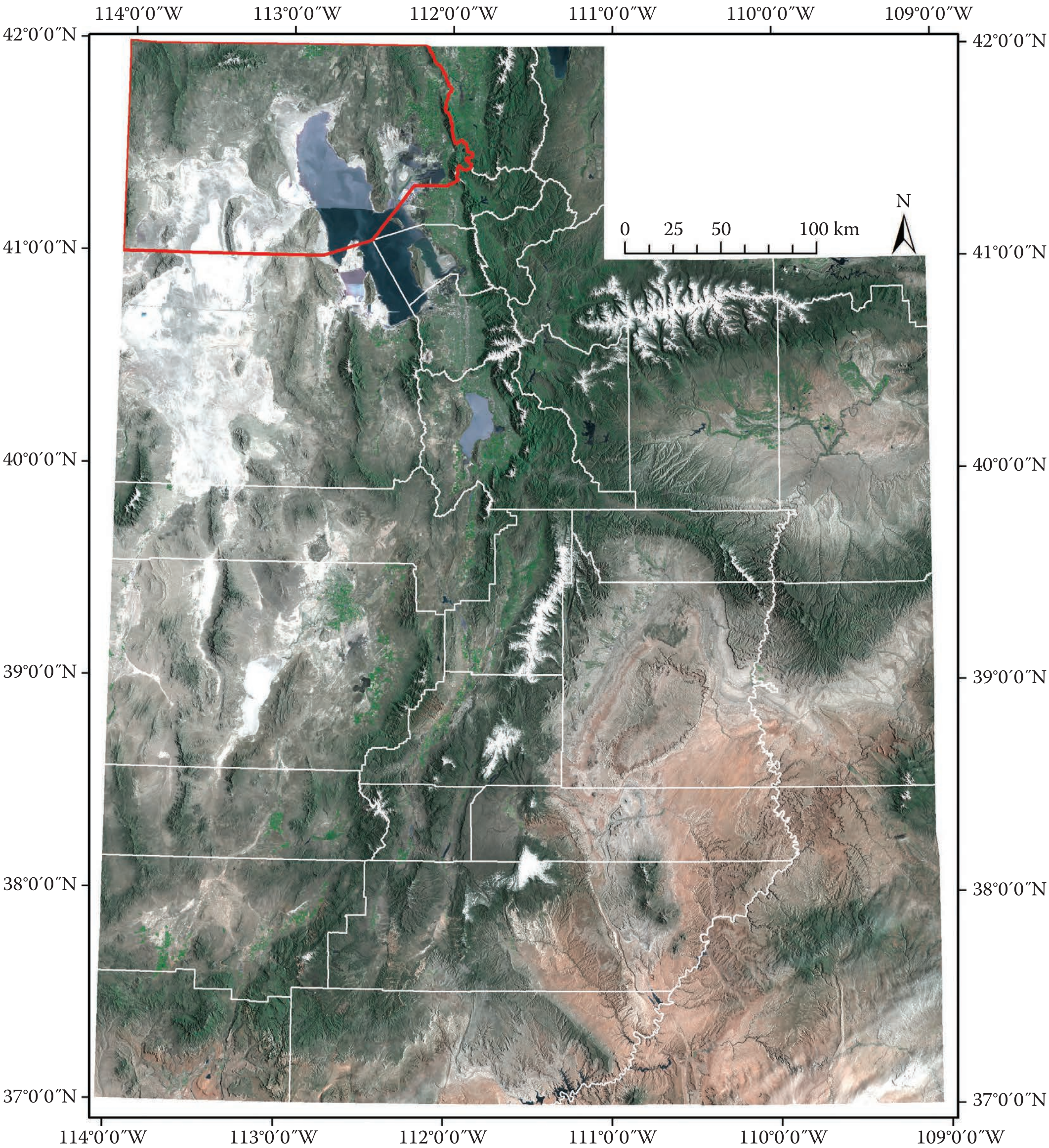

FIGURE 13.6 Utah image mosaic of 2013 Landsat 8 OLI imagery with Box Elder County highlighted in red.

geo-referenced field points and obtained from different sources: (a) 482 points collected by the South West Regional GAP (SWREGAP) project during 2001 (Lowry et al., 2007), (b) Points collected by The Nature Conservancy (TNC) for the Northwest Utah Landscape modeling project in 2007 (Conservancy, 2009), and (c) Field points that we collected during a field season in 2007. In total, 135 field observations were available for the year 2007. A fourth dataset was available from the Utah Division of Wildlife Resources (UDWR). Figure 13.8 contains the spatial distribution of the different datasets across the study area.

With the exception of the UDWR dataset, which are permanent sample plots and follow a standardized and quantitative data gathering method, the rest of the field points were visually assessed (qualitative assessment) in terms of percent canopy cover for shrubs, trees, herbaceous vegetation, and bare-ground on an area that resembled a 3 × 3 Landsat TM pixel (approximately 90 × 90 m). Cover estimates were taken independently at four cardinal directions from the center of the plot in the NE, SE, SW, and NW directions. These estimates were averaged to represent the entire plot.

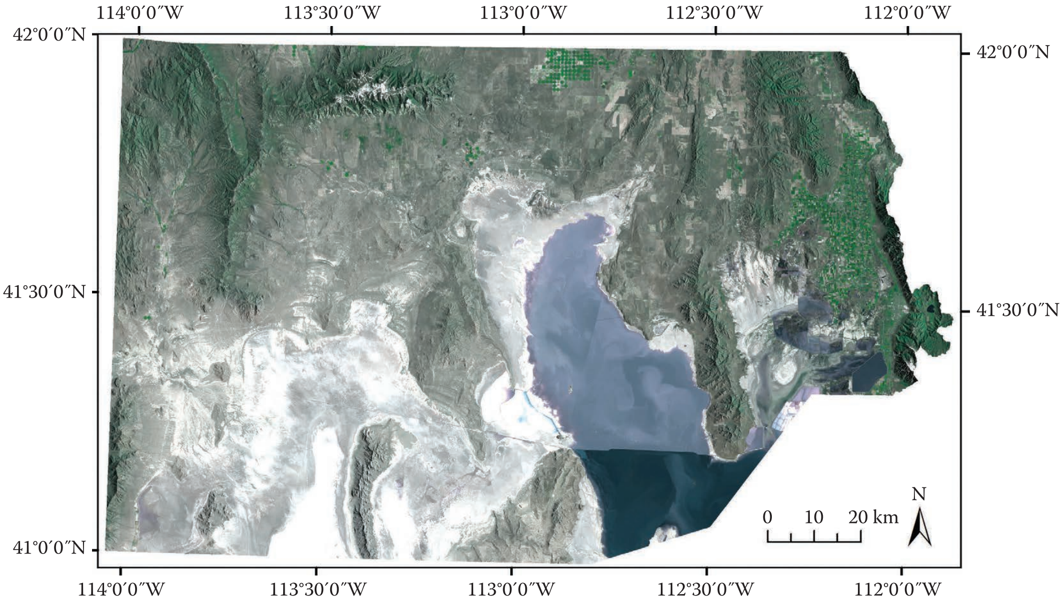

FIGURE 13.7 Landsat 8 OLI image mosaic (2013) of Box Elder County, Utah.

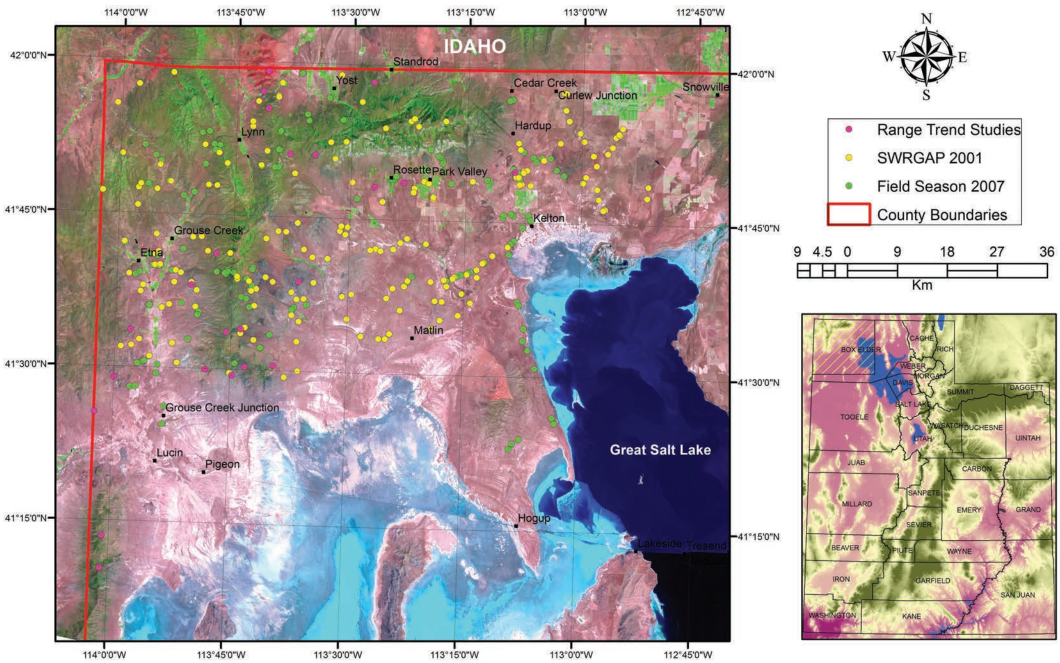

FIGURE 13.8 Distribution of field observations to model multi-temporal CVF.

The percent cover estimates were recorded using 5% increments for each life form and bare ground (i.e. 0%, 5%, 10%, etc.). The sum of the percent cover for shrubs, herbaceous vegetation, trees, and bare ground totaled 100% at each point. The sampling scheme consisted of locating sites along an elevation range that included Wyoming big sagebrush (Artemisia tridentata ssp. wyomingensis), basin big sagebrush (Artemisia tridentata ssp. tridentata), and mountain big sagebrush (Artemisia tridentata ssp. vaseyana) communities.

13.3.2.2.3 Explanatory Variables: Remote Sensing and Topography

Remotely sensed images and topographic datasets were used as explanatory variables for this modeling. With regards to the remotely sensed data, scenes from the Thematic Mapper (TM) sensor of the Landsat 5 satellite, Path 39 Row 31 were obtained. Due to the underlying differences in phenology that most vegetation types exhibit in semiarid landscapes (Bradley and Mustard, 2008), imagery from multiple dates during the summer months of 2001 were acquired. Within year seasonal imagery allowed us to capture major phenological variations that occur during the growing season. Landsat TM imagery collection was concentrated during late spring, mid-summer and early fall. An effort to obtain only imagery with the best quality (i.e., minimum cloud cover) was made. Three images were selected for this study. These were collected on April 28, July 01, and October 5, 2001.

Where necessary, imagery was rectified and resampled to a common map projection UTM Zone 12 WGS 1984. Standardization of the imagery was performed by converting the raw digital numbers to exo-atmospheric reflectance values using an image-based atmospheric correction procedure (Chavez, 1996) with the most up-to-date calibration coefficients for the Landsat TM sensor (Chander et al., 2009).

The Soil Adjusted Vegetation Index (SAVI) was computed for each date. SAVI may be calculated as follows:

$$SAVI = \frac{NIR - RED}{(NIR + RED + L)} * (1 + L) \tag{13.1}$$

In Equation 13.1, NIR = near-infrared reflected radiant flux, RED = red reflected radiant flux, and L = adjustment factor (typically a value of 0.5 is used).

SAVI has been reported to work well in semiarid ecosystems because it minimizes soil background effects that are known to affect other indices such as the Normalized Difference Vegetation Index (NDVI) (Huete, 1988; Jensen, 2007). It has been widely reported that a vegetation index such as SAVI may be used to follow the phenological trajectory or seasonal and inter-annual change in vegetation growth and activity (Jensen, 2007).

A new variable was created from the multi-temporal SAVI and named as NDSAVI or the normalized difference SAVI. The NDSAVI takes advantage of the contrast between the spring and the summer SAVI and may be used to improve our understanding of the phenological dynamics of grasses on the landscape. Higher values in the NDSAVI would correspond with higher greenness during the early spring relative to summer whereas low values of NDSAVI would relate to areas that become green later in the growing season. This new variable conveys a multi-temporal signature of greenness variation that may be used to discriminate among different land cover types and particularly focus on non-native grasses such as cheatgrass that follows this phenological pattern. Within this environment, this index allows us to identify areas where cheatgrass, a common and significant invasive annual grass, is a major component of the plant community.

NDSAVI was estimated as follows:

$$\frac{SAVIspr - SAVIsum}{SAVIspr + SAVIsum} \tag{13.2}$$

The Normalized Difference Water Index (NDWI; Gao, 1996) was also calculated for each image. NDWI takes advantage of the contrast found between the near and middle infrared bands to provide information about water content. Forest disturbances have been successfully detected using the NDWI (Jin and Sader, 2005), and thus it was appropriate to test its performance in our regression models. The brightness, greenness, and wetness (BGW) transformation (Crist and Kauth, 1986) was also derived for each image. This transformation has been used extensively to monitor condition and changes in soil brightness, vegetation, and moisture content, respectively (Jensen, 2007; Lowry et al., 2007).

In addition to the remotely sensed information (Landsat TM spectral bands, SAVI, NDWI, BGW), derivatives from a 30 m digital elevation model (DEM) including slope, aspect, and landform were obtained. Two transformations of aspect, namely southness and westness indices (Chang et al., 2004) and a modification to the original topographic relative moisture index TRMI (Parker, 1982) were generated. An existing land cover map from the SWRGAP project (Lowry et al., 2007) was included as an explanatory variable. The inclusion of this type of ancillary information has been shown to greatly improve classification and regression modeling in rangelands (Peterson, 2005).

13.3.2.2.4 Regression with Random Forests

13.3.2.2.4.1 Background Random Forests (RF) is a relatively new statistical method that emerged from the machine learning literature, and is based on the same philosophy as CARTs (De Cauwer et al., 2024; Arogoundade et al., 2023; Feizizadeh et al., 2023; Sharifi and Felegari, 2023; McCord and Pilliod, 2022; Matongera et al., 2021; Zhou et al., 2020; Hadian et al., 2019; Al-bukhari et al., 2018; Eddy et al., 2017; Gökalp et al., 2017). In RF, multiple bootstrapped regression trees without pruning are created. In a typical bootstrap sample, approximately 63% of the original observations occur at least once (Cutler et al., 2007). The data that are not used in the training set are termed "out-of-bag" observations and are customarily used to provide estimates of errors (Prasad et al., 2006). Out-of-bag samples are also used to calculate variable importance (Cutler et al., 2007). In RF, each tree is grown with a randomized subset of predictors, which equal the square root of the number of variables. In general, 500 to 2000 trees are grown, and averaging aggregates the results. The method is very effective in reducing variance and error in multi-dimensional datasets. One of the strengths of RF is that because it grows a large number of trees, the method tends not to overfit the data, and because the selection of predictors is random, the bias can be kept low (Prasad et al., 2006). More comprehensive descriptions of the method may be found in Sutton (2005), Lawler et al. (2006), Prasad et al. (2006), and Cutler et al. (2007). The application of RF was done in two phases. First, the best subset of variables to model each response variable: shrubs, trees, herbaceous vegetation, and bare-ground were identified. Second, the best subset of variables identified for each response variable was used to model the VCF for that variable.

13.3.2.2.5 Variable Importance and Parsimony

The underlying principle that the phenological pattern of a given vegetation type should dictate which remotely sensed datasets to use (Bradley and Mustard, 2008) was followed. For example, it is sensible to use only one scene (mid-summer for instance) to model bare ground percent cover due to its relatively constant spectral response throughout the year. On the other hand, it makes sense to utilize two to three images (i.e., mid-summer and early fall) to model herbaceous vegetation due to its conspicuous phenological signature which peaks during the summer and then significantly decreases during the fall.

In order to develop a simple yet effective model the concept of variable importance (Cutler et al., 2007) was used. This is based on the mean decrease in accuracy concept, and is assessed based on how much poorer the predictions would be if the data for that predictor were permuted arbitrarily. This provides a measure of the impact that a specific variable has in decreasing the precision of prediction. This is a somewhat subjective approach to choosing the most important variables since thresholds of decreasing precision tend to be arbitrary. Once the most important variables are chosen, the correlation coefficients between each variable are evaluated and further used to eliminate highly correlated variables (choosing the variable that makes most ecological/spectral sense) to arrive at a parsimonious set of predictor variables.

13.3.2.2.6 Regression

The R package RandomForest (Liaw and Wiener, 2002) was used to develop regression trees to calculate the VCF. Regressions were run separately for each of the four response variables (i.e., shrubs, trees, etc.) using the selected subset of variables determined to be most important. The R package YaImpute (Crookston and Finley, 2008) was used to extract the model for each VCF run, and then applied a predict function to generate a continuous geospatial response surface for the entire study area.

13.3.2.2.7 Validation and Comparison Metrics

For independent validation purposes, 20% of the field observations were withheld during model development. Pearson's correlation coefficients were calculated for each of the VCF predictions using this withheld set of data and two metrics were further calculated: mean absolute error (MAE) and root mean square error (RMSE). MAE is the average absolute difference of the predicted value from the field-observed estimate, while RMSE is the square root of the mean squared error (Prasad et al., 2006; Walton, 2008).

13.3.2.3 Results and Discussion

Table 13.4 contains the Pearson's Correlation Coefficients (PCC), mean absolute error (MAE), and root mean square error (RMSE). A global average of the PCC was 0.65. Our highest PCC was

TABLE 13.4
Validation Metrics between MRTS and RF

VCF	Pearson's Correlation	MAE*	RMSE**
Shrubs	0.72	7.81	10.00
Trees	0.52	12.56	16.69
Herbaceous	0.77	9.39	12.02
Bare ground	0.62	8.15	11.05
Average	0.65		

* Mean Absolute Error
** Root Mean Square Error

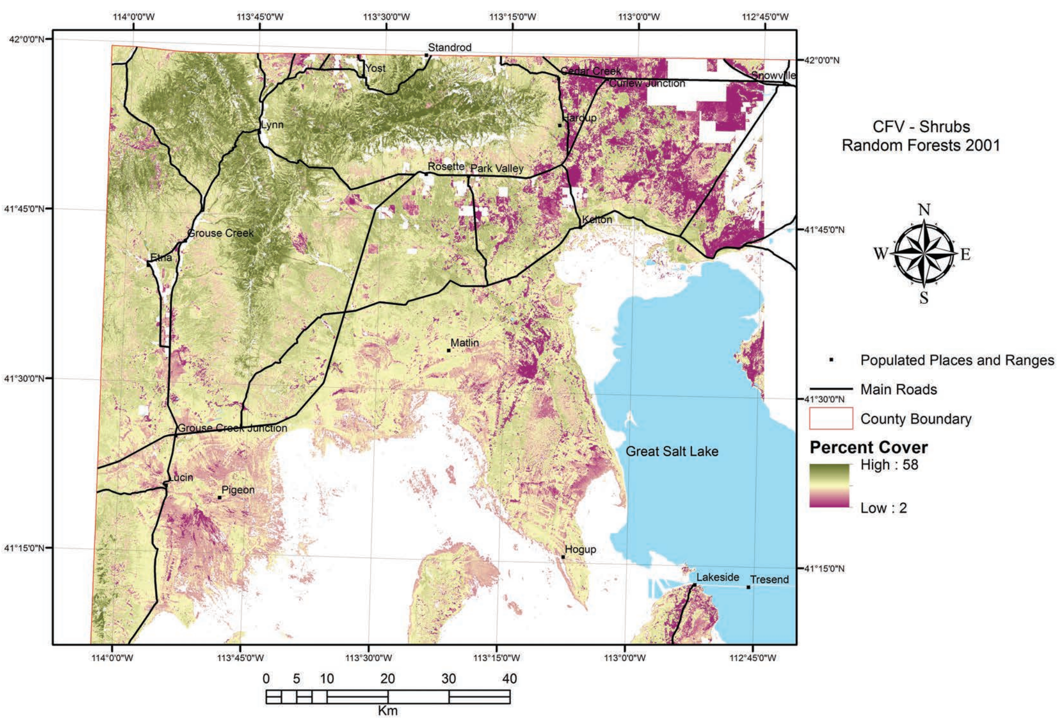

FIGURE 13.9 Percent canopy cover of shrubs as modeled using Random Forests.

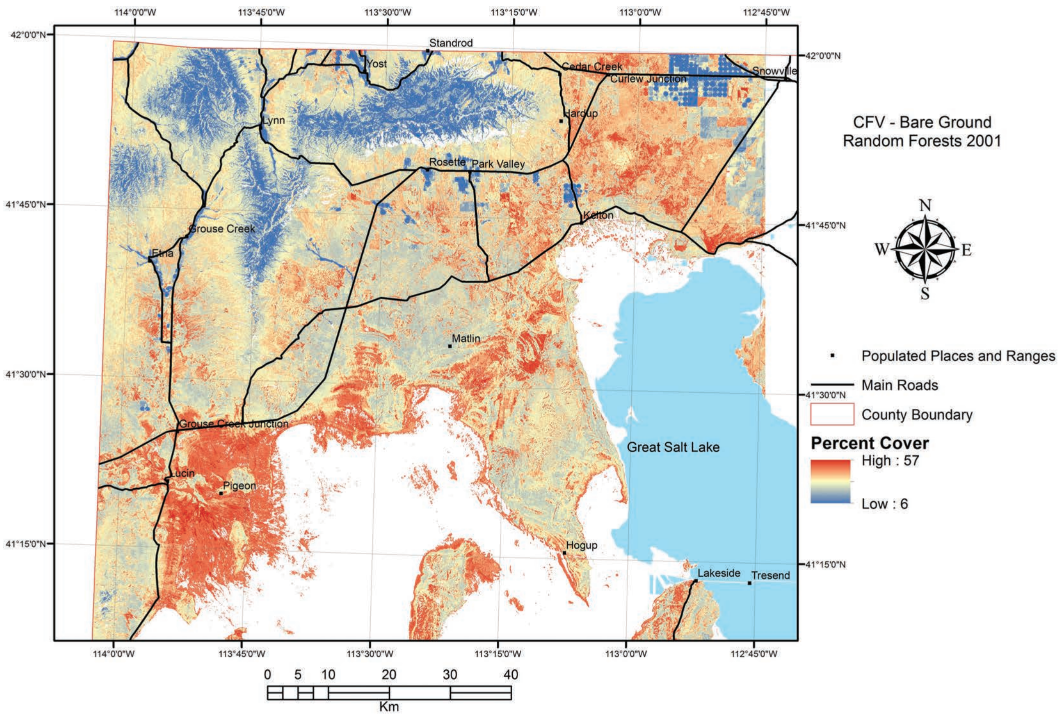

FIGURE 13.10 Percent canopy cover of bare ground as modeled using Random Forests.

for herbaceous cover at 0.77 and the lowest was for trees at 0.52. Figures 13.9 and 13.10 illustrate samples of the VCF spatial layers generated using RF.

The use of regression trees to depict sub-pixel heterogeneity has been widely reported in the literature. In rangeland environments, work has been conducted to model woody vegetation cover (Danaher et al., 2004), bare ground cover (Weber et al., 2009), and shrub cover and encroachment (Laliberte et al., 2004). With the exception of the MODIS global continuous vegetation maps (Danaher et al., 2004), the preceding examples dealt with only one response variable. In this work there were four response variables. Since a pixel is in essence an integrated multi-dimensional spectral response of vegetation, bare ground and other features, it makes sense to attempt to decompose that response to understand the land cover dynamics of a given pixel in relation to the surrounding landscape.

With regards to the ease of understanding, RF has been frequently described as a "black box" (Prasad et al., 2006) because the individual trees cannot be examined separately due to the sheer number of trees that may be generated. This can limit the ability of an analyst to understand the underlying dynamics of the resulting model. Random Forests does provide metrics to aid in interpretation. One metric is variable importance, which can be used to compare relative importance among predictor variables. Such a feature is not available in other regression tree tools and therefore the importance of variables must be determined with a careful data mining process.

13.3.2.4 Implications

The development of a multi-temporal collection of VCF may be used to update information about the status or condition of a particular ecological site as well as characterizing the states and transitions for that site. For instance, a specific spatial unit of an ecological site may be characterized in terms of its occupancy by shrubs, grasses, trees, and bare ground using modeled VCF. Knowledge about the relative dominance of these life forms in a particular unit may shed light about its current condition relative to a reference condition. The VCF process may provide knowledge about usage of the ground by major life forms and bare ground and in this way pinpoint areas that are diverging from a desired condition.

13.4 RANGELAND CHANGE DETECTION ANALYSIS

13.4.1 Rangeland Indicators

Numerous landscape metrics have been developed to characterize the patterns and configurations of different land cover types in a landscape. Categorical maps generated from remote sensing data can then be used for landscape characterization to better understand spatial arrangements between different cover classes, particularly forest fragments (Read and Lam, 2002). These spatial arrangements are expressed numerically in the form of landscape indices or pattern metrics and have been used in many studies to assess land cover change and its impact, ecosystem health, or as variables for models that support environmental assessment and planning efforts (e.g., Botequilha Leitão and Ahern, 2002; Fuller, 2001; Gergel, 2005; Griffith et al., 2000; Liu and Cameron, 2001).

More than 100 pattern metrics can be computed using freeware such as FRAGSTAT (McGarigal and Marks, 1995), Patch Metrics (Rempel et al., 1999) and others (Crews-Meyer, 2002; Cumming and Vervier, 2002; Stanfield et al., 2002). However, many pattern metrics are highly correlated (Cain et al., 1997; Riitters et al., 1995). Efforts have been made to identify a minimum set of pattern metrics that describe landscape patterns adequately. Multivariate data analysis using principal component analysis (PCA) and factor analysis (FA) are the most commonly used methods to reduce pattern metrics data (Griffith et al., 2000; Honnay et al., 2003; McAlpine and Eyre, 2002; Stanfield et al., 2002). These methods identify a small number of components, which are then interpreted in terms of their dominant characteristics and underlying causes (Griffith et al., 2000). Multivariate data analysis requires large datasets and several landscape units to be statistically consistent (e.g., Cumming and Vervier, 2002; Schmitz et al., 2003). A few empirical landscape studies apply pattern analysis to only one landscape (e.g., Griffith et al., 2000) and are useful because they tackle problems at relevant scales, but the validity of making statistical inferences with such an approach is seriously compromised (Li and Wu, 2004). Gustafson (1998) overcame this by generating artificial landscapes (called neutral models), but the technique was difficult to relate to pattern metrics in real landscapes (Li and Wu, 2004). Therefore, the behavior of pattern metrics in real landscapes over time needs further investigation (Griffith et al., 2003). Irrespective of the landscape unit used, pattern metrics require rigorous validation in order to be interpreted and applied with confidence (McAlpine and Eyre, 2002).

13.4.2 Pattern Metrics to Measure Landscape Attributes

Area: Area distribution pattern metrics include basic attributes of the landscape such as the number of patches (*NP*) and the total area (*CA*) of all class patches, expressed in hectares. Mean patch size (*AREA_MN* in ha) is an intuitive index for measuring aggregation and is particularly suitable for categorical maps (Matongera et al., 2021; Zhou et al., 2020). Other measures are the standard deviation of the mean patch size (*AREA_SD* in ha) and the coefficient of variation (*AREA_CV* in %), determined by Equation 13.3.

$$AREA\_CV = \frac{AREA\_SD}{AREA\_MN} * 100 \tag{13.3}$$

$AREA\_CV$ indicates patch area distribution by determining the difference among patches within one landscape class. Lower values indicate a more uniform class distribution (Batistella et al., 2003; McAlpine and Eyre, 2002), that is if a landscape class is dominated by big patches both $AREA\_SD$ and $AREA\_CV$ values are large. All of these pattern metrics assign equal weights to each patch. For measuring landscape resistance to fragmentation, large forest patches are most important (Batistella et al., 2003), therefore metrics such as largest patch index (LPI) are useful. LPI is equal to the percent of the total landscape made up by the largest patch (McAlpine and Eyre, 2002).

Edge: Total edge (TE) refers to the length of edge that exists at the interface between land classes (McGarigal and Marks, 1995) while mean patch edge (MPE) indicates the amount of edge per patch (Equation 13.4).

$$MPE = TE / NP \tag{13.4}$$

Patch Shape Complexity: Mean perimeter—area ratio (*PAR_MN*) is a simple index of patch shape complexity, computed as the mean ratio between patch perimeter and area; it describes the amount of edge per unit area of landscape unit (such as forest) (McGarigal and Marks, 1995). Since the simple ratio is usually affected by patch size, a modified perimeter—area ratio called Landscape index (*LSI*), implied as shape of landscape, is computed using Equation 13.5.

$$LSI = Perimeter / 2\left(area * \pi\right) \tag{13.5}$$

Higher LSI values indicate higher complexity (McAlpine and Eyre, 2002). Because *LSI* is influenced both by shape complexity and number of patches (*NP)*, preference is sometimes given to the mean shape index (*SHAPE_MN*) or the area-weighted mean shape index (*SHAPE_AM*), which weights larger patches more heavily than smaller patches (Batistella et al., 2003).

Fractal dimension (*FRAC*) has equally been used to describe patch shape complexity across a range of spatial scales (patch sizes). This overcomes one of the major limitations of the perimeter—area ratio as a measure of shape complexity. The value of *FRAC* ranges between 1 and 2 and is computed as:

$$FRAC = 2\log P / \log A \tag{13.6}$$

where P is the perimeter and A is the area of the patch. Fractal dimension approaches 1 for shapes with very simple perimeters such as squares, and approaches 2 for shapes with highly complex perimeters (Read and Lam, 2002). Mean patch fractal dimension (*FRAC_MN*) and the area-weighted mean patch fractal dimension (*FRAC_AW*) are derived measures of shape complexity, interpreted similarly to *FRAC* with the addition of an individual patch area weighting applied to each patch in the case of *FRAC_AW* (McGarigal and Marks, 1995).

Interior-to-edge (core area): Core area (CA) represents the area of patch greater than a specified depth-of-edge distance from the perimeter. It is determined by defining a vanishing distance as the distance from a patch boundary inward, to a point where edge effects are eliminated (Baskent and Jordan, 1995). The higher the ratio between the core area and the total area, the lesser the degree of fragmentation (Batistella et al., 2003; Tang et al., 2005). The vanishing distance is arbitrarily set. The number of core areas (*NCA*) is the number of distinct core areas contained within a patch boundary. Total core area (*TCA*) is the same as *CA* except that core area is aggregated (summed) over all patches, approaching *CA* as patch shapes are simplified. Core area distribution in the landscape is measured using the parameters mean core area per patch (ha) (*CORE_MN*), patch core area standard deviation (*CORE_SD*) and patch core area coefficient of variation (*CORE_CV*).

Isolation: The distance of patch to its nearest neighbor measures the degree of isolation of that patch. Averaging this distance for all individual land cover classes or patches in a landscape gives the mean nearest neighbor distance (*ENN_MN*). Mean proximity index (*PROX_MN*) is also computed (Equation 13.7) and is a measure of isolation and fragmentation:

$$PROX\_MN = \sum \frac{\sum_i^N \sum_j^{m'} \frac{a_{ij}}{h_{ij}}}{N} \tag{13.7}$$

where a_{ij} is the area of patch *ij* in the neighborhood of patch *i*, h_{ij} the distance between patch *i* and patch *ij*, *N* is the number of patches and *m'* is the number of patches in the neighborhood of patch *i*. This index allows comparison among landscapes of any size, as long as the search buffer around each patch is the same (Gustafson and Parker, 1992).

Contagion/Interspersion: Contagion (*CONTAG*) provides an effective summary of overall clumpiness of categorical data where lower values indicate fragmentation of larger patches into smaller patches, that is the patch types are maximally disaggregated and interspersed (equal proportions of all pairwise adjacencies) (Equation 13.8):

$$CONTAG = 1 + \frac{\sum_{i=1}^{m}\sum_{k=1}^{m}(P_i)\left(\frac{g_{ik}}{\sum_{k=1}^{m} g_{ik}}\right)*ln(P_i)\left(\frac{g_{ik}}{\sum_{k=1}^{m} g_{ik}}\right)}{2ln(m)}(100) \tag{13.8}$$

where P_i is the proportion of the landscape occupied by path type (class) *i*, g_{ik} is the number of adjacencies (joins) between pixels of patch types (classes) *i* and *k* based on the double-count method, and *m* is the number of patch types (classes) present in the landscape, including the landscape border if present.

Aggregation index (AI) is calculated from an adjacency matrix at the class level, AI equals 0 when the patch types are maximally disaggregated. *SPLIT* and *MESH* are two subdivision metrics computed as isolation measures (McGarigal and Marks, 1995). The interspersion and juxtaposition index (*IJI*), a configuration metric, is a measure of relative interspersion of each class at class level and each patch at landscape level (Crews-Meyer, 2002; McAlpine and Eyre, 2002). *IJI* approaches 100 when all patch types are equally adjacent to all other patch types, and as the distribution of class types depart from evenness, the *IJI* approaches 0 (Equation 13.9).

$$IJI = \frac{-\sum_{i=1}^{m}\sum_{k=i+1}^{m}\left(\frac{e_{ik}}{E}\right)*ln\left(\frac{e_{ik}}{E}\right)}{ln\left(0.5m(m-1)\right)}(100) \tag{13.9}$$

where e_{ik} is total length (m) of edge in the landscape between patch types (classes) *i* and *k*, *E* is total length (m) of edge in the landscape, excluding background, and *m* is the number of patch types (classes) present in the landscape, including the landscape border, if present.

Spatial heterogeneity: Spatial diversity representing the extent to which all patches are equally adjacent to each other, number of different land cover classes, and interspersion metrics determine the spatial arrangements of land cover classes (Trani and Giles, 1999). Patch richness (*PR*) is a simple metric equal to the number of different patch types present within the landscape boundary. Shannon's diversity index (*SHDI*) assesses the diversity of patches, and the extent to which one or a few patch types dominate the landscape (McAlpine and Eyre, 2002). *SHDI* starts at zero and increases without limit and is more sensitive to the number of patch types than evenness. *SHDI* is given by Equation 13.10 (Read and Lam, 2002):

$$SHDI = -\sum_{i=1}^{m}\left(P_i*lnP_i\right) \tag{13.10}$$

where P_i is the proportion of landscape occupied by patch type (class) *i*, and *m* is the number of patch types (classes) present in the landscape, excluding the landscape border, if present.

The Shannon's evenness index (*SHEI*) is expressed such that an even distribution of area among patch types results in maximum evenness (Equation 13.11):

$$SHEI = -\frac{\sum_{i=1}^{m}(P_i*lnP_i)}{\ln m} \tag{13.11}$$

SHEI varies between 0 and 1, and the highest value is reached when the distribution among patch types is perfectly even (Wickham and Rhtters, 1995). The modified Simpson's diversity (*MSIDI*) is similar to the *SHEI* (Equation 13.12):

$$MSIDI = -\ln \sum_{i=1}^{m} \left(P_i^2\right) \tag{13.12}$$

where P_i is the proportion of the landscape occupied by patch type (class) i. Diversity metrics represent landscape composition in terms of the relative proportions of each patch types (evenness), together with the number of patch types (richness). Detailed information on these indices and their computation can be found in Wickham and Rhtters (1995).

Ludwig et al. (2004) Monitored ecological indicators of rangeland functional integrity and their relation to biodiversity at local to regional scales. Functional integrity is the intactness of soil and native vegetation patterns and the processes that maintain these patterns. The integrity of these patterns and processes has been modified by clearing, grazing and fire. Intuitively, biodiversity should be strongly related to functional integrity. Ludwig et al. (2004), based on published work on Australian rangelands, identified several indicators of landscape functional integrity at finer patch and hillslope scales. These indicators, based on the quantity and quality of vegetation patches and inter patch zones, are related to biodiversity. These vegetation-cover and bare-soil patches can be measured using remote-sensing data at various resolutions depending on specific rangeland areas. De Cauwer et al. (2024) used Landsat MSS for prevailing dry periods before the major rainfall events and about six weeks after them when vegetation growth had peaked for the assessment of biodiversity condition in a rangelands in central Australia. They computed Contagion and Interspersion scores for land systems and vegetation types. The Contagion and Interspersion values, as indices of the spatial arrangement of patches in the landscape, indicated the extent to which both water development and land degradation associated with pastoralism had fragmented habitat types. Non-degraded and water-remote patches of pastorally more productive land systems or vegetation types were more dispersed and more fragmented relative to their original state, than for patches of pastorally less productive land systems or vegetation types.

13.4.2.1 Resilience

Ecological resilience is defined as the degree, manner, and pace of the restoration of vegetation attributes after a disturbance (Westman, 1985). Ecological resilience and its characteristics have been quantified statistically in ecosystem simulations (O'Neill, 1976; Westman and O'Leary, 1986), plant community field studies (Westman and O'Leary, 1986), and regional analyses of land degradation (Wessels et al., 2004, 2007). O'Neill (1976) simulated energy flow through a three-compartment (autotrophs, heterotrophs, and detrivores) model for six different biomes to test their ability to recover from a 10% reduction in plant biomass over a 25-year period. A recovery index, that is, a measure of the amount of deviation from a reference equilibrium value or initial state after a disturbance (a measure of malleability), was computed for each year over the 25-year period. The mean malleability of each biome for this period was interpreted to indicate which biomes were least and most resistant to disturbance (O'Neill, 1976). Westman and O'Leary (1986) developed four measures of ecological resilience: elasticity, that is, the rate of recovery from a disturbance; amplitude, that is, the threshold beyond which recovery to a previous reference state no longer occurs; damping, that is, the extent and duration of an ecosystem parameter following disturbance, and malleability. These were used to estimate the responses of various plant functional types within a coastal sage scrub plant community at 5–6 years after fire using field data and for 200 years after fire using a simulation model. Wessels et al. (2004, 2007) used an inter-annual time series of AVHRR- and Moderate Resolution Imaging Spectroradiometer (MODIS)-derived NDVI (or ANPP) from 1985 to 2005 to examine the resilience of a landscape in northeastern South Africa that had been subject to both overpopulation and apparent overgrazing by the forced settlement of pastoralists into "homelands" during the apartheid era from 1910 to 1994. A spatially aggregated approach was used in which the mean annual ΣNDVI for the period of 1985–2005 was compared between non-degraded benchmark areas and degraded areas within the homelands as

$$RDI\ or\ PD = \frac{non-degraded\sum NDVI - degraded\sum NDVI}{non-degraded\sum NDVI} \times 100 \tag{13.13}$$

where RDI is the relative degradation index or the percent difference (PD) between the mean NDVIs of non-degraded and degraded sites (Wessels et al., 2004, 2007). Wessels et al. (2004, 2007) found that these paired sites were significantly different from each other and that degraded sites had significantly lower mean annual NDVI than did non-degraded sites. Also, there was no indication of recovery (malleability) of degraded sites toward the mean conditions of non-degraded sites from the end of the apartheid era in 1994 to 2005 (Wessels et al., 2004, 2007). This provided evidence in support of the hypothesis that the observed migrations of former rural homeland populations to jobs in major urban centers, such as Johannesburg and Durban, were due in part to environmental degradation of the homelands. However, at the coarse resolution of MODIS (0.25 km^2) and AVHRR (1 km^2), it was observed that finer-scale phenomena at the community and species levels were masked or averaged out (Wessels et al., 2007). A number of scaling studies in drylands suggest characteristic length scales for vegetation and bare soil patches of approximately 1–100 m; these scales are probably not amenable to analysis using spatially coarse-resolution sensors such as MODIS or AVHRR (Hudak and Wessman, 1998; Rietkerk et al., 2004). To account for this disparity, Wessels et al. (2007) suggested a staged remote sensing approach to monitoring at regional and national scales in which both coarse-resolution sensors such as MODIS are used in conjunction with relatively finer-resolution datasets such as Landsat.

13.4.3 Change Detection Methods

It is important to monitor and understand change in rangelands so that effective action can be taken to maintain ecological, economic and social values. Both seasonal conditions and grazing management play a role in vegetation dynamics on pastoral areas. For example, De Cauwer et al. (2024) determined the effect of seasonal spectral variability on vegetation and land cover classification of Landsat TM by comparing accuracies in different seasons in a mid-latitudinal (29°30′–31°0′S) region with summer and winter rainfall, a broad altitudinal range, a temperate to subtropical climate and diverse land uses (e.g., summer and winter crops, and nature conservation). By comparing the observed changes with those expected under the prevailing seasonal conditions and by investigating the response of species known to be adversely or positively affected by livestock grazing, it was possible to conclude that at least some of the positive changes observed could be attributed to the type of grazing management, rather than seasonal conditions alone. In a similar study, De Cauwer et al. (2024) used three-date composite land cover maps through a process called referential refinement and aggregation for understanding the level of land exploitation (extensive vs intensive) activities carried out in the region. Landscape-scale monitoring is important for providing regional to national-scale intelligence on habitat quality and trends in threats to or drivers of biodiversity, with data obtained using systematic ground-based and remote methods. Landscape-scale monitoring is typically based on remotely obtained or extrapolated data that can be mapped, and use temporal scales appropriate to the indicator (Ludwig et al., 2004). The advantage of landscape-scale monitoring is that it is often relatively cheap to undertake over space and time and provides a broader context for national reporting.

There are a variety of opinions and suggestions about the selection of the most effective and appropriate techniques for change detection studies (Lu et al., 2004). Therefore, it is difficult to specify which change detection algorithm will suit a specific problem. A review of different change detection techniques used in previous research would be of great help in selecting methods to aid in producing good quality change detection results. For any change detection project, the following conditions must be satisfied (Lu et al., 2004): (1) accurate and precise registration between multi-temporal images; (2) precise radiometric and atmospheric normalization between multi-temporal images; (3) similar phenological or seasonal conditions between multi-temporal images; and (4) selection of the same spatial and spectral resolution images if possible.

The aim of change detection studies is to compare the spatial representation of two points in time by controlling all variance caused by differences in variables that are not of interest and to measure changes caused by differences in the variables of interest (Green et al., 1994). Since there are many change detection techniques that can be used in one study, the selection of the most suitable method for a given project is not easy since different approaches, with the same environmental conditions, produce different results (Coppin et al., 2004).

13.4.3.1 Classification Based Change Detection

Broadly, image classification is a process of drawing meaningful information by differentiation and extraction of different classes or types (e.g., land use types, vegetation species) from remote sensing data through a number of image processing procedures including image pre-processing. Image is classified either using traditional methods or improved or modified techniques.

The classification group of change detection techniques includes supervised and unsupervised classification followed by post-classification comparison of results of change/no-change identification. The aim of these methods is to produce high quality, accurate classification results from remote sensing data through the use of adequate numbers of accurate training sample data, to produce accurate change results after comparison. However, the selection of sufficient numbers of high quality training samples to truly represent each land use/land cover class is laborious and time consuming and requires a thorough knowledge of the study area in order to obtain high quality classification results. The situation is more difficult in the classification of historical data when there is no or insufficient ground or area information, making accurate classification a challenge and often leading to unsatisfactory change detection results (Lu et al., 2004). The change detection results are often represented in the form of matrix showing land use/land cover dynamics of pixel changes from one class to another, providing a detailed description of changes over a specified period of time and minimizing the effect of atmospheric and environment difference between the multi-date images. A detailed review of quality assessment of different image classification algorithms for land cover mapping and accuracy assessment has been summarized by Arogoundade et al., (2023) and Feizizadeh et al., 2023. These techniques have been used by many researches in different types of land cover change detection analysis with good results (e.g., Xiuwan, 2002; Petit and Lambin, 2002; Li and Zhou, 2009).

Among traditional methods of classifying remote sensing data, unsupervised and supervised techniques are the most commonly used algorithms. ISODATA clustering and K-means methods are mainly used in unsupervised techniques while the Maximum Likelihood Classification (MLC) and Minimum Distance to Mean (MDM) are commonly applied techniques in supervised methods since the beginning of digital image feature extraction using statistical software. Unsupervised approaches, such as ISODATA clustering and K-means algorithms, are easy to apply for thematic mapping of landcover or vegetation classification using statistical software packages (Hadian et al., 2019 and Al-bukhari et al., 2018) based on iterative learning of remote sensing data defined by the user. In this classification approach, an arbitrary initial cluster vector is assigned first, based on which each pixel is classified as closest to that cluster value. Finally, based on all the pixels present in one cluster, the new cluster mean vector is calculated and the process is repeated until the gap between the iterations becomes smaller than the threshold value (Xie et al., 2008). This method does not require any prior knowledge of the area or theme being studied (Tso and Olsen, 2005) and classifies the image based on natural grouping or spectrally homogenous thematic classes using spectral values of each pixel. The analyst then assigns the spectral classes into thematic information classes of interest (Jensen, 2005). It has the benefit of automatically converting the raw image data into useful information so long as higher accuracy is achieved (Tso and Olsen, 2005). However, since each pixel is treated as spatially independent, a traditional unsupervised classification based on spectral data alone results in poor accuracy. To overcome this, Tso and Olsen (2005) introduced

Hidden Markov Model (HMM) as a fundamental framework to incorporate both the spectral and contextual information for unsupervised classification and achieved higher classification accuracies.

In supervised classification, a prior knowledge about some cover types are obtained in advance through a combination of field work, aerial photo interpretation, existing maps and other sources. Based on this, the analyst attempts to locate specific sites (class representation) for these cover classes in remote sensing data. These sites are called training sites and used to train the classification algorithm based on spectral characteristics of each site to classify the rest of the image. Statistical parameters such as mean, standard deviation, covariance matrices, correlation matrices etc. are computed for each training site, based on these statistics, every pixel is then evaluated and assigned to a class of which it has the highest likelihood of being a member of (Jensen, 2005). Various supervised classification algorithms such as Parallelpiped (PAR), Minimum Distance (MID), Nearest Neighborhood (NN), and Maximum Likelihood (MLC) may be used to assign an unknown pixel to one of the possible classes; therefore the choice of a particular classifier or decision rule depends on the nature of input data and desired output (Jensen, 2005). MLC is considered to be classic and most widely used supervised classification technique, applied by many researchers in different studies for satellite image classification (Laba et al., 1997; Langford and Bell, 1997; Rogan et al., 2002; Xiuwan, 2002; Abdulaziz et al., 2009). In rangeland studies, Abdulaziz et al. (2009) evaluated the potential of multispectral Landsat images (MSS and TM) and applied MLC to classify vegetation cover in the degraded land of MuUs sandy land in China. Torahi (2012), in monitoring rangeland dynamics between 1990–2006, used MLC for classifying TM and ASTER data and generated detailed rangeland maps and also separated grazing intensity levels in rangelands.

However, in complex areas, the assumption of MLC that data follow Gaussian distribution is not always applicable, resulting in less satisfactory results. Strahler (1980) demonstrated the effective use of modified prior probabilities into MLC to improve image classification. In addition to MLC alone, there are studies conducted by researchers using a combination of other supervised classification algorithms, for example Miller et al. (1998) applied parallelepiped technique to classify water, open land, clouds and cloud shadows, assuming them as discrete classes in spectral space, while other forest classes were classified using MLC in landcover change study in Northern Forest of New England. Xiuwan (2002) compared several classification methods such as PAR, MID, Mahalanobis Distance (MAD), MLC, ISODATA and a method combining an unsupervised algorithm and training data (CUT) to develop a new classification method and suitable change detection technique for analysis of landcover change and its regional impacts on sustainable development in Korea. J. Im et al. (2008) used nearest neighborhood classification techniques for landuse and landcover classification and compared the accuracy with other techniques. Munyati et al. (2011) used the hybrid image classification approach to monitor savanna rangeland deterioration in Mokopane, South Africa. For classification, initial clustering was undertaken by unsupervised classification using the ISODATA algorithm. On the resulting cluster image, the field data sites were then located and the spectral signature clusters were assigned names. The named spectral signatures were then used for a final supervised classification.

13.4.3.1.1 Improved/Modified Classifiers

Depending upon different geographic conditions and other factors, there is a possibility that same ground covers or vegetation types show different spectral response or different covers show similar spectral response on remote sensing imagery due to spectral mixing, therefore an accurate classification result is very difficult to obtain from traditional supervised or unsupervised classification techniques. Hence, there is always a need for improvement in the classification methods for better classification results. Some of the new methods have been based on traditional supervised or unsupervised approaches through a process of combination, extension or as an expansion to provide better classification results from remote sensing data. Sohn and Rebello (2002) developed the new spectral angle classifier (SAC), a combination of supervised spectral angle classifier (SSAC) and unsupervised spectral angle classifiers (USAC), based on the fact that the spectra of same types of surface objects are approximately linearly scaled variations of one another due to atmospheric and topographic effects. SAC allows the spectral angle to be used as a metric for measuring angular distances in feature space for classification and clustering of multispectral satellite data and was successfully applied in biotic and landcover classification (Sohn and Qi, 2005). Collado et al. (2002) found use of spectral mixture analysis (SMA) to be valuable in monitoring desertification processes in the crop-rangeland boundary of Argentina. Savanna rangeland degradation in Namibia was classified by Vogel and Strohbach (2009), who used Landsat TM and ETM+ data. The decision tree classifier was also used. Their results showed that savanna degradation could be classified into the following six classes: vegetation densification, vegetation decrease, complete vegetation loss, long-term vegetation patterns, the recovery of vegetation on formerly bare soils, and no change with an overall accuracy of 73.4%, with class pair accuracies ranging from 80 to 100% for producer and user accuracies. Okin et al. (2001) assessed the utility of AVIRIS satellite imagery for accurately discriminating among vegetation types in the Mojave Desert, USA. Multiple Endmember Spectral Mixture Analysis (MESMA) and Spectral Mixture Analysis (SMA) were performed to estimate the proportion of each ground pixels area that fitted with different cover types. They concluded that AVIRIS showed low potential for classifying vegetation types, with an overall accuracy of only 30% due to low vegetation cover. This is a common problem in rangelands, where the overall classification accuracies are generally lower than for forest or well vegetated areas.

James et al. (2003) suggested that ecological condition of rangelands is a major factor in their environmental quality, their overall performance as watersheds and in wildlife and livestock production. They pointed out that to maintain the quality of rangelands, they must be monitored over time and space and also must take into account topography, climate, soils, plant communities, and animal population. Several studies have shown that extensive field knowledge and support data improves classification accuracy, for example, Wang et al. (2009) used stratified classification approaches based on segmentation of an image into focused area and categories based on existing GIS landcover data in order to improve classification accuracy. Franklin and Wilson (1992) developed a three-stage classifier that incorporated a quadtree-based segmentation operator, a Gaussian minimum-distance to mean test and final test involving ancillary geomorphometric data and a spectral curve measure and attained significant increase in classification accuracy in less time and with minimum field training data as compared to MLC. Jianlong et al. (1998) used green herbage yield data, environment, and remote sensing data recorded in different grassland types in Fukang County, Xinjiang from 1991 to 1996. They explored the methods of processing images, analyzing information, and linking of remote sensing data with ground grassland data. Tagestad and Downs (2007) studied landscape measures of rangeland condition using texture methods, highlighting the apparent roughness in the visible surface due to drastic changes in brightness between adjacent pixels. The texture model reduces the color signal in the image and maximizes the texture signal. The field-measured shrub canopy cover in each plot was compared to the corresponding texture ratio values for pixels representing that plot to develop a simple linear regression relationship between shrub canopy cover and image texture. Franklin et al. (2001) used spatial co-occurrence texture measures and MLC to generate higher forest species composition classification accuracies in New Brunswick forest stand than the use of spectral patterns alone. Gong and Howarth (1992) developed and evaluated a contextual method of landuse classification using SPOT data involving two steps: gray-level vector reduction and frequency based classification and found that the frequency based classification method was comparatively fast, efficient and could improve landuse classification accuracies over MLC and was effective in identification of spatially heterogeneous landuse classes. Pin˜eiro et al. (2006) estimated seasonal variation in aboveground production and radiation-use efficiency of temperate rangelands using remote sensing. They evaluated, at a seasonal scale, the relationship between ANPP and the NDVI and estimated the seasonal variations in the coefficient of conversion of absorbed radiation into aboveground biomass and also identified the environmental controls on such temporal changes. Their results indicated that NDVI produced good, direct estimates of ANPP only if NDVI, PAR, and aboveground biomass were correlated throughout the seasons and hence suggested seasonal variations of aboveground biomass associated with temperature and precipitation to be taken into account to generate seasonal ANPP estimates with acceptable accuracy.

Fuzzy methods in the classification of remote sensing images have become popular because of their ability to deal with situations where the geographical boundary is inherently fuzzy or heterogeneous due to the presence of mixed pixels and traditional methods of classification are often incapable of performing satisfactorily (Okeke and Karnieli, 2006). For example, Tagestad and Downs (2007) investigated the fuzzy approach for the classification of sub-urban landcover from remote sensing imagery and reported to have advantages over both conventional hard method and partially fuzzy approach. Other similar applications have been by Okeke and Karnieli (2006) for vegetation change study, and Sha et al. (2008) for grassland classification. Discriminating and mapping vegetation degradation at Fowlers Gap Arid Zone Research Station in Western New South Wales, Australia, Okeke and Karnieli (2006) used Random Forest method to classify perennial vegetation, chenopod shrubs and trees using hyperspectral imaging (CASI). An area of less than 25% was discriminated and mapped. Okeke and Karnieli (2006) concluded that high-spectral resolution imagery had potential for the discrimination of vegetation cover in arid regions.

Recently, decision tree (DT) classifiers have been used for landcover and vegetation classification from remote sensing data based on the concept of splitting a complex decision into several simpler decisions which may be easier to interpret. DT is based on multistage or hierarchal decision scheme or a tree like structure composed of a root node (containing all data), a set of internal nodes (splits) and a set of terminal nodes (leaves) and processes from top to bottom by moving down the tree where each node of the decision tree structure makes a binary decision that separates either one class or some of the classes from the remaining classes (Xu et al., 2005; Chen and Rao, 2008). DT is relatively simple, explicit, computationally fast, makes no statistical assumptions and can handle data on different measurement scales (Friedl and Brodley, 1997; Pal and Mather, 2003). Chen and Rao (2008) determined the rate and status of grassland degradation and soil salinization based on DT and field investigation with overall classification accuracy of more than 85%. Xu et al. (2005) employed a decision tree regression approach to determine class proportions within a pixel so as to produce a soft classification and the accuracy achieved by DT regression was found to be significantly higher as compared to MLC applied in soft mode and supervised version of fuzzy-c-soft classification, especially when data contained a large proportion of mixed pixels.

Pal and Mather (2003) assessed the utility of DT classifier for landcover classification using multispectral and hyperspectral data and compared the performance of univariate and multivariate DT with that of ANN and MLC. They concluded that DT performance was always affected by training data size, univariate DT was more systematic than multivariate DT for common training and test datasets and, in the case of univariate DT, a minimum of 300 training pixels per class were needed to the achieve most suitable classification accuracy. They further concluded that DT classifiers were not recommended for high-dimensional datasets. Friedl and Brodley (1997) tested univariate DT, multivariate DT and a hybrid DT on three different remote sensing datasets and compared the classification results from each DT algorithm with those of MLC and linear discriminant function classifier, and reported that DT, hybrid DT in particular, consistently outperformed MLC and linear function discriminant classifier in regard to classification accuracy. Rogan et al. (2002) compared MKT, MSMA MLC and DT to accurately identify changes in vegetation cover in south California and showed that DT classification approach outperformed MLC by nearly 10% regardless of enhancement technique used and using DT classification, MSMA change fractions outperformed MKT change features by nearly 5%. Borak and Strahler (1999) developed a tree-based model for landcover identification from satellite data for a semiarid region in Cochise County, Arizona and compared the results with other classifiers such as fuzzy ARTMAP, MLC and reported that DT could reduce a high-dimension dataset to a manageable set of inputs that retained most of the information of the original database. However fuzzy ARTMAP achieved the highest accuracy in comparison to MLC or DT classifier. Muchoney et al. (2000) compared the classification results obtained from MODIS data for vegetation and landcover mapping using DT, Gaussian ART and Fuzzy ART ANN algorithms in Central America and attained high accuracies from DT (88%), Gaussian ART (83%), and Fuzzy ART NN (79%).

Jarman et al. (2011) studied rangeland conditions in the regions of Kvemo Kartli and Samtskhe-Javakheti in southern Georgia, USA using remote sensing data. They used (NDVI) as the indicator of condition and used object based image analysis. The Landsat scenes and ancillary datasets were collated within eCognition following a two tiered (multi-level) hierarchical approach. The first level brought together the non-rangeland datasets and the second level classified the rangeland area into relative states of rangeland condition (good, moderate, poor). A rule based classification was undertaken within eCognition to map the classes. Laliberte et al. (2011) applied IHS transformation on remote sensing data followed by object based segmentation and classification for structure and species level rangeland mapping. They developed specific rules to define threshold for broader classes and nearest neighborhood classification for finer species level classification. They reported that classification accuracies were highly dependent on the level of detail, number of classes, size of area and specific mapping objectives.

13.4.3.2 Image Differencing and Image Ratioing

The algebraic technique of change detection analysis is based on the selection of a threshold to determine the changed areas (Lu et al., 2004). In this group of change detection techniques, many researchers have applied image differencing and image ratioing with different combinations of spectral bands as their first choice for identifying change, and derived satisfactory results. Conclusions and recommendations vary about whether image differencing and regression, vegetation index differencing or image ratioing is the best change detection technique. Since each method has been applied to different areas, with different datasets and under different environmental conditions, the decision on the selection of a suitable method is not an easy task (Coppin et al., 2004). For example, Sinha and Kumar (2013a) tested 11 different binary change detection methods and compared their capability in detecting land-cover change/no-change information in different seasons using multi-date Thematic Mapper (TM) data. They proposed a relatively new approach for optimal threshold value determination for separation of change/no-change areas and found improved results with this as compared to traditional thresholding (Sinha and Kumar, 2013b).

13.4.3.2.1 Transformation

Various linear data transformation techniques such as Principal Component Analysis (PCA), Tasselled Cap (TC), Gramm-Schmidt (GS), and chi-square transformations have been applied to multi-temporal remote sensing data to identify changes in various land use/land cover classes. In PCA, only two bands of the multi-date image are used as input instead of all bands (Richards, 1986), and hence reducing the data volume and redundancy between bands. After transformation using two bands, the derived components contain information about change and no change areas as the first and second components, respectively, based on information common or unique in the two input bands (Chavez and Kwarteng, 1989). PCA is based on three steps: calculation of a variance—covariance matrix, computation of eigenvectors and linear transformation of datasets (Richards, 1986). Two types of PCA, standardized PCA (uses correlation matrix) and non-standardized PCA (uses covariance matrix), have been used for change detection (De Cauwer et al., 2024; Arogoundade et al., 2023). PCA has certain disadvantages in not providing detailed change matrices and difficulty in interpretation, identification and labelling of changed areas.

TC transformation is carried out by assigning tasseled cap coefficients to spectral bands of two dates, a positive coefficient to the first date and a negative coefficient to the second date, as explained by Crist and Cicone (1984). This is followed by Gramm-Schmidt transformation to make the derived vectors orthogonal to each other. The three transformed images thus obtained contain information about differences in greenness, brightness and wetness, with highest classification accuracy in the greenness change image. Maynard et al. (2007) classified Landsat 7 ETM+ to identify spectrally anomalous locations on satellite data and their correlation with corresponding ground locations for rangeland evaluation. Their classification was carried out using TC brightness, greenness and wetness components stratified by ecological site descriptions. PCA and TC have been the most used approaches for detecting change/no-change information. An additional advantage of TC transformation is that the TC coefficients are scene independent compared to PCA coefficients, which are scene-dependent.

13.4.4 Case Study: Spectral-Spatial Characteristics of Selected Ecological Sites

13.4.4.1 Introduction

Ecological sites (ES) characterize land of specific biophysical and plant community properties. Spatially distinct land areas of the same ecological site respond similarly to management actions and natural disturbances (U.S. Department of Agriculture, NRCS 2012). Therefore, the identification and mapping of ecological sites across large landscapes can be an important tool for rangeland managers. Ecological sites, as they are applied by the United States Department of Agriculture Natural Resources Conservation Service (NRCS) are defined on the basis of soils, geomorphology, hydrology, and the plant species composition that occur on those soils. The NRCS spatially ties ESs to soil components mapped within soil map units (SMU) contained in their spatial digital soil surveys.

Bestelmeyer et al. (2009) formulated an approach to identify ESs from Landsat (or similar platforms) interpreted into land cover maps to identify vegetation distribution. These mapped vegetation areas are used to infer possible ecological sites. In addition to this effort, Maynard et al. (2007) found that there was a high correlation between field measures of productivity and exposed soil when compared to the tasseled cap brightness component extracted from Landsat Thematic Mapper (TM) imagery. Differences in brightness have been shown to discriminate between deciduous shrubs (or harvested forest stands) and closed canopy forests (Dymond et al. 2002).

Gamon et al. (1995) discussed the usefulness of the NDVI as an indicator of photosynthetic activity as well as canopy structure and plant nitrogen content. Jensen (2000) showed that NDVI was sensitive to canopy variations including soil visible through canopy openings. While the sensitivity to soil background has typically been seen as a disadvantage of NDVI for vegetation assessment, it could prove useful for studying ESs because areas of the same ES may have a similar amount and type of bare soil. The NDVI values within a polygon, such as an SMU, and the variation in the NDVI within that polygon has also been used to distinguish between cover types (Pickup and Foran, 1987).

Accurately classifying and identifying the spatial extent of ESs on a landscape level is a time consuming process involving extensive field-work to characterize soils. While remotely sensed data cannot yet be used to obtain detailed data about soils, it can be used to identify the unique vegetation components of ESs. Being able to accurately identify the vegetation component of ESs should provide a means by which soil field sample locations can be identified more efficiently. Based on past research, the use of satellite derived NDVI and brightness, coupled with biophysical geospatial data (elevation, slope, and aspect) should allow areas of the same ES vegetation components to be mapped.

13.4.4.2 Methods

13.4.4.2.1 Study Area

This research was conducted in Rich County, Utah, U.S. (Figure 13.11), located in the northeastern corner of the state (long 111°30′38.5″—long 111°2′42.2″ West and lat 42°0′0″- lat 42°08′24.3″ North). The western portion of the study area is characterized by high elevations with vegetation consisting of aspen forests, subalpine conifer forests, and scattered mountain sagebrush steppe. Moving east, elevation decreases, and the mountain sagebrush steppe becomes dominant. Central and eastern Rich County is made up of relatively lower elevations with vegetation consisting of basin big sagebrush steppe and shrubland, subalpine grasslands, and agriculture (Figure 13.12). The average elevation is 2093 m. The highest point is Bridger Peak at 2821 m and the lowest point is about 1800 m. The climate is variable and is affected by the changing topography of the county.

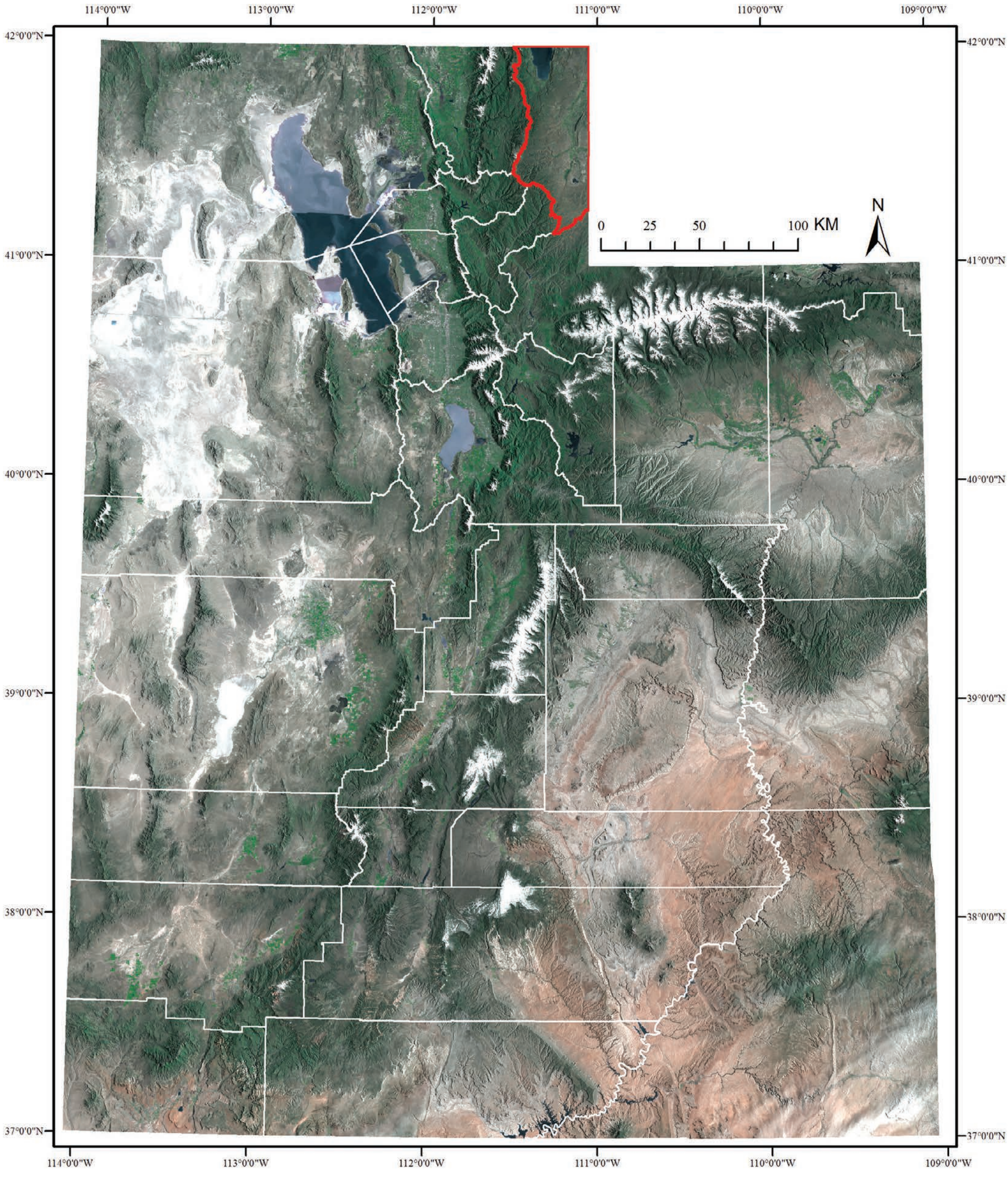

FIGURE 13.11 Utah natural color mosaic from the Landsat 8 Operational Land Imager (OLI) showing Rich County outlined in red.

13.4.4.2.2 Biophysical Geospatial Datasets

A series of Landsat 5 TM images (Path 38/Row 31) for each year between 1984–2011 with Julian date as close to 207 (July 26th) as possible (given acceptable cloud cover) were collected from the U.S. Geological Survey Global Visualization Viewer (GLOVIS). The Julian date of 207 was chosen by averaging the date for each year that displayed the greatest variance in NDVI between different land cover types. The dates were obtained by examining line graphs of mean NDVI values collected by the Moderate Resolution Imaging Spectroradiometer (MODIS) of evergreen forests, shrubs, and deciduous forests. Figure 13.13 is an example of one of these graphs from 2009.

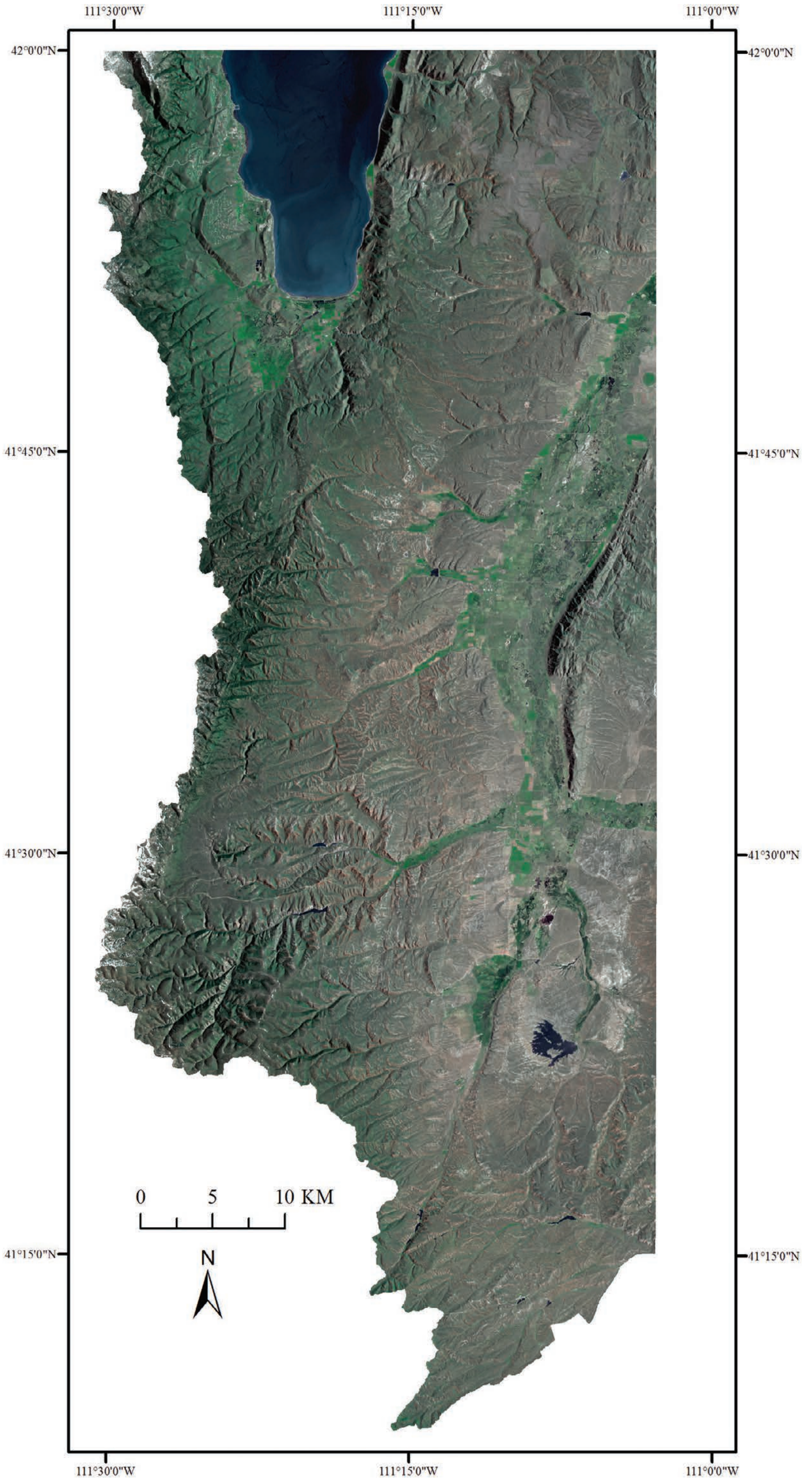

FIGURE 13.12 Rich County, Utah, natural color image from Landsat 8 OLI.

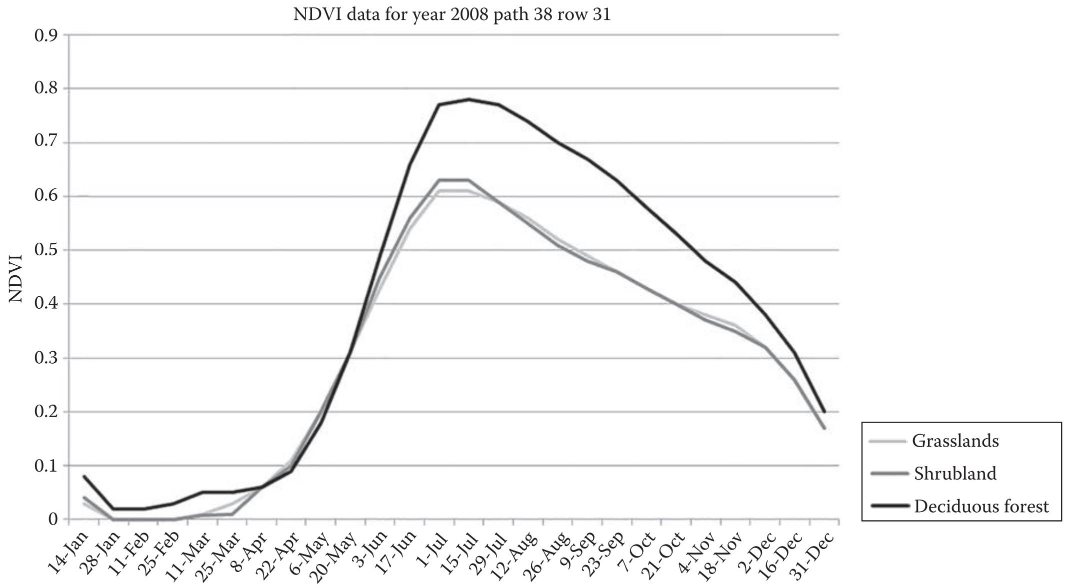

FIGURE 13.13 Line graph of annual fluctuations in NDVI for evergreen forests, shrublands, and deciduous forests. The largest differences in NDVI can be seen in mid-summer.

Of the 28 years' images, 18 were within 20 days of 207, five more were within 30 days of 207, and three more were within 40 days of 207. The cloud free scene closest to Julian date 207 from 1987 had a Julian date of 153 and was 54 days off. The year 2001 was the only year that an image was not available due to cloud cover.

Raw pixel values were converted to reflectance using an image-based atmospheric correction (Chavez, 1996) using appropriate calibration coefficients for Landsat 5 TM (Chander et al., 2009). The NDVI was calculated for each image (Rouse et al., 1974) and for each NDVI product we calculated the spatial standard deviation of the NDVI using a 5 × 5 pixel focal window. The brightness component for each year was calculated using the published transformation coefficients for Landsat 5 TM (Crist and Cicone, 1984). Images from every year were utilized, based on literature indicating that longer time series of remotely sensed data were necessary to adequately characterize different ecological states due to inherent year-to-year variance (Hernandez, 2011).

A 30 m digital elevation model (DEM) produced by the USGS National Elevation Dataset program was used to extract slope and aspect. Elevation, slope, and aspect have been shown to drive microclimatic variation and therefore the spatial distribution and patterns of vegetation (Jin et al., 2008).

13.4.4.2.3 Ecological Sites

To test the process, land cover types representing five ESs were selected. These were Wyoming big sagebrush (*Artemisia tridentata* ssp. *wyomingensis*) steppe, mountain big sagebrush (*Artemisia tridentata* ssp. *vaseyana*), Utah juniper (*Juniperus osteosperma*), Douglas-fir (*Pseudotsuga menziesii*), and aspen (*Populus tremuloides*). With the exception of Utah juniper, these vegetation components were selected because of their prevalence in the county. Wyoming big sagebrush accounts for much of the foothill vegetation in the study area, and aspen is prevalent in the mountainous section, with Douglas-fir, and mountain big sagebrush as secondary and tertiary types. Utah juniper is not prevalent within the study area; however, it is an important vegetation component due to its potential to encroach into sagebrush steppe communities (Miller and Rose, 1999). Together, these vegetation components represent approximately 71% of the county by area.

Twenty polygons were digitized for each of the five ESs using 2009 National Agricultural Imagery Project (NAIP) 1m resolution aerial orthoimagery. In total, one-hundred polygons were created (20 for each ES vegetation component).

Polygons were intersected with the topographic data layers, yearly NDVI imagery, and yearly brightness component images. For each polygon, the mean values of topographic and brightness variables were extracted along with the mean and standard deviation of each NDVI image for each year. From these data, a 28-year mean of the average brightness as well as the mean of the average NDVI and the mean NDVI standard deviation (sdNDVI) were produced. This was done to minimize the effects of inter-annual climate variability and clouds and provide long-term average values for each polygon of each land cover type. Inter-annual climate variability has been shown to affect plant species productivity (Goulden et al., 1996; Arain et al., 2002) and ecological processes (Westerling and Swetnam, 2003). The resulting data matrix was therefore composed of the ES vegetation component name followed by three columns for the DEM derivatives, and three columns for the NDVI, sdNDVI, and brightness.

13.4.4.2.4 Results

Figure 13.14 shows the 28-year mean of the average NDVI value for each polygon plotted against the 28-year mean of the sdNDVI for each polygon showing that the five ESs occupied unique NDVI mean and spatial variance "niches." Some overlap occurred between Wyoming big sagebrush and Utah juniper and between Douglas-fir and aspen ESs. Figure 13.15 shows the same data points with 28-year mean of the average NDVI value plotted against the 28-year mean of the average brightness. The brightness component was able to cleanly separate Aspen polygons from the Douglas-fir polygons. However, brightness provided little separation between Utah juniper and Wyoming big sagebrush.

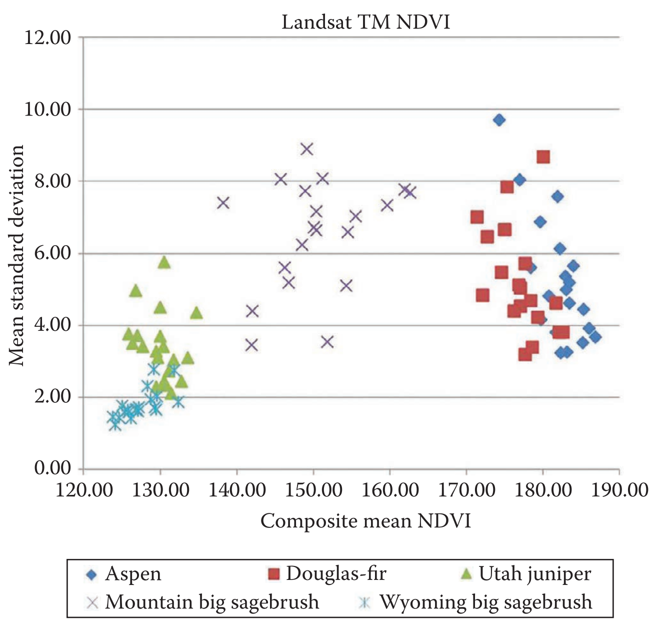

FIGURE 13.14 Scatter-plot showing the distribution of each ecological site vegetation component in our study with average NDVI value on the x-axis and the average standard deviation in NDVI on the y-axis. Both of these variables provide separation between vegetation classes.

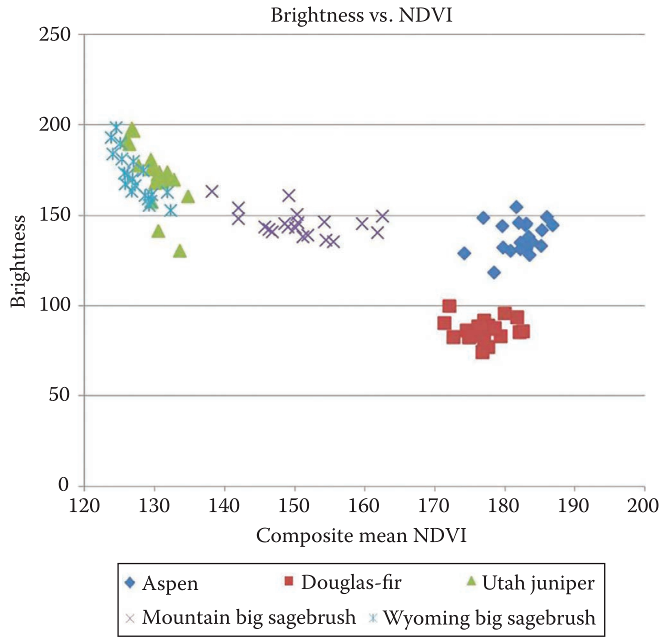

FIGURE 13.15 Scatter-plot showing the distribution of each ecological site vegetation component in our study with average NDVI value on the x-axis and the average brightness component (obtained from the tasseled cap transformation) value on the y-axis.

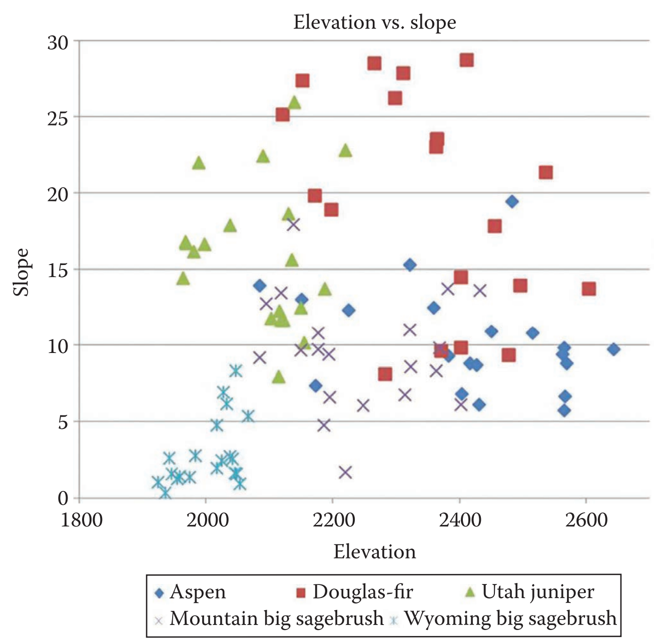

FIGURE 13.16 Scatter-plot showing the distribution of each ecological site vegetation component in our study with elevation on the x-axis and slope on the y-axis. Most vegetation classes overlap one another. However, slope does help with separating Wyoming big sagebrush from Utah juniper.

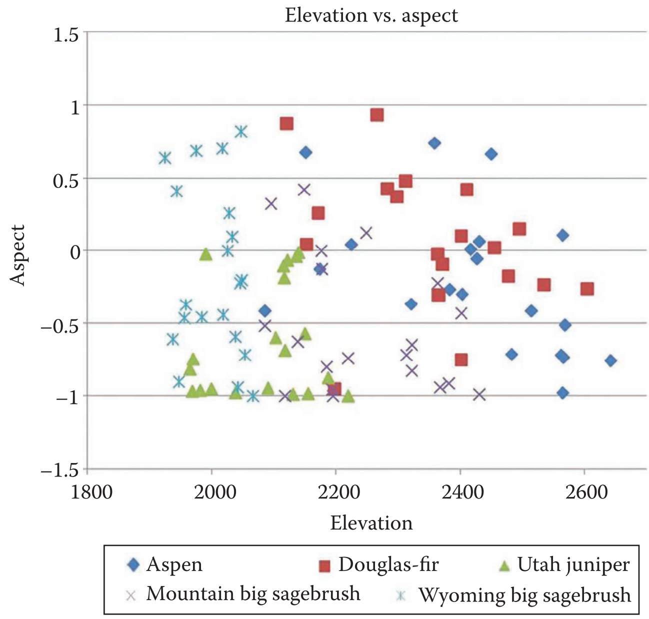

FIGURE 13.17 Scatter-plot showing the distribution of each ecological site vegetation component in our study with elevation on the x-axis and aspect on the y-axis. Aspect does not appear to separate any vegetation classes.

Each polygon was plotted against elevation and slope (Figure 13.16) and also against elevation and the cosine of aspect (Figure 13.17). Topographic variables alone were able to somewhat separate vegetation components along an elevation gradient (as expected). Slope seemed to be a good variable to separate Utah Juniper from Wyoming big sagebrush and Douglas-fir from Aspen. Aspect was not useful for distinguishing between any vegetation types.

The Wyoming big sagebrush polygons collectively had low NDVI and low spatial variation in NDVI. Utah juniper sites had similarly low average NDVI, but due to high contrast between green juniper trees and a relatively larger amount of bare ground, these sites had higher spatial variation in NDVI. Mountain big sagebrush had higher average NDVI values. This was expected since mountain big sagebrush occurs at higher elevations that receive more precipitation than either Wyoming big sagebrush or Utah juniper and therefore is associated with higher plant production. Aspen polygons tended to have higher NDVI values compared to Douglas-fir polygons with both ESs having a similar, relatively large distribution of spatial variance. Where the aspen sites are concerned, there was a slight but distinct trend of decreasing composite mean NDVI with increasing mean standard deviation (sdNDVI). Indeed considering the four aspen sites with the highest sdNDVI, three sites consisted of lower aspen canopy cover and the site with the highest sdNDVI contained a mix of immature aspen trees and shrubs. The remaining 16 aspen sites were all similar in canopy cover.

13.4.4.2.5 Discussion

This case study has shown that using variables derived from remotely sensed images as well as biophysical geospatial data, selected ESs can be discriminated on a per-pixel basis. Prediction of the spatial distribution of ESs on a pixel basis has been suggested as the next step in remote sensing applications to rangeland conservation (Hernandez, 2011). This research has shown that selected ESs can be somewhat cleanly discriminated by utilizing spectral (NDVI and Brightness) and spectral-spatial (sdNDVI) variables and therefore could be mapped by utilizing remotely sensed imagery. This is, of course, not surprising since the remote sensing community has clearly shown the ability to map land cover. What is important here is that by identifying the spatiotemporal spectral nature of selected land cover types, land cover change can be tracked. Ecological sites are used by the USDA-NRCS as a benchmark condition to develop state and transition models (Briske et al., 2005; Bestelmeyer et al., 2009). Ecological sites linked to soil map units provide a means to compare current land cover condition to historic conditions (as defined by the ES). By establishing the spectral nature of ESs, the spectral/spatial signature of soil map polygons can be compared with an expected ES for that polygon. Deviations from the expected response could indicate type and directionality of change, thus providing managers with a powerful land management tool.

13.5 CONCLUSION

Rangelands are dynamic environments that probably exhibit change more frequently and profoundly than many other systems (De Cauwer et al., 2024; Arogoundade et al., 2023; Sharifi and Felegari, 2023; McCord and Pilliod, 2022; Matongera et al., 2021; Hadian et al., 2019; Al-bukhari et al., 2018; Eddy et al., 2017). Land management, livestock grazing, invasive species, prolonged droughts and fire have the potential to alter rangeland community structure at both the micro and macro levels. Vegetation communities can be dominated by either C_3 or C_4 grass species or have permanent shrublands; thus productivity is very phenology dependent. Biomass production in rangelands by C_3 and C_4 plants displays significantly different phenological timing that is detectable using satellite remote sensing. The phenological differences are also useful for identifying vegetation types. Such information about rangeland productivity, vegetation species and timing are useful for rangeland managers in adjusting stocking rate, broad-scale movement of stock, land degradation monitoring and long-term trends in the health and condition of the systems. This chapter has highlighted numerous methods of achieving the preceding by using remotely sensed imagery.

Accurately classifying and identifying the spatial extent of Ecological Sites on a landscape scale is a laborious task involving extensive fieldwork to characterize soils. Case studies presented in this chapter show that variables extracted from remote sensing images, together with biophysical geospatial data, can be used to discriminate Ecological Sites on a per pixel basis with a relatively high degree of confidence. Ecological Sites are widely used as a benchmark condition to develop state and transition models and provide a means to compare current land cover condition with historic conditions, thus indicating type and directionality of change and helping in rangeland management.

Monitoring of fuel in rangelands is also important and this chapter has provided examples of how high temporal resolution satellite remote sensing can be used for quantifying fuel loads in rangeland landscapes. We have also summarized a range of change detection techniques relevant to rangeland monitoring and discussed, through a case study, the effectiveness of a Regression Tree algorithm (Random Forest) in modeling estimates of percent cover and developing Vegetation Continuous Fields for a range of vegetation communities in a rangeland environment.

Remote Sensing has undergone major transformations since its mainstream application began about 50 years ago. Spatial resolutions of images have shrunk from a few kilometers range to the sub-meter range, spectral resolutions have moved to the hyperspectral domain and temporal resolutions enable images to be available almost on a daily basis. In conjunction with this development, image classification techniques have made major progress and continue to be developed. New techniques include neural networks, random forest and object based classifications, and research cited earlier show that they have led to a marked increase in classification accuracies. All these developments have greatly enhanced our ability to map and monitor rangelands to a degree not possible in the past and no doubt will continue to be improved into the future as new techniques and sensor capabilities become mainstream. This chapter has covered some of these developments and highlighted the importance and usefulness of remote sensing for rangeland mapping and monitoring (De Cauwer et al., 2024; Arogoundade et al., 2023; Sharifi and Felegari, 2023; McCord and Pilliod, 2022; Matongera et al., 2021; Hadian et al., 2019; Al-bukhari et al., 2018; Eddy et al., 2017).

REFERENCES

Abdulaziz, A. M., Hurtado, J. M., & Al-Douri, R. 2009. Application of multitemporal Landsat data to monitor land cover changes in Eastern Nile Delta region, Egypt. International Journal of Remote Sensing, 30, 2977–2996.

Ajorlo, M., & Abdullah, B. R. 2007. Develop an Appropriate Vegetation Index for Assessing Rangeland Degradation in Semi-Arid Areas. In: Proceedings of 28th Asian Conference on Remote Sensing, 12–16 November, Kuala Lumpur, Malaysia.

Al-bukhari, A., Hallett, S., & Brewer, T. 2018. A review of potential methods for monitoring rangeland degradation in Libya. Pastoralism, 8(13). https://doi.org/10.1186/s13570-018-0118-4

Amiri, F., & Shariff, A. R. B. M. 2010. Using remote sensing data for vegetation cover assessment in semi-arid rangeland of center province of Iran. World Applied Sciences Journal, 11(12), 1537–1546.

Anderson, H. 1982. Aids to Determining Fuel Models for Estimating Fire Behavior. General Technical Report GTR INT-122. USDA Forest Service, Intermountain Forest and Range Experiment Station: Ogden, Utah. p. 22.

Anderson, M. A. 1997. Two-source time-integrated model for estimating surface fluxes using thermal infrared remote sensing.Remote Sensing of Environment, 60, 195– 216.

Andrews, P. L., & C. D. Bevins. 2003. BehavePlus Fire Modeling System, Version 2.0: Overview. In: Proceedings of the Second International Wildland Fire Ecology and Fire Management Congress and Fifth Symposium on Fire and Forest Meteorology, 16–20 November, American Meteorological Society, Orlando, FL. P5.11.

Arain, M. A., Black, T. A., Barr, A. G., Jarvis, P. G., Massheder, J. M., Verseghy, D. L., & Nesic, Z. 2002. Effects of seasonal and interannual climate variability on net ecosystem productivity of boreal deciduous and conifer forests. Canadian Journal of Forest Research, 32, 878–891.

Arogoundade, A. M., Mutanga, O., Odindi, J., & Odebiri, O. 2023. Leveraging Google Earth Engine to estimate foliar C: N ratio in an African savannah rangeland using Sentinel 2 data. Remote Sensing Applications: Society and Environment, 30, 2023, 100981, ISSN 2352–9385, https://doi.org/10.1016/j.rsase.2023.100981. (www.sciencedirect.com/science/article/pii/S2352938523000630)

Arroyo, L. A., Pascual, C., & Manzanera, J. A. 2008. Fire models and methods to map fuel types: The role of remote sensing. Forest Ecology and Management, 256, 1239–1252.

Asrar, G., Kanemasu, E., & Yoshida, M. 1985. Estimates of leaf area index from spectral reflectance of wheat under different cultural practices and solar angles. Remote Sensing of Environment, 17, 1–11.

Badeck, F.-W., Bondeau, A., Bottcher, K., Doktor, D., Lucht, W., Schaber, J., & Sitch, S. 2004. Responses of spring phenology to climate change. New Phytologist, 162(2), 295–309.

Bailey, R. G., & Hogg, H. C. 1986. A world ecoregions map for resource reporting. Environmental Conservation, 13, 195–202. https://doi.org/10.1017/S0376892900036237.

Baret, F., Guyot, G., & Major, D. J. 1989. TSAVI: A Vegetation Index Which Minimizes Soil Brightness Effects on LAI and APAR Estimation. 12th Canadian Symp. on Remote Sensing and IGARSS' 90, Vancouver, Canada, 10–14 July, 1989.

Baskent, E. Z., & Jordan, G. A. 1995. Characterizing spatial structure of forest landscapes. Canadian Journal of Forest Research, 25, 1830–1849.

Batistella, M., Robeson, S., & Moran, E. F. 2003. Settlement design, forest fragmentation, and landscape change in Rondônia, Amazônia. Photogrammetric Engineering and Remote Sensing, 69, 805–811.

Bestelmeyer, B. T., Tugel, A. J., Peacock, G. L., Robinett, D. G., Shaver, P. L., Brown, J. R., Herrick, J. E., Sanchez, H., & Havstad, K. M. 2009. State-and-transition models for heterogeneous landscapes: A strategy for development and application. Rangeland Ecology & Management, 52, 1–15.

Birth, G. S., & McVey, G. 1968. Measuring the color of growing turf with a reflectance spectrophotometer. Agronomy Journal, 60, 640–643.

Blumenthal, D., Booth, D. T., Cox, S. E., & Ferrier, C. E. 2007. Large-scale aerial images capture details of invasive plant populations. Rangeland Ecological Management, 60, 523–528.

Borak, J. S., & Strahler, A. H. 1999. Feature selection and land cover classification of MODIS-like data set for a semiarid environment. International Journal of Remote Sensing, 20, 919–938.

Bowers, S. A., & Hanks, R. J. 1965. Reaction of radiant energy from soil. Soil Science, 100, 130–138.

Boyte, S. P., Wylie, B. K., Major, D. J., & Brown, J. F. 2014. The integration of geophysical and eMODIS NDVI data into a rule-based, piecewise regression-tree model to estimate cheatgrass beginning of spring growth. International Journal of Digital Earth, 8, 118–132.

Bradley, B. A., & Mustard, J. F. 2008. Comparison of phenology trends by land cover class: A case study in the Great Basin, USA. Global Change Biology, 14, 334–346.

Briggs, J. M., & Knapp, Z. A. K. 1995. Interannual variability in primary production in tallgrass prairie: Climate, soil moisture, topographic position, and fire as determinants of aboveground biomass. American Journal of Botany, 82, 1024–1030.

Briske, D. D., Fuhlendorf, S. D., & Smeins, F. E. 2005. State-and-transition models, thresholds, and rangleland health: A synthesis of ecological concepts and perspectives. Rangeland Ecology & Management, 58, 1–10.

Cain, D. H., Riitters, K., & Orvis, K. 1997. A multi-scale analysis of landscape statistics. Landscape Ecology, 12, 199–212.

Chander, G., Markham, B. L., & Helder, D. L. 2009. Summary of current radiometric calibration coefficients for Landsat MSS, TM, ETM+, and EO-1 ALI sensors. Remote Sensing of Environment, 113, 893–903.

Chang, C. R., Lee, P. F., Bai, M. L., & Lin, T. T. 2004. Predicting the geographical distribution of plant communities in complex terrain—a case study in Fushian Experimental Forest, northeastern Taiwan. Ecography, 27, 577–588.

Chavez, P. S. 1996. Image-based atmospheric corrections revisited and improved. Photogrammetric Engineering and Remote Sensing, 62, 1025–1036.

Chavez, P. S. Jr., & Kwarteng, A. Y. 1989. Extracting spectral contrast in Landsat Thematic Mapper image data using selective principal component analysis. Photogrammetric Engineering and Remote Sensing, 55, 339–348.

Chen, S., & Rao, P. 2008. Land degradation monitoring using-multi-temporal Landsat TM/ETM data in a transition zone between grassland and cropland of northeast China. International Journal of Remote Sensing, 29, 2055–2073.

Cheney, P., & Sullivan, A. 1997. Grassfires: Fuel, Weather and Fire Behaviour. CSIRO Publishing, Collingwood, Australia.

Chopping, M., Lihong, S., Rango, A., Martonchik, J. V., Peters, D. P. C., & Laliberte, A. 2006. Remote sensing of woody shrub cover in desert grasslands using MISR with a geometric-optical canopy reflectance model. Remote Sensing of Environment, 112, 19–34.

Collado, A. D., Chuvieco, E., & Camarasa, A. 2002. Satellite remote sensing analysis to monitor desertification processes in the crop-rangeland boundary of Argentina. Journal of Arid Environment, 52, 121–133.

Conservancy, T. N. 2009. Spatial Modeling of the Cumulative Effects of Land Management Actions on Ecological Systems of the Grouse Creek Mountains—Raft River Mountains Region, Utah. Salt Lake City, Utah. p. 243.

Coppin, P., Joncheere, I., Nackaerts, K., & Muys, B. 2004 Digital change detection methods in ecosystem monitoring: A review. International Journal of Remote Sensing, 25, 1565–1596.

Crews-Meyer, K. A. 2002. Characterizing landscape dynamism using pane-pattern metrics. Photogrammetric Engineering & Remote Sensing, 68, 1031–1040.

Crist, E. P. 1983. The Thematic Mapper Tasseled Capped a Preliminary Formulation. In: Proceedings of 1983 Machine Processing of Remotely Sensed Data Symposium, Environmental Research Institute of Michigan, Ann Arbor, Michigan, pp. 357–363.

Crist, E. P., & Cicone, R. C. 1984. Application of the tasseled cap concept to simulated Thematic Mapper data. Photogrammetric Engineering and Remote Sensing, 50, 343–352.

Crist, E. P., & Cicone, R. C. 1984. A physically-based transformation of thematic mapper data—the TM tasseled cap. IEEE Transactions on Geosciences and Remote Sensing, 22, 256–263.

Crist, E. P., & Kauth, R. J. 1986. The Tasseled Cap De-Mystified. Photogrammetric Engineering and Remote Sensing, 52, 81–86.

Crookston, N. L., & Finley, A. O. 2008. yaImpute: An R package for kNN imputation. Journal of Statistical Software, 23, 1–16.

Cumming, S., & Vervier, P. 2002. Statistical models of landscape pattern metrics, with applications to regional scale dynamic forest simulations. Landscape Ecology, 17, 433–444.

Cutler, D. R., Edwards, T. C., Beard, K. H., Cutler, A., & Hess, K. T. 2007. Random forests for classification in ecology. Ecology, 88, 2783–2792.

Danaher, T., Armston, J., & Collett, L. 2004. A Regression Model Approach for Mapping Woody Foliage Projective Cover Using Landsat Imagery in Queensland, Australia. In: Geoscience and Remote Sensing Symposium, 2004. IGARSS '04. Proceedings. 2004 IEEE International, Anchorage, AK, pp. 523–527.

De Cauwer, V., Colace, M. P., Mendelsohn, J., Antonio, T., & Van Der Waal, C. 2024. A Rangeland Management-Oriented Approach to Map Dry Savanna—Woodland Mosaics. Available at SSRN: https://ssrn.com/abstract=4703486 or https://doi.org/10.2139/ssrn.4703486

Defries, R. S., Hansen, M. C., & Towsend, J. R. G. 2000. Global continuous fields of vegetation characteristics: A linear mixture model applied to multi-year 8 km AVHRR data. International Journal of Remote Sensing, 21, 1389–1414.

Desalew, T., Tegegne, A., Nigatu, L., & Teka, W. 2010. Rangeland Condition and Feed Resources in Metema District, North Gondar Zone, Amhara Region, Ethiopia, IPMS (Improving Productivity and Market Success) of Ethiopian Farmers Project Working Paper 25: Nairobi, Kenya.

Dunn, B. H., Smart, A. J., Gates, R. N., Johnson, P. S., Beutler, M. K., Diersen, M. A., & Janssen, L. L. 2010. Long-term production and profitability from grazing cattle in the northern mixed grass prairie. Rangeland Ecology and Management, 63, 233–242.

Dymond, C. C., Mladenoff, D. J., & Radeloff, V. C. 2002. Phenological differences in tasseled cap indices improve deciduous forest classification. Remotes Sensing of Environment, 80, 460–472.

Eddy, I. M. S., Gergel, S. E., Coops, N. C., Henebry, G. M., Levine, J., Zerriffi, H., & Shibkov, E. 2017. Integrating remote sensing and local ecological knowledge to monitor rangeland dynamics. Ecological Indicators, 82, 2017, 106–116, ISSN 1470–160X, https://doi.org/10.1016/j.ecolind.2017.06.033. (www.sciencedirect.com/science/article/pii/S1470160X17303746)

Ellis, E. C., & Ramankutty, N. 2008. Putting people in the map: Anthropogenic biomes of the world. Frontier in Ecology and the Environment, 6, 439–447.

Elvidge, C. D., & Lyon, R. J. P. 1985. Influence of rock-soil spectral variation on the assessment of green biomass. Remote Sensing of Environment, 17, 37–53.

Feizizadeh, B., Omarzadeh, D., Garajeh, K. M., Lakes, T., & Blaschke, T. (2023) Machine learning data-driven approaches for land use/cover mapping and trend analysis using Google Earth Engine. Journal of Environmental Planning and Management, 66(3), 665–697, https://doi.org/10.1080/09640568.2021.2001317.

Foody, G. M., & Dash, J. 2007. Discriminating and mapping the C3 and C4 composition of grasslands in the northern Great Plains, USA. Ecological Informatics, 2, 89–93.

Franklin, S. E., & Wilson, B. A. 1992. A three-stage classifier for remote sensing of mountain environments. Photogrammetric Engineering and Remote Sensing, 58, 449–454.

Franklin, S. E., Maudie, A. J., & Lavigne, M. B. 2001. Using spatial co-occurrence texture to increase forest structure and species composition classification accuracy. Photogrammetric Engineering and Remote Sensing, 67, 849–855.

Friedl, M. A., & Brodley, C. E. 1997. Decision tree classification of land cover from remotely sensed data. Remote Sensing of Environment, 61, 399–409.

Fry, J. A., Xian, G., Jin, S., Dewitz, J. A., Homer, C. G., Yang, L., Barnes, C. A., Herold, N. D., & Wickham, J. D. 2011. Completion of the 2006 national land cover database for the conterminous united states. Photogrammetric Engineering and Remote Sensing, 77, 858–864.

Fuller, D. O. 2001. Forest fragmentation in Loudoun County, Virginia, USA evaluated with multitemporal Landsat imagery. Landscape Ecology, 16, 627–642.

Gamon, J. A., Field, C. B., Goulden, M. L., Griffin, K. L., & Hartley, A. E. 1995. Relationships between NDVI, canopy structure, and photosynthesis in three Californian vegetation types. Ecological Applications, 5, 28–41.

Gao, B. C. 1996. NDWI—a normalized difference water index for remote sensing of vegetation liquid water from space. Remote Sensing of Environment, 58, 257–266.

Gergel, S. E. 2005. Spatial and non-spatial factors: When do they affect landscape indicators of watershed loading? Landscape Ecology, 20, 177–189.

Gilmanov, T. G., Aires, L., Barcza, Z., Baron, V. S., Belelli, L., Beringer, J., Billesbach, D., Bonal, D., Bradford, J., Ceschia, E., Cook, D., Corradi, C., Frank, A., Gianelle, D., Gimeno, C., Gruenwald, T., Guo, H., Hanan, N., Haszpra, L., Heilman, J., Jacobs, A., Jones, M. B., Johnson, D. A., Kiely, G., Li, S., Magliulo, V., Moors, E., Nagy, Z., Nasyrov, M., Owensby, C., Pinter, K., Pio, C., Reichstein, M., Sanz, M. J., Scott, R., Soussana, J. F., Stoy, P. C., Svejcar, T., Tuba, Z., & Zhou, G. 2010. Productivity, respiration, and light-response parameters of world grassland and agroecosystems derived from flux-tower measurements. Rangeland Ecology and Management, 63, 16–39.

Gitelson, A. A., Kaufman, Y., & Merzlyak, M. N. 1996. Use of green channel in remote sensing of global vegetation from EOS-MODIS. Remote Sensing of Environment, 58, 289–298.

Glenn, E. P., Huete, A. R., Nagler, P. L., & Nelson, S. G. 2008. Relationship between remotely-sensed vegetation indices, canopy attributes and plant physiological processes: What vegetation indices can and cannot tell us about the landscape. Sensors, 8, 2136–2160.

Glenn, E., Huete, A., Nagler, P., Hirschboeck, K., & Brown, P. 2007. Integrating remote sensing and ground methods to estimate evapotranspiration. Critical Reviews in Plant Sciences, 26, 139–168.

Gökalp, A. E., Akar, Ö., & Yılmaz, V. 2017. Improving classification accuracy of spectrally similar land covers in the rangeland and plateau areas with a combination of WorldView-2 and UAV images. Geocarto International, 32(9), 990–1003, https://doi.org/10.1080/10106049.2016.1178816.

Gong, P., & Howarth, P. J. 1992. Frequency based contextual classification and gray-level vector reduction for land use identification. Photogrammetric Engineering & Remote Sensing, 58, 423–437.

Goulden, M. L., Munger, J. W., Fan, S., Daube, B. C., & Wofsy, S. C. 1996. Exchange of carbon dioxide by a deciduous forest: Response to interannual climate variability. Science, 271, 1576–1578.

Graetz, R. D., Pech, R. P., & Davis, A. W. 1988. The assessment and monitoring of sparsely vegetated rangelands using calibrated Landsat data. International Journal of Remote Sensing, 9, 1201–1222.

Green, K., Kempka, D., & Lackey, L. 1994. Using remote sensing to detect and monitor land-cover and land-use change. Photogrammetric Engineering & Remote Sensing, 60, 331–337.

Grice, A. C., & Hodgkinson, K. C. 2002. Global Rangelands: Progress and Prospects. CABI Publishing, Wallingford, Oxfordshire, UK.

Griffith, J., Stehman, S., Sohl, T., & Loveland, T. 2003. Detecting trends in landscape pattern metrics over a 20-year period using a sampling-based monitoring programme. International Journal of Remote Sensing, 24, 175–181.

Griffith, J. A., Martinko, E. A., & Price, K. P. 2000. Landscape structure analysis of Kansas at three scales. Landscape and Urban Planning, 52, 45–61.

Gustafson, E. J. 1998. Quantifying landscape spatial pattern: What is the state of the art? Ecosystems, 1, 143–156.

Gustafson, E. J., & Parker, G. R. 1992. Relationships between landcover proportion and indices of landscape spatial pattern. Landscape Ecology, 7, 101–110.

Hadian, F., Jafari, R., Bashari, H. et al. 2019. Estimation of spatial and temporal changes in net primary production based on Carnegie Ames Stanford Approach (CASA) model in semi-arid rangelands of Semirom County, Iran. Journal of Arid Land 11, 477–494. https://doi.org/10.1007/s40333-019-0060-3.

Hansen, M. C., DeFries, R. S., Townshend, J. R. G., Carroll, M., Dimiceli, C., & Sohlberg, R. A. 2003a. Development of 500 Meter Vegetation Continuous Field Maps Using MODIS Data. In: Geoscience and Remote Sensing Symposium, 2003. IGARSS '03. Proceedings. 2003 IEEE International, pp. 264–266.

Hansen, M. C., DeFries, R. S., Townshend, J. R. G., Carroll, M., Dimiceli, C., & Sohlberg, R. A. 2003b. Global percent tree cover at a spatial resolution of 500 meters: First results of the MODIS vegetation continuous fields algorithm. American Meteorological Society, 7, 1–15.

Hansen, M. C., DeFries, R. S., Townshend, J. R. G., Sohlberg, R., Dimiceli, C., & Carroll, M. 2002. Towards an operational MODIS continuous field of percent tree cover algorithm: Examples using AVHRR and MODIS data. Remote Sensing of Environment, 83, 303–319.

Hardisky, M. A., Klemas, V., & Smart, R. M. 1983. The influence of soil salinity, growth form, and leaf moisture on the spectral radiance of Spartina alterniflora canopies. Photogrammetric Engineering & Remote Sensing, 49, 77–83.

Hernandez, A. 2011. Spatiotemporal modeling of threats to big sagebrush ecological sites in northern Utah [dissertation]. Logan, UT, USA: Utah State University. 163 p.

Heumann, B. W., Seaquis, J. W., Eklundh, L., & Jönsson, P. 2007. AVHRR derived phenological change in the Sahel and Soudan, Africa, 1982–2005. Remote Sensing of Environment, 108, 385–392.

Hoffer, R. M., & Johannsen, C. J. 1969. Ecological potentials in spectral signature analysis. Chapter 1 in Remote Sensing in Ecology, edited by P. C. Johnson (Athens: University of Georgia Press), 1–6.

Honnay, O., Piessens, K., Van Landuyt, W., Hermy, M., & Gulinck, H. 2003. Satellite based land use and landscape complexity indices as predictors for regional plant species diversity. Landscape and Urban Planning, 63, 241–250.

Hudak, A. T., & Wessman, C. A. 1998. Textural analysis of historical aerial photography to characterize woody plant encroachment in South African savanna. Remote Sensing of Environment, 66(3), 317–330.

Huete, A. R. 1988. A soil-adjusted vegetation index (Savi). Remote Sensing of Environment, 25, 295–309.

Huete, A. R., & Jackson, R. D. 1987. Suitability of spectral indices for evaluating vegetation characteristics on arid rangelands. Remote Sensing of Environment, 25, 89–105.

Huete, A. R., Jackson, R. D., & Post, D. F. 1985. Spectral response of a plant canopy with different soil backgrounds. Remote Sensing of Environment, 17, 37–53.

Huete, A., Didan, K., Miura, T., Rodriguez, E. P., Gao, X., & Ferreira, L. G. 2002. Overview of the radiometric and biophysical performance of the MODIS vegetation indices. Remote Sensing of Environment, 83, 195–213.

Im, J., Jensen, J. R., & Tylliss, J. A. 2008. Object based change detection using correlation image analysis and image segmentation. International Journal of Remote Sensing, 29, 399–423.

James, L. F., Young, J. A., & Sanders, K. 2003. A new approach to monitoring rangelands. Arid Land Research and Management, 17, 319–328.

Jensen, J. R. 2000. Remote Sensing of the Environment: An Earth Resources Perspective. Prentice-Hall, Upper Saddle River, NJ, USA. 592 p.

Jensen, J. R. 2007. Remote Sensing of the Environment: An Earth Resource Perspective. Pearson Prentice Hall, Upper Saddle River, NJ.

Jensen, J., 2005. Introductory Digital Image Processing: A Remote Sensing Perspective. Pearson Prentice Hall, Upper Saddle River, NJ.

Jiang, Z., Huete, A. R., Chen, J., Chen, Y., Li, J., & Yan, G. 2006. Analysis of NDVI and scaled difference vegetation index retrievals of vegetation fraction. Remote Sensing of Environment, 101, 366–378.

Jianlong, L., Tiangang, L., & Quangong, C. 1998. Estimating grassland yields using remote sensing and GIS technologies in China. New Zealand Journal of Agricultural Research, 41, 31–380028–8233/98/4101–0031 $7.00/0 © The Royal Society of New Zealand 1998.

Jin, S. M., & Sader, S. A. 2005. Comparison of time series tasseled cap wetness and the normalized difference moisture index in detecting forest disturbances. Remote Sensing of Environment, 94, 364–372.

Jin, S., Yang, L., Danielson, P., Homer, C., Fry, J., & Xian, G. 2013. A comprehensive change detection method for updating the National Land Cover Database to circa 2011. Remote Sensing of Environment, 132, 159–175.

Jin, X. M., Zhang, Y. K., Schaepman, M. E., Clevers, J. G., & Su, Z. 2008. Impact of elevation and aspect on the spatial distribution of vegetation in the Qilian mountain area with remote sensing data. The International Archives of the Photogrammetry, Remote Sensing and Spatial Information Sciences, 37, 1385–1390.

John, R., Chen, J., Lu, N., Guo, K., Liang, C., Wei, Y., Noormets, A., Ma, K., & Han, X. 2008. Predicting plant diversity based on remote sensing products in the semi-arid region of Inner Mongolia. Remote Sensing of Environment, 112, 2018–2032.

Kaloudis, S. T., Lorentzos, N. A., Sideridis, A. B., & Yialouris, C. P. 2005. A decision support system for forest fire management. Operational Research, 5(1), 141–152.

Kamp, K. V., Rigge, M., Troelstrup Jr, N. H., Smart, A. J., & Wylie, B. 2013. Detecting channel riparian vegetation response to best-management-practices implementation in ephemeral streams with the use of spot high-resolution visible imagery. Rangeland Ecology and Management, 66, 63–70.

Kauth, R. J., & Thomas, G. S. 1976. The Tasseled Cap: A Graphic Description of the Spectratemporal Development of Agricultural Crops as Seen by Landsat. In: Proceedings of the Symposium on Machine Processing of Remotely Sensed Data, Purdue University, West Lafayette, Indiana, pp. 4B41–4B51.

Keane, R. E. 2013. Describing wildland surface fuel loading for fire management: A review of approaches, methods and systems. International Journal of Wildland Fire, 22, 51–62.

Kovalskyy, V., & Henebry, G. M. 2012. A new concept for simulation of vegetated land surface dynamics-Part 1: The event driven phenology model. Biogeosciences, 9, 141–159.

Kumar, L., Rietkerk, M., van Langevelde, F., van de Koppel, J., van Andel, J., Hearne, J., de Ridder, N., Stroosnijder, L., Prins, H. H. T., & Skidmore, A. K. 2002. Relationship between vegetation recovery rates and soil type in the Sahel of Burkina Faso: Implications for resource utilization at large scales. Ecological Modelling, 149, 143–152.

Kustas, W., & Norman, J. 1996. Use of remote sensing for evapotranspiration monitoring over land surfaces. Hydrological Sciences Journal—Journal des Sciences Hydrologiques, 41, 495–516.

Laba, M., Smith, S. D., & Degloria, S. D. 1997. Landsat based land cover mapping in the lower Yuna river watershed in the Dominican Republic. International Journal of Remote Sensing, 18, 3011–3025.

Laliberte, A. S., Rango, A., Havstad, K. M., Paris, J. F., Beck, R. F., McNeely, R., & Gonzalez, A. L. 2004. Object-oriented image analysis for mapping shrub encroachment from 1937 to 2003 in southern New Mexico. Remote Sensing of Environment, 93, 198–210.

Laliberte, A. S., Winters, C., & Rango, A. 2011. UAS remote sensing missions for rangeland applications. Geocarto International, 26(2), 141–156.

Langford, M., & Bell, W. 1997. Land cover mapping in a tropical hillsides environment: A case study in the Cauca region of Colombia. International Journal of Remote Sensing, 18, 1289–1306.

Lauenroth, W. K., & Sala, O. E. 1992. Long-term forage production of North American shortgrass steppe. Ecological Applications, 2, 397–403.

Lawler, J. J., White, D., Neilson, R. P., & Blaustein, A. R. 2006. Predicting climate-induced range shifts: Model differences and model reliability. Global Change Biology, 12, 1568–1584.

Le Houerou, H. N., & Hoste, C. H. 1977. Rangeland production and annual rainfall relations in the mediterranean basin and in the African Sahelo-Sudanian Zone. Journal of Range Management, 30, 181–189.

Leitão, B., & Ahern, A., J. 2002. Applying landscape ecological concepts and metrics in sustainable landscape planning. Landscape and Urban Planning, 59, 65–93.

Li, B., & Zhou, Q. 2009. Accuracy assessment on multi-temporal land-cover change detection using a trajectory error matrix. International Journal of Remote Sensing, 30, 1283–1296.

Li, H., & Wu, J. 2004. Use and misuse of landscape indices. Landscape Ecology, 19, 389–399.

Liaw, A., & Wiener, M. 2002. Classification and Regression by randomForest. R News, 2, 5.

Liu, A. J., & Cameron, G. N. 2001. Analysis of landscape patterns in coastal wetlands of Galveston Bay, Texas (USA). Landscape Ecology, 16, 581–595.

Lowry, J., Ramsey, R. D., Thomas, K., Schrupp, D., Sajwaj, T., Kirby, J., Waller, E., Schrader, S., Falzarano, S., Langs, L., Manis, G., Wallace, C., Schulz, K., Comer, P., Pohs, K., Rieth, W., Velasquez, C., Wolk, B., Kepner, W., Boykin, K., O'Brien, L., Bradford, D., Thompson, B., & Prior-Magee, J. 2007. Mapping moderate-scale land-cover over very large geographic areas within a collaborative framework: A case study of the Southwest Regional Gap Analysis Project (SWReGAP). Remote Sensing of Environment, 108, 59–73.

Lu, D., Mausel, P., Brondizio, E., & Moran, E. 2004. Change detection techniques. International Journal of Remote Sensing, 25, 2365–2407.

Ludwig, J. A., Tongway, D. J., Bastin, G. N., & James, C. D. 2004. Monitoring ecological indicators of rangeland functional integrity and their relation to biodiversity at local to regional scales. Austral Ecology, 29, 108–120.

Lutes, D. C., Keane, R. E., & Caratti, J. F. 2009. A surface fuels classification for estimating fire effects. International Journal of Wildland Fire, 18, 802–814.

Matongera, T. N., Mutanga, O., Sibanda, M., & Odindi, J. 2021. Estimating and monitoring land surface phenology in rangelands: A review of progress and challenges. Remote Sensing, 13, 11, 2060. https://doi.org/10.3390/rs13112060.

Maynard, C. L., Lawrence, R. L., Nielsen, G. A., & Decker, G. 2007. Ecological site descriptions and remotely sensed imagery as a tool for rangeland evaluation. Canadian Journal of Remote Sensing, 33(2), 109–115.

McAlpine, C. A., & Eyre, T. J. 2002. Testing landscape metrics as indicators of habitat loss and fragmentation in continuous eucalypt forests (Queensland, Australia). Landscape Ecology, 17, 711–728.

McCord, S. E., & Pilliod, D. S. 2022. Adaptive monitoring in support of adaptive management in rangelands. Rangelands, 44(1), 2022, 1–7, ISSN 0190–0528, https://doi.org/10.1016/j.rala.2021.07.003. (www.sciencedirect.com/science/article/pii/S0190052821000663)

McGarigal, K., & Marks, B. J. 1995. Spatial Pattern Analysis Program for Quantifying Landscape Structure. Gen. Tech. Rep. PNW-GTR-351. US Department of Agriculture, Forest Service, Pacific Northwest Research Station: Portland, Oregon.

Means, J. E., Krankina, O. N., Jiang, H., & Li, H. 1996. Estimating Live Fuels for Shrubs and Herbs With BIOPAK. Gen. Tech. Rep. PNW-GTR-372. U.S. Department of Agriculture, Forest Service, Pacific Northwest Research Station: Portland, OR. p. 28.

Merrill, D. F., & Alexander, M. E. 1987. Glossary of Forest Fire Management Terms, 4th Edition. National Research Council of Canada, Canadian Committee on Forest Fire Management, Ottawa, Ontario.

Milchunas, D. G., Laurenroth, W. K., Chapman, P. L., & Kazempour, M. K. 1989 Effects of grazing, topography, and precipitation on the structure of a semiarid grassland. Vegetation, 80, 11–23.

Miller, A. B., Bryant, E. S., & Birnie, R. W. 1998. An analysis of land cover changes in the northern forest of New England using multi temporal Landsat MSS data. International Journal of Remote Sensing, 19, 245–265.

Miller, R. F., & Rose, J. A. 1999. Fire history and western juniper encroachment in sagebrush steppe. Journal of Range Management, 52, 550–559.

Monteith, J., & Unsworth, M. 1990. Principles of Environmental Physics. 2nd. Edition, Edward Arnold, London.

Muchoney, D. M., Borak, J., Chi, H., Friedl, M., Gopal, S., Hodges, J., Morrow, N., & Strahler, A. 2000. Application of the MODIS global supervised classification model to vegetation and land cover mapping of Central America. International Journal of Remote Sensing, 21, 1115–1138.

Munyati, C., Shaker, P., & Phasha, M. G. 2011. Using remotely sensed imagery to monitor savanna rangeland deterioration through woody plant proliferation: A case study from communal and biodiversity conservation rangeland sites in Mokopane, South Africa. Environmental Monitoring Assessment, 176, 293–311.

O'Neill, R. V. 1976. Ecosystem persistence and heterotrophic regulation. Ecology, 57(6), 1244–1253.

Ode, D. J., Tieszen, L. L., Lerman, J. C. 1980. The seasonal contribution of C3 and C4 plant species to primary production in a mixed prairie. Ecology, 61, 1304–1311.

Okeke, F., & Karnieli, A. 2006. Methods for fuzzy classification and accuracy assessment of historical aerial photographs for vegetation change analyses. Part I: Algorithm development. International Journal of Remote Sensing, 27, 153–176.

Okin, G. S., Roberts, D. A., Murray, B., & Okin, W. J. 2001. Practical limits on hyperspectral vegetation discrimination in arid and semiarid environments. Remote Sensing of Environment, 77(2), 212–225.

Ottmar, R. D., Sandberg, D. V., Riccardi, C. L., & Prichard, S. 2007. An overview of the fuel characteristic classification system—quantifying, classifying, and creating fuelbeds for resource planners. Canadian Journal of Forest Research, 37, 2381–2382.

Pal, M., & Mather, P. M. 2003. An assessment of the effectiveness of decision tree methods for landcover classification. Remote Sensing of Environment, 86, 554–565.

Parker, A. J. 1982.The topographic relative moisture index: An approach to soil-moisture assessment in mountain terrain. Physical Geography, 3, 160–168.

Paruelo, J. M., & Lauenroth, W. K. 1998. Interannual variability of NDVI and its relationship to climate for North American shrublands and grasslands. Journal of Biogeography, 25, 721–733.

Peterson, D. L., Spanner, M. A., Running, S. W., & Teuber, K. B. 1987. Relationships of Thematic Mapper simulator data to leaf area index of temperate coniferous forests. Remote Sensing of Environment, 22, 323–341.

Peterson, E. B. 2005. Estimating cover of an invasive grass (Bromus tectorum) using tobit regression and phenology derived from two dates of Landsat ETM plus data. International Journal of Remote Sensing, 26, 2491–2507.

Petit, C. C., & Lambin, E. F. 2002. Impact of data integration technique on historical land-use/landcover change: Comparing historical maps with remote sensing data in the Belgian Ardennes. Landscape Ecology, 17, 117–132.

Pickup, G., & Foran, B. D. 1987. The use of spectral and spatial variability to monitor cover change on inert landscapes. Remote Sensing of Environment, 23, 351–363.

Pinty, B., & Verstraete, M. M. 1992. GEMI: A non-linear index to monitor global vegetation from satellites. Vegetation, 101, 15–20.

Prasad, A. M., Iverson, L. R., & Liaw, A. 2006. Newer classification and regression tree techniques: Bagging and random forests for ecological prediction. Ecosystems, 9, 181–199.

Program, U. N. G. A. 2004.Provisional Digital Land Cover Map for the Southwestern United States. Version 1.0. United States Geological Survey.

Rauzi, F., & Dobrenz, A. K. 1970. Seasonal variation of chlorophyll in Western wheatgrass and blue grama. Journal of Range Management, 23, 372–373.

Read, J., & Lam, N. S. 2002. Spatial methods for characterising land cover and detecting land-cover changes for the tropics. International Journal of Remote Sensing, 23, 2457–2474.

Reed, B. C., Brown, J., VanderZee, D., Loveland, T. R., Merchant, J. W., & Ohlen, D. O. 1994a. Measuring phenological variability from satellite imagery. Journal of Vegetation Science, 5, 703–714.

Reed, B. C., Brown, J. F., Vanderzee, D., Loveland, T. R., Merchant, J. W., & Ohlen, D. O. 1994b. Measuring phenological variability from satellite imagery. Journal of Vegetation Science, 5, 703–714.

Reed, B. C., Loveland, T. R., & Tieszen, L. L. 1996. An approach for using AVHRR data to monitor U.S. Great Plains grasslands. Geocarto International, 11, 13–22.

Reeves, M., Ryan, K. C., Rollins, M. G., & Thompson, T. 2009. Spatial fuel data products of the LANDFIRE Project. International Journal of Wildland Fire, 18, 250–267.

Rempel, R. S., Carr, A., & Elkie, P. C. 1999. Patch Analyst User's Manual: A Tool for Quantifying Landscape Structure. Ontario Ministry of Natural Resources, Boreal Science, Northwest Science & Technology, Ontario, Canada.

Riaño, D., Chuvieco, E., Salas, J., Palacios-Orueta, A., & Bastarrika, A. 2002. Generation of fuel type maps from Landsat TM images and ancillary data in Mediterranean ecosystems. Canadian Journal of Forest Research, 32(8), 1301–1315.

Riaño, D., Chuvieco, E., Ustin, Salas, S., Rodríguez-Pérez, J., Ribeiro, L., Viegas, D., Moreno, J., & Fernández, H. 2007. Estimation of shrub height for fuel-type mapping combining airborne LiDAR and simultaneous color infrared ortho imaging. International Journal of Wildland Fire, 16(3), 341–348.

Riaño, D., Meier, E., Allgöwer, B., Chuvieco, E., & Ustin, S. L. 2003. Modeling airborne laser scanning data for the spatial generation of critical forest parameters in fire behavior modeling. Remote Sensing of Environment, 86(2), 177–186.

Richards, J. A. 1986, Thematic mapping from multitemporal image data using the principal components transformation. Remote Sensing of Environment, 16, 35–46.

Richardson, A. J., & Wiegand, C. L. 1990. Comparison of two models for simulating the soil-vegetation composite reflectance of a developing cotton canopy. International Journal of Remote Sensing, 11, 447–459.

Richardson, A. J., & Wiegand, C. L. 1977. Distinguishing vegetation from soil background information. Photogrammetric Engineering & Remote Sensing, 43, 1541–1552.

Rietkerk, M., Dekker, S. C., de Ruiter, P. C., & van de Koppel, J. 2004. Self-organized patchiness and catastrophic shifts in ecosystems. Science, 305(5692), 1926–1929.

Rigge, M., Smart, A., Wylie, B., Gilmanov, T., & Johnson, P. 2013. Linking phenology and biomass productivity in South Dakota mixed-grass prairie. Rangeland Ecology and Management, 66, 579–587.

Riitters, K. H., O'neill, R., Hunsaker, C., Wickham, J. D., Yankee, D., Timmins, S., Jones, K., & Jackson, B. 1995. A factor analysis of landscape pattern and structure metrics. Landscape Ecology, 10, 23–39.

Rock, B. N., Williams, D. L., & Vogelmann, J. E. 1985. Field and Airborne Spectral Characterization of Suspected Acid Deposition Damage in Red Spruce (Picea Rubens) from Vermont. Proc., Symp. on Machine Processing of Remotely Sensed Data, Purdue Univ., West Lafayette, IN, pp. 71–81.

Rogan, J., Franklin, J., & Roberts, D. A. 2002. A comparison of methods for monitoring multitemporal vegetation change using Thematic Mapper imagery. Remote Sensing of Environment, 80, 143–156.

Rollins, M. 2009. LANDFIRE: A nationally consistent vegetation, wildland fire and fuel assessment. International Journal of Wildland Fire, 18, 235–249.

Rouse, J. W., Haas, R. H., Schell, J. A., & Deering, D. W. 1974. Monitoring vegetation systems in the Great Plains with ERTS. Proc. Third ERTS-1 Symposium, NASA Goddard, NASA SP-351, pp. 309–317.

Sandberg, D. V., Ottmar, R. D., & Cushon, G. H. 2001. Characterizing fuels in the 21st Century. International Journal of Wildland Fire, 10, 381–387.

Sharifi, A., & Felegari, S. 2023. Remotely sensed normalized difference red-edge index for rangeland biomass estimation. Aircraft Engineering and Aerospace Technology, 95(7), 1128–1136. https://doi.org/10.1108/AEAT-07-2022-0199.

Schmitz, M., De Aranzabal, I., Aguilera, P., Rescia, A., & Pineda, F. 2003. Relationship between landscape typology and socioeconomic structure: Scenarios of change in Spanish cultural landscapes. Ecological Modelling, 168, 343–356.

Scott, J. H., & Burgan, R. E. 2005. Standard fire behavior fuel models: A comprehensive set for use with Rothermel's surface fire spread model. General Technical Report RMRS-GTR-153. U.S. Department of Agriculture, Forest Service, Rocky Mountain Research Station: Fort Collins, CO. p. 72.

Scott, J. M., Davis, F., Csuti, B., Noss, R., Butterfield, B., & Groves, C. 1993. Gap analysis: A geographic approach to protection of biological diversity. Wildlife Monographs, 123, 3–41.

Sellers, P. 1985. Canopy reflectance, photosynthesis and transpiration. International Journal of Remote Sensing, 6, 1335–1372.

Sexton, J. O., Song, X. P., Feng, M., Noojipady, P., Anand, A., Huang, C., Kim, D. H., Collins, K. M., Channan, S., DiMiceli, C., & Townshend, J. R. 2013. Global, 30-m resolution continuous fields of tree cover: Landsat-based rescaling of MODIS vegetation continuous fields with lidar-based estimates of error. International Journal of Digital Earth, 6, 427–448.

Sha, Z., Baiy, Y., & Xie, Y. 2008. Using a hybrid fuzzy classifier (HFC) to map typical grassland vegetation in Xilinhe River Basin, Inner Mongolia, China. International Journal of Remote Sensing, 29(8), 2317–2337.

Sims, P. L., & Singh, J. S. 1978a. The structure and function of ten western North American grasslands. II. Intra-seasonal dynamics in primary producer compartments. Journal of Ecology, 66, 547–572.

Sims, P. L., & Singh, J. S. 1978b. Primary production of the central grassland region of the United States. Ecology 69, 40–45.

Sinha, P., & Kumar, L. 2013a. Binary images in seasonal land-cover change identification: A comparative study in parts of NSW, Australia. International Journal of Remote Sensing, 34(6), 2162–2182.

Sinha, P., & Kumar, L. 2013b. Independent two-step thresholding of binary images in inter-annual land cover change/no-change identification. ISPRS Journal of Photogrammtery and Remote Sensing, 81(7), 31–43.

Sinha, P., Kumar, L., & Reid, N. 2012a. Seasonal variation in landcover classification accuracy in diverse region. Photogrammetric Engineering & Remote Sensing, 78(3), 770–781.

Sinha, P., Kumar, L., & Reid, N. 2012b. Three-date Landsat TM composite in seasonal land-cover change identification in a mid-latitudinal region of diverse climate and land-use. Journal of Applied Remote Sensing, 6(1), 063595, https://doi.org/10.1117/1.JRS.6.063595.

Smart, A. J., Dunn, B. H., Johnson, P. S., Xu, L., & Gates, R. N. 2007. Using weather data to explain herbage yield on three great plains plant communities. Rangeland Ecology Management, 60, 146–153.

Sohn, Y., & Qi, J. 2005. Mapping detailed biotic communities in the upper San Pedro Valley of southeastern Arizona using Landsat 7 ETM+ data and supervised spectral angle classifier. Photogrammetric Engineering & Remote Sensing, 71, 709–718.

Sohn, Y., & Rebello, N. S. 2002. Supervised and unsupervised spectral angle classifiers. Photogrammetric Engineering & Remote Sensing, 68, 1271–1280.

Sparks, T. H., Jeffree, E. P., & Jeffree, C. E. 2000. An examination of the relationship between flowering times and temperature at the national scale using long-term phenological records from the UK. International Journal of Biometeorology, 44(2), 82–87.

Stanfield, B. J., Bliss, J. C., & Spies, T. A. 2002. Land ownership and landscape structure: A spatial analysis of sixty-six Oregon (USA) Coast Range watersheds. Landscape Ecology 17, 685–697.

Strahler, A. H., 1980. The use of prior probabilities in maximum likelihood classification of remotely sensed data. Remote Sensing of Environment, 10, 1135–1163.

Sutton, C. D. 2005. Classification and regression trees, bagging, and boosting. Handbook of Statistics: Data Mining and Data Visualization, edited by C. R. Rao, E. J. Wegman & J. L. Solka (Elsevier), 303–329.

Tagestad, J. D., & Downs, J. L. 2007. Landscape Measures of Rangeland Condition in the BLM Owyhee Pilot Project: Shrub Canopy Mapping, Vegetation Classification, and Detection of Anomalous Land Areas. Report prepared for U.S. Department of Interior Bureau of Land Management under a Related Services Agreement with the U.S. Department of Energy Contract DE-AC05–76RL01830 Pacific Northwest National Laboratory Richland, Washington 99352.

Tang, J., Corresponding, L. W., & Zhang, S. 2005. Investigating landscape pattern and its dynamics in Daqing, China. International Journal of Remote Sensing, 26, 2259–2280.

Tao, F., Yokozawa, M., Zhang, Z., Hayashi, Y., & Ishigooka, Y. 2008. Land surface phenology dynamics and climate variations in the North East China Transect (NECT), 1982–2000. International Journal of Remote Sensing, 29, 5461–5478.

Tateishi, R., & Ebata, M. 2004. Analysis of phenological change patterns using 1982–2000 advanced very high resolution radiometer (AVHRR) data. International Journal of Remote Sensing, 25, 2287–2300.

Teague, W. R., Ansley, J. R., Pinchak, W. E., Dowhower, S. L., Gerrard, S. A., & Waggoner, J. A. 2008. Interannual herbaceous biomass response to increasing honey mesquite cover on two soils. Rangeland Ecological Management, 61, 496–508.

Tieszen, L. L., Reed, B. C., Bliss, N. B., Wylie, B. K., & DeJong, D. D. 1997. NDVI, C3 AND C4 production, and distributions in Great Plains grassland land cover classes. Ecological Applications, 7, 59–58.

Timmerman, W., Kustas, W., Anderson, M., & French, A. 2007. An intercomparison of the surface energy balance algorithm for land (SEBAL) and the two-source energy balance (TSEB) modeling schemes. Remote Sensing of Environment, 108, 369–384.

Todd, S. W., & Hoffer, R. M. 1997. Responses of spectral indices to variations in vegetation cover and soil background. Photogrammetric Engineering & Remote Sensing, 64(9), 915–921.

Todd, S. W., Hoffer, R. M., & Milchunas, D. G. 1998. Biomass estimation on grazed and ungrazed rangelands using spectral indices. International Journal of Remote Sensing, 19(3), 427–438.

Torahi, A. A. 2012. Rangeland Dynamics Monitoring Using Remotely-Sensed Data, in Dehdez Area, Iran. In: International Conference on Applied Life Sciences (ICALS2012), 10–12 September, Turkey.

Trani, M. K., & Giles, R. H. 1999. An analysis of deforestation: Metrics used to describe pattern change. Forest Ecology and Management, 114, 459–470.

Tso, B., & Olsen, R. C. 2005. Combining spectral and spatial information into hidden Markov models for unsupervised image classification. International Journal of Remote Sensing, 26, 2113–2133.

Tucker, C. 1979. Red and photographic infrared linear combinations for monitoring vegetation. Remote Sensing of Environment, 8, 127–150.

Tucker, C., Townshend, J., & Goff, T. 1985. African land cover classification using satellite data. Science, 227, 229–235.

Tucker, C. J., & Sellers, P. J. 1986. Satellite remote sensing of primary production. International Journal of Remote Sensing, 7, 1395–1416.

Tymstra, C., Bryce, R. W., Wotton, B. M., Taylor, S. W., & Armitage, O. B. 2010. Development and Structure of Prometheus: The Canadian Wildland Fire Growth Simulation Model. Natural Resources Canada, Canadian Forest Service, Northern Forestry Centre, Edmonton, AB. Information Report NOR-X-417. p. 88. Available at: http://cfs.nrcan.gc.ca/bookstore_pdfs/31775.pdf. Accessed 16 March 2011.

U.S. Department of Agriculture, National Resources Conservation Service. 2008. Field Office Technical Guide, Major Land Resource Area 063A: Northern Rolling Pierre Shale Plains, Ecological Site Description: Clayey.

U.S. Department of Agriculture, NRCS. 2012. Ecological Sites. Available at: www.nrcs.usda.gov/wps/portal/nrcs/detail/national/landuse/rangepasture/?cid=STELPRDB1043235. Accessed 17 October 2011.

van Leeuwen, W. J. D., Davison, J. E., Casady, G. M., & Marsh, S. E. 2010. Phenological characterization of desert sky island vegetation communities with remotely sensed and climate time series data. Remote Sensing, 2, 388–415.

Vierling, L. A., Xu, Y., Eitel, J. U. H., & Oldow, J. S. 2012. Shrub characterization using terrestrial laser scanning and implications for airborne LiDAR assessment. Canadian Journal of Remote Sensing, 38(6), 709–722.

Vogel, M., & Strohbach, M. 2009. Monitoring of savanna degradation in Namibia using Landsat TM/ETM+ data, Int. Geosci. Remote Sensing (IGARSS) IEEE, Cape Town, S. Afr., pp. III-931–III-934.

Vogelmann, J. E., Xian, G., Homer, C., & Tolk, B. 2012. Monitoring gradual ecosystem change using Landsat time series analyses: Case studies in selected forest and rangeland ecosystems. Remote Sensing of Environment, 122, 92–105.

Walton, J. T. 2008. Subpixel urban land cover estimation: Comparing cubist, random forests, and support vector regression. Photogrammetric Engineering & Remote Sensing, 74, 1213–1222.

Wang, C., Jamison, B. E., & Spicci, A. A. 2010. Trajectory-based warm season grassland mapping in Missouri prairies with multi-temporal ASTER imagery. Remote Sensing of Environment, 114, 531–539.

Wang, Y., Mitchell, B. R., Nugranad-Marzilli, J., Bonynge, G., Zhou, Y., & Shriver, G. 2009. Remote sensing of land-cover change and landscape context of National Parks: A case study of northeast temperate network. Remote Sensing of Environment, 113, 1453–1461.

Weber, K. T., Alados, C. L., Bueno, C. G., Gokhale, B., Komac, B., & Pueyo, Y. 2009. Modeling bare ground with classification trees in Northern Spain. Rangeland Ecology & Management, 62, 452–459.

Weiser, R. L., Asrar, G., Miller, G. P., & Kanemasu, E. T. 1986 Assessing grassland biophysical characteristics from spectral measurements. Remote Sensing of Environment, 20, 141–152.

Wessels, K. J., Prince, S. D., Carroll, M., & Malherbe, J. 2007. Relevance of rangeland degradation in semiarid northeastern South Africa to the nonequilbrium theory. Ecological Applications, 17(3), 815–827.

Wessels, K. J., Prince, S. D., Frost, P. E., & Van Zyl, D. 2004. Assessing the effects of human-induced land degradation in the former homelands of northern South Africawith a 1km AVHRR NDVI time-series. Remote Sensing of Environment, 91, 47–67.

Westerling, A. L., & Swetnam, T. W. 2003. Interannual to decadal drought and wildfire in the western United States. Transactions American Geophysical Union, 84, 545–560.

Westman, W. E. 1985. Ecology, Impact Assessment, and Environmental Planning. Wiley, New York, USA.

Westman, W. E., & O'Leary, J. F. 1986. Measures of resilience: The response of coastal sage scrub to fire. Vegetation, 65(3), 179–189.

White, M. A., de Beurs, K. M., Didan, K., Inouye, D. W., Richardson, A. D., Jensen, O. P., O'Keefe, J., Zhang, G., Nemani, R. R., van Leeuwen, W. J. D., Brown, J. F., de Wit, A., Schaepman, M., Lin, X., Dettinger, M., Bailey, A. S., Kimball, J., Schwartz, M. D., Baldocchi, D. D., Lee, J. T., & Lauenroth, W. K. 2009. Intercomparison, interpretation, and assessment of spring phenology in North America estimated from remote sensing for 1982–2006. Global Change Biology, 15, 2335–2359.

Wickham, J., & Rhtters, K., 1995. Sensitivity of landscape metrics to pixel size. International Journal of Remote Sensing, 16, 3585–3594.

Wisdom, M., Rowland, M., Suring, L., Shueck, L., Meinke, C., & Knick, S. 2005. Evaluating species of conservation concern at regional scales. Habitat Threats in the Sagebrush Ecosystem: Methods of Regional Assessment and Applications in the Great Basin, edited by M. Wisdom, M. Rowland & L. Suring (Lawrence, Kansas: Alliance Communications Group), 5–74.

Wotton, B. M. 2009. Interpreting and using outputs from the Canadian Forest Fire Danger Rating System in research applications. Environmental and Ecological Statistics, 16(2), 107–131.

Xie, Y., Sha, Z., & Yu, M. 2008. Remote sensing imagery in vegetation mapping: A review. Journal of Plant Ecology, 1, 9–23.

Xiuwan, C. 2002. Using remote sensing and GIS to analyse land cover change and its impacts on regional sustainable development. International Journal of Remote Sensing, 23, 107–124.

Xu, M., Watanachaturaporn, P., Varshney, P. K., & Arora, M. K. 2005. Decision tree regression for soft classification of remote sensing data. Remote Sensing of Environment, 97, 322–336.

Zhang, L., Wylie, B. K., Ji, L., Gilmanov, T. G., & Tieszen, L. L. 2010. Climate-driven interannual variability in net ecosystems exchange in the northern Great Plains grasslands. Rangeland Ecology and Management, 63, 40–50.

Zhou, B., Okin, G. S., & Zhang, J. 2020. Leveraging Google Earth Engine (GEE) and machine learning algorithms to incorporate in situ measurement from different times for rangelands monitoring. Remote Sensing of Environment, 236, 2020, 111521, ISSN 0034–4257. https://doi.org/10.1016/j.rse.2019.111521. (www.sciencedirect.com/science/article/pii/S0034425719305401)